

# POLITECNICO DI TORINO

Dipartimento di Ingegneria dell'Ambiente, del Territorio e delle Infrastrutture

**Corso di Laurea Magistrale  
in Ingegneria per l'Ambiente e il Territorio**

Tesi di Laurea Magistrale

## **A STUDY ON SOIL TEMPERATURE AND MOISTURE IN THE SWISS PLATEAU USING THE MODEL SNOWPACK**



**Relatore:** Costantino Manes

**Correlatore:** Michael Lehning  
**Supervisor:** Adrien Michel

**Candidato:**  
Edoardo Brovero

Ottobre 2019

## Acknowledgements

## Abstract

The extension of the well-known surface process model SNOWPACK to the soil is relatively new. Studies have mostly been conducted in high-altitude alpine areas, characterized by coarse-grained soils. Investigating the role of soil at all altitudes is crucial for various fields, such as catchment hydrology, geotechnical engineering, geochemistry, and agriculture. A thorough understanding of the model behavior can provide a tool to assess water cycle, soil moisture and other phenomena in future variable climate change scenarios.

This work focuses on a seasonal analysis of ground temperature, soil moisture, water loss by evapotranspiration and produced runoff, which, despite often being studied separately, are highly interconnected. SNOWPACK allows evaluating all of them together. By applying the model to low-altitude sites with fine-grained soils, this thesis pursues a double purpose: on the one hand, a sensitivity analysis is carried out in Payerne (Canton Vaud, Switzerland), to determine how various configurations and soil parameters affect the mentioned hydrologic quantities. On the other hand, the model is tested in ten other locations, most of which in the Swiss Plateau, through the application of the soil parametrization obtained in Payerne and the comparison with ground temperature and soil moisture field data sets.

A sensitivity analysis is initially performed: the results are divided based on the water infiltration model and the soil evaporation method. A simple Bucket model is found to reproduce summer and spring temperatures well and autumn and winter ones decently (underestimation of 1 °C), but only when associated with the Evaporation Resistance method. If Richards equation is implemented, temperatures are underestimated by about 1-2 °C in all seasons, whereas evapotranspiration and soil moisture are satisfactorily simulated. Ground temperature evolution with depth appears largely affected by thermal conductivity and heat capacity, while surface summer temperatures turn out to be highly sensitive to roughness length variations. The average soil grain size is, by construction, the variable that influences the most evapotranspiration, runoff and soil moisture. It is noted that the introduction of canopy, together with every canopy parameter variation which contributes to its increased effect (increases in height, Leaf Area Index and others), causes a ground temperature reduction. Evapotranspiration, instead, responds with a general increase, except for the case in which the canopy height is raised.

SNOWPACK validation in the ten new sites is overall successful. The ground temperature underestimation observed in Payerne is generally reduced or inverted, with overestimation occurring especially in the sandy loam soils; ground temperature gradients are not well reproduced in autumn and occasionally in winter. The fitting's accuracy with respect to the modelled data is therefore very variable. Modelled evapotranspiration (assessed in three sites) has the same bias as in Payerne, with the difference that Root Mean Square Error values are much lower in Rietholzbach. Regarding soil moisture, this is well reproduced (Root Mean Square Error < 0.05) in most of the sites; variations are satisfyingly captured, even though accuracy is not uniform among the simulations. Moreover, it can be affirmed that no evident difference in soil moisture is manifested between the seven loamy soils and the other four (silt loam and sandy loam soils) when a new soil type is set, but the same other soil parameters are maintained.

Finally, Payerne runoff is assessed at a catchment scale using Alpine3D. The cumulative runoff is found to have the same order of magnitude of the cumulative river discharge. Runoff exceeds discharge more with Bucket than with Richards (43% and 21% respectively), a result consistent with the strong underestimation of evapotranspiration by the Bucket model and which allows to confirm Richards as the most accurate hydrological model at yearly scale.

Key words: ground temperature, evapotranspiration, soil moisture, runoff, Richards equation, Bucket model, soil evaporation method, sensitivity analysis, SNOWPACK, Alpine3D

# Contents

Acknowledgements .....	- 2 -
Abstract .....	i
List of figures .....	v
List of tables .....	viii
Abbreviations .....	ix
1 INTRODUCTION .....	10
2 MODELS USED .....	14
2.1 MeteoIO .....	14
2.2 SNOWPACK .....	14
2.3 Alpine3D .....	15
3 THEORETICAL NOTIONS .....	17
3.1 Water flow in porous media .....	17
3.1.1 Saturated conditions: Darcy's Law .....	17
3.1.2 Non-saturated conditions: Richards equation .....	19
3.2 Theory on thermal transfer in soil .....	23
3.3 Thermal boundary conditions and phase changes .....	27
4 SNOWPACK .....	30
4.1 Type of files and variables .....	30
4.2 Richards equation in SNOWPACK .....	31
4.3 Bucket scheme in SNOWPACK .....	32
4.4 Soil evaporation method .....	33
4.5 Other variables and phenomena .....	34
4.5.1 Thermal boundary conditions .....	34
4.5.2 Atmospheric stability correction .....	36
4.5.3 Roughness length .....	36
4.5.4 Thermal parameters .....	37
4.5.5 Canopy .....	39
5 DATA AND ANALYSIS TOOLS .....	41
5.1 Origin of the data .....	41
5.2 Output processing .....	44
6 RESULTS - PAYERNE SENSITIVITY ANALYSIS .....	47
6.1 Bucket model .....	48
6.2 Richards equation .....	59

6.3	Discussion .....	66
6.4	Canopy module.....	70
6.4.1	Canopy module implementation .....	70
6.4.2	Canopy height .....	73
6.4.3	Canopy Leaf Area Index .....	75
6.4.4	Canopy Direct Throughfall .....	77
6.4.5	Canopy root depth.....	78
6.4.6	Other canopy parameters .....	80
7	RESULTS – VALIDATION.....	82
7.1	Ground temperature.....	83
7.2	Evapotranspiration.....	87
7.3	Soil moisture.....	90
7.4	Runoff.....	93
8	CONCLUSIONS.....	100
	BIBLIOGRAPHY .....	104
	APPENDICES .....	108

## List of figures

Figure 3-1: Typical values for hydraulic conductivity (adapted from Freeze and Cherry, 1979).....	18
Figure 3-2: Characteristic curve relating moisture content to pressure head (Blaskó Lajos, 2008).....	21
Figure 3-3: The initial drainage curve (IDC), the main wetting curve (MWC), the main drainage curve (MDC), and a scanning curve. $\theta$ refers to the volumetric water content and the subscripts r, o, and s, to residual, satiated, and saturated (Dane, Lenhard, 2005) .....	22
Figure 3-4: Typical soil water characteristic curves for soils of different texture (Tuller, Or, 2003) .....	23
Figure 3-5: Annual temperature waves in the weekly averaged subsurface soil temperatures at two depths in a sandy loam soil (West, 1952).....	27
Figure 3-6: Relevant processes in the snow cover model SNOWPACK (SLF) .....	28
Figure 4-1: Field capacity in function of $r_g$ , when the Bucket model is applied.....	33
Figure 4-2: Swiss Geotraverse, crossing all the regions defined by differing geothermal heat fluxes (Vedova, 1991) .....	35
Figure 5-1: Location of SwissSMEX stations for soil monitoring ( <a href="https://iac.ethz.ch">https://iac.ethz.ch</a> ) .....	41
Figure 5-2: Payerne station for soil monitoring ( <a href="https://iac.ethz.ch">https://iac.ethz.ch</a> ) .....	42
Figure 5-3: Plaffeien station for soil monitoring ( <a href="https://iac.ethz.ch">https://iac.ethz.ch</a> ).....	42
Figure 6-1: Soil moisture vs time, modelled and measured. Bucket, ER. Depth: 50 cm .....	48
Figures 6-2: Seasonal and yearly average GT vs depth, modelled and measured. Soil evaporation methods: ER (left panel), RH (right panel).....	49
Figures 6-3: Seasonal average ET vs time, modelled and measured. Soil evaporation methods: ER (left panel), RH (right panel) .....	50
Figures 6-4: Seasonal and yearly average GT vs depth, modelled and measured. $r_g$ : 0.5 mm, clay (left panel), 40 mm, gravel (right panel).....	51
Figures 6-5: Seasonal and yearly average GT vs depth, modelled and measured. $r_g$ : 0.75 mm, sandy clay (left panel), 40 mm, gravel (right panel) .....	52
Figures 6-6: Modelled runoff (left panel) and difference in ET (right panel) trends with the two soil evaporation methods ER and RH.....	53
Figures 6-7: Seasonal and yearly average GT vs depth, modelled and measured. $c_m$ : 500 J/kg·K (left panel), 2300 J/kg·K (right panel) .....	54
Figures 6-8: Seasonal and yearly average GT vs depth, modelled and measured. $\lambda_m$ : 0.5 W/m·K (left panel), 2.3 W/m·K (right panel) .....	55
Figures 6-9: Seasonal and yearly average GT vs depth, modelled and measured. Solid fraction: 0.40 (left panel), 0.70 (right panel) .....	56
Figures 6-10: Seasonal and yearly average GT vs depth, modelled and measured. Dry compacted density: 2000 kg/dm <sup>3</sup> (left panel), 3200 kg/dm <sup>3</sup> (right panel) .....	57
Figures 6-11: Seasonal and yearly average GT vs depth, modelled and measured. Roughness length: 0.005 m (left panel), 0.05 m (right panel) .....	58
Figure 6-12: Difference between measured and modelled OSWR and its average. Soil albedo: 0.21... 59	59
Figures 6-13: Seasonal and yearly average GT vs depth, modelled and measured. Soil evaporation methods: ER (left panel), RH (right panel).....	60
Figures 6-14: Seasonal average ET vs time, modelled and measured. Soil evaporation methods: ER (left panel), RH (right panel).....	61
Figures 6-15: Soil moisture vs time, modelled and measured. Depth: 30 cm (top left panel), 50 cm (top right panel), 80 cm (bottom left panel). Seasonal and yearly average soil moisture vs depth, modelled and measured (bottom right panel) .....	62

Figures 6-16: Silty clay. Soil moisture vs time, modelled and measured, depth: 80 cm (left panel). Seasonal and yearly average soil moisture vs depth, modelled and measured (right panel) .....	64
Figures 6-17: Sand. Soil moisture vs time, modelled and measured, depth: 80 cm (left panel). Seasonal and yearly average soil moisture vs depth, modelled and measured (right panel) .....	64
Figures 6-18: Seasonal and yearly average GT vs depth, modelled and measured. Final soil parametrization with: Bucket, ER (left panel), Richards, ER (right panel) .....	67
Figures 6-19: Seasonal average ET vs time, modelled and measured. Final soil parametrization with: Bucket, ER (left panel), Richards, ER (right panel) .....	68
Figures 6-20: Modelled and measured GT vs time. Depth: 5 cm (left panel), 10 cm (right panel).....	69
Figures 6-21: Modelled and measured GT vs time. Depth: 30 cm (left panel), 50 cm (right panel).....	69
Figure 6-22: Modelled and measured GT vs time. Depth: 80 cm.....	70
Figures 6-23: Seasonal average ET vs time, modelled and measured. Richards, ER. Canopy OFF (left panel), ON (right panel) .....	72
Figures 6-24: Seasonal average ET vs time, modelled and measured. Richards, ER. Canopy height: 0.50 m (left panel), 0.90 m (right panel) .....	74
Figures 6-25: Seasonal average ET vs time, modelled and measured. Richards, ER. Canopy LAI: 1 (left panel), 4 (right panel).....	76
Figures 6-26: Seasonal average ET vs time, modelled and measured. Richards, ER. Canopy DT: 0.45 (left panel), 0.90 (right panel) .....	78
Figures 6-27: Seasonal average ET vs time, modelled and measured. Richards, ER. Root depth: 0.05 m (left panel), 0.90 m (right panel) .....	79
Figure 7-1: Seasonal and yearly average GT vs depth, modelled and measured. Bucket, ER. Taenikon (left panel), Basel (right panel) .....	85
Figures 7-2: Seasonal and yearly average GT vs depth, modelled and measured. Bucket, ER. Rietholzbach (left panel), Sion (right panel).....	85
Figures 7-3: Payerne. Seasonal average ET vs time, modelled and measured. Infiltration model: Bucket, ER (left panel), Richards, ER (right panel) .....	88
Figures 7-4: Bern. Seasonal average ET vs time, modelled and measured. Infiltration model: Bucket, ER (left panel), Richards, ER (right panel).....	88
Figures 7-5: Rietholzbach. Seasonal average ET vs time, modelled and measured. Infiltration model: Bucket, ER (left panel), Richards, ER (right panel) .....	89
Figures 7-6: Soil moisture vs time, modelled and measured. Nyon Changins, depth: 50 cm (left panel); Basel, depth: 80 cm (right panel) .....	92
Figures 7-7: Soil moisture vs time, modelled and measured. Bern, depth: 50 cm (left panel); Sion, depth: 50 cm (right panel).....	92
Figure 7-8: Map of the Broye catchment, equipped with coordinates and elevation (Michel, 2018) ....	94
Figures 7-9: Alpine3D results: cumulative runoff vs cumulative discharge. Bucket, ER, rg = 1.8 (left panel), Richards, ER, soil type = loam (right panel).....	97
Figures 7-10: SNOWPACK results: cumulative runoff vs cumulative ET, measured and modelled. Extract relative to Alpine3D simulations' time window. Bucket, ER, rg = 1.8 (left panel), Richards, ER, soil type = loam (right panel).....	97
Figures 7-11: SNOWPACK results: cumulative runoff vs cumulative ET, measured and modelled. Full temporal window, as in other SNOWPACK plots. Bucket, ER, rg = 1.8 (left panel), Richards, ER, soil type = loam (right panel).....	98
Figures 7-12: SNOWPACK produced runoff. Bucket, ER, rg = 1.8 (left panel), Richards, ER, soil type = loam (right panel).....	98
Figures 7-13: Alpine3D results: runoff vs discharge. Bucket, ER, rg = 1.8 (left panel), Richards, ER, soil type = loam (right panel).....	99

Figures 0-1: Seasonal and yearly average GT vs depth, modelled and measured. Payerne (left panel), Basel (right panel).....	113
Figures 0-2: Seasonal and yearly average GT vs depth, modelled and measured. Bern (left panel), Nyon Changins (right panel).....	114
Figures 0-3: Seasonal and yearly average GT vs depth, modelled and measured. Reckenholz (left panel), Rietholzbach (right panel).....	114
Figure 0-4: Seasonal and yearly average GT vs depth, modelled and measured. Taenikon.....	114
Figures 0-5: Seasonal and yearly average GT vs depth, modelled and measured. Magadino Cadenazzo (left panel), Wynau (right panel).....	115
Figures 0-6: Seasonal and yearly average GT vs depth, modelled and measured. Plaffeien (left panel), Sion (right panel) .....	115
Figures 0-7: Seasonal and yearly average GT vs depth, modelled and measured. Payerne (left panel), Basel (right panel).....	116
Figures 0-8: Seasonal and yearly average GT vs depth, modelled and measured. Bern (left panel), Nyon Changins (right panel).....	116
Figures 0-9: Seasonal and yearly average GT vs depth, modelled and measured. Reckenholz (left panel), Rietholzbach (right panel).....	117
Figure 0-10: Seasonal and yearly average GT vs depth, modelled and measured. Taenikon.....	117
Figures 0-11: Seasonal and yearly average GT vs depth, modelled and measured. Magadino Cadenazzo (left panel), Wynau (right panel).....	118
Figures 0-12: Seasonal and yearly average GT vs depth, modelled and measured. Plaffeien (left panel), Sion (right panel) .....	118
Figures 0-13: Seasonal and yearly average soil moisture vs depth, modelled and measured. Payerne (left panel), Basel (right panel) .....	119
Figures 0-14: Seasonal and yearly average soil moisture vs depth, modelled and measured. Bern (left panel), Nyon Changins (right panel).....	119
Figures 0-15: Seasonal and yearly average soil moisture vs depth, modelled and measured. Reckenholz (left panel), Rietholzbach (right panel) .....	120
Figure 0-16: Seasonal and yearly average soil moisture vs depth, modelled and measured. Taenikon.....	120
Figures 0-17: Seasonal and yearly average soil moisture vs depth, modelled and measured. Magadino Cadenazzo (left panel), Wynau (right panel) .....	121
Figures 0-18: Seasonal and yearly average soil moisture vs depth, modelled and measured. Plaffeien (left panel), Sion (right panel).....	121

## List of tables

Table 3-1: Values of thermal conductivity of three soil classes in function of humidity and density (Belarbi, 2013) .....	26
Table 3-2: Typical values of albedo for natural surfaces (Nathan Cs, 2010) .....	28
Table 3-3: Typical values of emissivity for natural surfaces (An et Hemmati, 2017) .....	29
Table 4-1: van Genuchten values relative to a loamy soil .....	31
Table 4-2: Terrain classification due to Davenport and quoted by Wieringa (1960) .....	36
Table 5-1: Geographical and physical data of the stations analyzed in chapter 7 .....	43
Table 6-1: The tested soil types, reported with their characteristics and results .....	63
Table 6-2: Final soil parametrization .....	67
Table 6-3: Effect of canopy implementation on GT at 80 cm depth .....	71
Table 6-4: Effect of canopy implementation on average difference in ET .....	71
Table 6-5: Effect of canopy height change (from 0.5 m to 0.9 m) on GT at 80 cm depth .....	73
Table 6-6: Effect of canopy height change (from 0.5 m to 0.9 m) on average difference in ET .....	74
Table 6-7: Partitioning of ET before and after canopy height change (from 0.5 to 0.9 m) .....	75
Table 6-8: Effect of canopy LAI change (from 1 to 4) on GT at 80 cm depth .....	75
Table 6-9: Effect of canopy LAI change (from 1 to 4) on average difference in ET .....	76
Table 6-10: Partitioning of ET before and after canopy LAI change (from 1 to 4) .....	76
Table 6-11: Effect of canopy DT change (from 0.45 to 0.90) on GT at 80 cm depth .....	77
Table 6-12: Effect of canopy DT change (from 0.45 to 0.90) on average difference in ET .....	77
Table 6-13: Partitioning of ET before and after canopy DT change (from 1 to 4) .....	78
Table 6-14: Effect of root depth change (from 0.05 m to 0.90 m) on average difference in ET .....	79
Table 6-15: Partitioning of ET before and after root depth change (from 0.05 m to 0.90 m) .....	80
Table 7-1: RMSE values on ground temperature, at different depths, for the 11 studied sites. The starred values stand for values that are less representative than the others because of bias in the measurement. ....	85
Table 7-2: RMSE values on ground temperature, at different depths, for the 11 studied sites. The starred values stand for values that are less representative than the others because of bias in the measurement. ....	86
Table 7-3: Difference in ET with Bucket, ER and Richards, ER, for the three sites .....	89
Table 7-4: RMSE values on ET, with Richards, ER, for the three sites and for each season .....	89
Table 7-5: RMSE values on soil moisture, at different depths, for the 11 studied sites. The starred values stand for values that are less representative than the others because of bias in the measurement. ....	93
Table 7-6: Soil parametrization used in Alpine3D simulations .....	94
Table 7-7: Description of the six simulations' setup and results .....	95
Table 0-1: Rosetta class average values of hydraulic parameters .....	108
Table 0-2: Duration of the simulations and available information for each site .....	112

## Abbreviations

GT: Ground Temperature

ET: Evapotranspiration

ER: Evaporation Resistance (method)

RH: Relative Humidity (method)

LWC: Liquid Water Content

OSWR: Outgoing Short Wave Radiation

OLWR: Outgoing Long Wave Radiation

PAY: Payerne, BAS: Basel, BER: Bern, CGI: Nyon Changins, MAG: Magadino Cadenazzo, PLA: Plaffeien,

REC: Reckenholz, RHB: Rietholzbach, SIO: Sion, TAE: Taenikon, WYN: Wynau

## 1 INTRODUCTION

Future water cycle and soil moisture are topics that need to be addressed in the context of climate change predictions. This thesis contributes to this large field by validating the well-known surface process model SNOWPACK in a series of soil sites in the Swiss Plateau. This work is in the context of a larger project, which looks at coupled stream temperature and discharge in Switzerland from the Alpine catchments to the Swiss Plateau rivers.

Since the early 2000s, SNOWPACK has been used predominantly in alpine regions, followed by polar ones. Initially developed to simulate the snow cover in alpine areas and to assess avalanche risk (Bartelt et Lehning, 2002), it was then continuously adapted to study all types of snow-related phenomena more comprehensively. A soil module was introduced with the former purpose of creating a physically realistic lower boundary condition for snow. The first studies analyzing or accounting for soil were all primarily focused on permafrost. Luetschg et al. (2003) investigated the influence of the permafrost typical grain size on the thermal behavior and the liquid water content (LWC) of three soil samples, from coarse-grained to rocky types, under low temperatures. They obtained a satisfying representation of ground temperatures (GT) and an underestimation of soil moisture, as well as a strong linear dependency between air temperature and ground surface temperature. Later, a sensitivity study on the relationship between the snowpack and the soil thermal regime was realized by Luetschg et al. (2008). They identified snow depth as the most critical factor in terms of thermal insulation by the snow. Secondly, the variations in mean annual air temperature together with the dates of first winter snow and summer snow disappearance, hence the duration of the snow insulation, were found to be important. This last point governs the slope of the linear dependence between mean air temperature and mean ground surface temperature.

Passing to water dynamics schemes, Wever et al. (2014) were the first to introduce a Richards equation (Richards, 1931) solver in SNOWPACK, which is the same used in this work. In two mountain sites, precisely Col de Porte (1325 m a.s.l.) and Weissfluhjoch (2540 m a.s.l.), snow-only produced runoff with the classic Bucket and the new Richards model was verified against measurements from a snow lysimeter. Richards was found to predict slightly better cumulative values and a lot better values at sub-daily time scales. Once more, SNOWPACK was run in Weissfluhjoch, where the reproduction of GT in the gravel soil characterizing the place was evaluated, using the same Bucket and Richards models

(Wever et al., 2015). The target, consisting in providing a correct boundary for the snowpack, was achieved and Richards was confirmed to be a more accurate tool for both GT and water dynamics modelling, even though a significant bias remained between the observed and the modelled data. Wever et al. (2017) took the analysis one step forward, assessing soil moisture in two Swiss mountain sites (Uf den Chaiseren and SLF2) and runoff in the whole Dischma catchment using Alpine3D. Interesting findings were reported, such as SNOWPACK tendency to overestimate soil freezing, causing an underestimation of soil moisture in winter. Further issues were identified in the impossibility to reproduce a high groundwater table in the melting season and in the modelling of nonexistent soil moisture fluctuations at the sub-daily scale. LWC was overall well captured, even though significant bias remained between modelled and observed data as well as within different field datasets.

Both with Bucket and Richards model, an incorrect prediction of soil water budget components often occurs. Regarding Bucket models, Romano et al. (2011) suggest determining the field capacity through field drainage experiments instead of simply relating it to a specific suction head value of the water retention curve. As for Richards equation, Wever et al. (2017) propose to calibrate the water retention curves to actual soil moisture measurements to achieve a better agreement.

Many other soil hydrological models exist, that can simulate in detail soil physics, soil thermal regime and soil water dynamics. Among these, the CoupModel and HYDRUS-1D are worth mentioning, because of their historic importance and robustness. The former represents a platform of multiple modules which have seen a development since 1979 (Jansson et Halldin, 1979), whereas the latter traces its roots in the late 1980s, based on the works by van Genuchten (1978), van Genuchten (1987), Vogel (1987), and Kool et van Genuchten (1989). Both models combine Richards equation for water flow and Fourier equation for heat flow in a 1D domain. In its early years, the CoupModel was mainly used in Boreal forest ecosystems (Jansson et al., 1999), being then extended to all types of systems, from semiarid regions (Rockström et al., 1998) to permafrost soils (Holleisen et al., 2011). Chemical processes such as the nitrogen and carbon cycles were implemented in the model, followed by the inclusion of plants development. HYDRUS-1D, the 1D version of the HYDRUS software (which also includes HYDRUS 2D/3D), is the reference soil hydrological model and is able, among other things, to well simulate solutes transport of various chemical substances such as carbon dioxide.

These two models were not developed for crop-related use. However, there is a variety of models specialized in specific crop evolution which can mimic soil water dynamics and GT. A good example is

offered by DDSAT, the Decision Support System for Agrotechnology Transfer (DSSAT), a package that incorporates 16 different crops (Jones et al., 2003). The Cropping System Model (CSM) within DSSAT, featuring a modular structure (soil, crop, weather modules), is equipped with a tipping bucket model. Sándor et Fodor (2012) decided to test the response of the coupled model DSSAT-HYDRUS-1D in terms of both soil water dynamics and crop growth and yield. The results were positive: in fact, LWC, evapotranspiration (ET) and crop-related parameters were reproduced better than with the simple DSSAT CSM model. In another study by Shelia et al. (2018), HYDRUS-1D was compared to CERES, a DSSAT model developed for cereals, focusing on GT simulations. Both highlighted a reduction in overall GT and in diurnal GT amplitude due to vegetation. Some critical points were found, such as the underestimation of GT, the overestimation of GT oscillations in winter and the impossibility to account for the snow cover insulation effect. HYDRUS-1D performed better than the simpler CERES model, even though the former requires many input parameters which, if estimated, can lead to a decrease in accuracy.

In the field of stream temperature prediction, an increasing number of studies has been presented over the past few years. In some cases, hydrological models which reproduced stream discharge were modified to consider water temperature too. The understanding of soil thermal behavior is crucial in this context because it directly affects the interflow routed to the stream. Studies such as the one by St-Hilaire et al. (2000) reported that stream temperature prediction is enhanced with the incorporation of soil temperature as a parameter influencing interflow temperature. Gallice et al. (2016) produced a list of semi-distributed models which simulate both stream discharge and temperature; in their work, they improved StreamFlow 1.0, an external extension to the physically-based snow model Alpine3D, and applied it in the Dischma catchment. Stream temperature was found to be highly sensitive to the approach used to model the subsurface flow temperature. Wever et al. (2017) found that “relating the water flux at 30 cm depth in the soil to streamflow in the Dischma catchment using a travel time distribution approach provided a higher agreement with observed streamflow than directly using the water flux at the top of the soil or at 60 cm depth”.

The present master thesis has been developed within the CRYOS research group, part of the School of Architecture, Civil and Environmental Engineering (ENAC) at EPFL.

The snow and land-surface model SNOWPACK has been widely used in high-altitude alpine areas, with the focus being a thorough description of the snowpack characteristics and evolution with respect to the atmosphere. Its application to soil is more recent and has so far regarded coarse-grained soils in the alpine sector near Davos (Switzerland). The aim of this work is validating the model SNOWPACK in the low-altitude region of the Swiss Plateau, where snow cover is only present for a restricted time of the year. To do so, a sensitivity analysis is first performed in the site of Payerne, where the best parametrization is sought for both a Bucket scheme and the Richards equation model.

Consequently, the hydro-meteorological and soil-related configuration obtained in Payerne is extended to ten sites bearing very similar soil characteristics. The analysis focuses on the seasonal average of four main quantities, i.e. GT, LWC, ET, and runoff. The first three can be evaluated via a comparison to field measurements data lasting several years. As for runoff, this can be roughly validated in the hydrographic catchment where Payerne is encountered. Here, the runoff produced by the spatial, three-dimensional snow cover and earth surface model Alpine3D in a 14-month period is compared to the cumulative river discharge over the same time window.

The thesis is organized as follows: second chapter describing the used models; third theoretical chapter explaining soil water dynamics and thermal transfer in soil; a fourth chapter treating all relevant SNOWPACK's characteristics and phenomena implementation; a fifth chapter gathering data and a summary of the MATLAB script; a sixth chapter covering the sensitivity analysis realized in Payerne; a seventh chapter intended for validation, made up of four sections, each one assessing a different quantity; a final chapter presenting the conclusions.

## 2 MODELS USED

This thesis will make use of the models MeteolO, SNOWPACK and Alpine3D. All of them were developed at the Swiss Institute for Snow and Avalanche Research (SLF) in Davos and at the CRYOS laboratory at EPFL. They are all available for free on <https://models.slf.ch/> under LGPL version 3 license. They are all coded in C++.

### 2.1 MeteolO

MeteolO is a library developed to handle the input and output of numerical models that make use of meteorological data. A complete description is found in Bavay et Egger (2014). The library is able to retrieve, filter and resample the data. An API is provided, which is used in the models to mask the complexity of the data processing steps. By applying different algorithms, MeteolO achieves the spatial and temporal extrapolation of the data. These come in most cases from the MeteoSwiss automatic monitoring network and from the IMIS stations. The latter are operated by SLF and are separated into two types, wind and snow stations, both well spread over the Alps. In the case of spatial extrapolation, the elevation is included thanks to a Digital Elevation Model (DEM). The DEM is also responsible for the topographic shading for short wave radiation. Many generators are present in the library for missing data and different filters can be applied, allowing to skip the editing of the input data. MeteolO is arranged through a text configuration file.

### 2.2 SNOWPACK

SNOWPACK is a one dimensional, physically based, numerical model initially developed for avalanche warning (Bartelt et Lehning, 2002; Lehning et al., 2002a; Lehning et al., 2002b). It provides information about the state of the snowpack, such as snow depth, snow temperature and density. Snow is reproduced as a tri-phase porous medium (ice, water, air) where each phase is characterized by its volumetric content. At a microscopical level, four independent structural parameters exist: sphericity, dendricity, grain size, bond size.

Over the last 15 years, SNOWPACK has seen constant improvements: a better description of weak layers characterization, the implementation of a soil module (Luetschg et al., 2003), the addition of a more

physical water transport scheme in soil and snow from Richards Equation (Wever et al., 2014) and the inclusion of a two-layer canopy module (Gouttevin et al., 2015). Mass, energy transport and phase change processes are modelled the same way in soil and snow (Lehning et al., 2002b). The model solves the partial differential equations governing the mass, energy and momentum conservation within the snowpack and soil layers using a Lagrangian finite element method (Bartelt et Lehning, 2002).

Soil is described as a four elements material: water, air, ice and soil minerals. Different soil types can be distinguished from one another by parameters such as density, grain size and thermal properties of the dry material. These are related to each other and are used to determine other characteristics: for instance, the water retention depends on the grain size, while the thermal conductivity is computed based on the water and ice contents (Luetschg M. , 2005).

The model has been validated in multiple locations and conditions, and it has fulfilled diverse goals, including studies on climate change scenarios and permafrost evolution.

### 2.3 Alpine3D

Alpine3D is a spatial, three-dimensional snow cover and earth surface model developed by the SLF. It is a distributed version of SNOWPACK (Lehning et al., 2006) and it simulates the key physical processes (mass and energy exchange) that occur between the atmosphere, snow and soil on mountain topography. The simulation of the snowpack remains one-dimensional, but a 3D radiation module, together with 3D atmospheric and topographic features, is implemented. One of the main reasons for the development of Alpine3D was building a physical model for catchment scale hydrology to be used predominantly in alpine environments. The model has been proved valid for this purpose by several authors (Comola et al., 2015a; Gallice et al., 2016; Brauchli et al., 2017; Wever et al., 2017). The model resolution is determined from the DEM one and its relative land cover grids. A sensitivity study has shown that resolution can have a relevant impact on the SWE (Snow Water Equivalent) for the Dischma catchment (Schlogl et al., 2016), situated in the eastern Swiss Alps. However, running Alpine3D with the highest possible resolution leads to high computational time, which is the reason why it can be run in parallel.

In this work, Alpine3D will be primarily used to estimate the runoff at a catchment scale. This quantity will be compared with the river discharge at a gauging station to assess the correctness of the simulated

runoff. In addition, soil temperature, which is an important factor for river temperature because it conditions the temperature of the infiltrating water, can directly be computed in Alpine3D. The soil module provides a physical residence time for the water in the top part of the soil.

## 3 THEORETICAL NOTIONS

### 3.1 Water flow in porous media

#### 3.1.1 Saturated conditions: Darcy's Law

The total hydraulic head  $h$  (m) of a fluid, also known as the piezometric head, is the sum of two components: *pressure head*  $\psi$  (m) and *elevation head*  $z$  (m). The head equation, coming from the Stevino law valid for static fluids (for which  $h = \text{const}$ ), reads as:

$$h = \psi + z \quad (1)$$

The pressure head can be expressed as:

$$\psi = \frac{P}{\gamma} = \frac{P}{\rho g} \quad (2)$$

where  $P$  is the gauge pressure (Pa),  $\gamma$  is the unit weight of the liquid ( $\text{N}/\text{m}^3$ ),  $\rho$  is the density of the liquid ( $\text{kg}/\text{m}^3$ ),  $g$  is the gravitational acceleration ( $\text{m}/\text{s}^2$ ).  $P$  is a positive term in case of saturated flow, while it is negative in non-saturated flow. In the latter case, the pressure head takes the name of *suction* and  $P$  is found to be:

$$P = -2\gamma \frac{\cos \theta_w}{r} \quad (3)$$

where  $\theta_w = \frac{V_w}{V_{tot}}$  is the volumetric water content (-) and  $r$  (m) is the bond radius of the soil particles. The elevation head  $z$  relates to a reference elevation.

The equation describing a fluid motion in a saturated porous media was empirically obtained by Henry Darcy (1856). By realizing multiple experiments with different materials and pipe lengths, he found a direct proportionality relation between the flow rate  $Q$  ( $\text{m}^3/\text{s}$ ) passing through a pipe connecting two tanks having different piezometric heads  $h_1 > h_2$  and all the following: the section area of the pipe  $A$ , the head difference  $\Delta h = h_1 - h_2$  and a coefficient  $K$ . An inverse proportionality relation held between  $Q$  and the pipe length  $L$ . He expressed these links in the famous Darcy's Law:

$$Q = \frac{KA\Delta h}{L} \quad (4)$$

Let the ratio  $\frac{Q}{A}$  be defined as *specific flow rate*  $q$  or *apparent velocity*  $V$  (m/s) and see in the ratio  $\frac{\Delta h}{L}$  the piezometric head gradient  $i = -\frac{\partial h}{\partial s}$  (-). Therefore, the law can be reformulated as:

$$\mathbf{q} = -K \frac{\partial h}{\partial s} \quad (5)$$

$K$  (m/s), denominated *hydraulic conductivity*, is defined as the ease with which a certain fluid can move through pore spaces or fractures of a solid matrix. Its range of values goes from  $10^{-12}$  to  $10^{-1}$  m/s (Freeze et Cherry, 1979). Figure 3-1 displays the possible  $K$  values associated with a variety of different soil types.

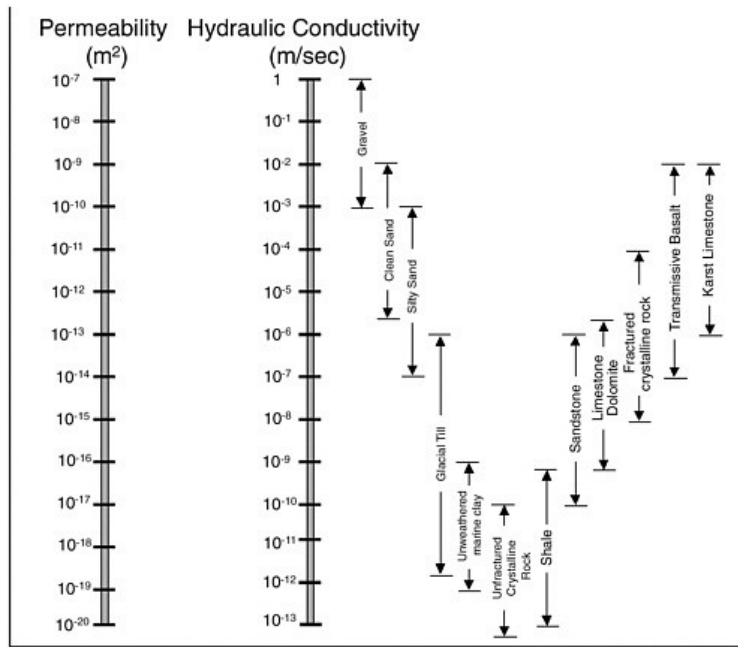


Figure 3-1: Typical values for hydraulic conductivity (adapted from Freeze and Cherry, 1979)

Expanding the analysis to three dimensions, Darcy's law in the three main directions becomes:

$$\mathbf{q}_x = -K \frac{\partial h}{\partial x} \quad \mathbf{q}_y = -K \frac{\partial h}{\partial y} \quad \mathbf{q}_z = -K \frac{\partial h}{\partial z} \quad (6)$$

Which can be summarized in the form:

$$\mathbf{q} = -K \mathbf{grad}(h) \quad (7)$$

The hypothesis admitted so far in Darcy's formulation is a condition of isotropy, with the value of  $K$  independent of the direction. However, a marked anisotropy exists for properties such as the

permeability  $k$  ( $m^2$ ). This behavior is marked for example in the case of sandy to clay sedimentary and alluvial deposits, for which  $k_x, k_y \gg k_z$  (De Marsily, 1986).

Following, the continuity equation is presented, from which the formulation of the Richards equation derives. The form displayed here below is valid in conditions of isotropy and uniformity:

$$\frac{D\rho}{Dt} + \rho \cdot \text{div}(\mathbf{q}) = 0 \quad (8)$$

Hypothesizing  $\rho$  as constant in space and time ( $\frac{D\rho}{Dt} = 0$ ),

$$\text{div}(\mathbf{q}) = 0 \quad (9)$$

is obtained.

### 3.1.2 Non-saturated conditions: Richards equation

In a porous medium, the infinitesimally small control volume for which the continuity equation (8) is derived, is composed of both solid matter and voids. The amount of fluid mass per unit volume of bulk porous material is thus given by  $\rho_w \cdot \theta_w$ , where  $\rho_w$  is the density of water ( $kg/m^3$ ). Likewise, the mass flux per unit area is defined as  $\rho_w \cdot \mathbf{q}$  (or  $q_i$ ). Therefore, the continuity equation (8) for a fluid with constant density but variable saturation, takes the form:

$$\text{div}(\mathbf{q}) = -\frac{\partial \theta_w}{\partial t} \quad (10)$$

If Darcy's law is substituted in the last equation, Richards Equation (Richards, 1931) is obtained:

$$\text{div}(K \mathbf{grad}(h)) = \frac{\partial \theta_w}{\partial t} \quad (11)$$

or written out in full,

$$\frac{\partial}{\partial x} \left( K \frac{\partial h}{\partial x} \right) + \frac{\partial}{\partial y} \left( K \frac{\partial h}{\partial y} \right) + \frac{\partial}{\partial z} \left( K \frac{\partial h}{\partial z} \right) = \frac{\partial \theta_w}{\partial t} \quad (12)$$

Under conditions of steady flow or fully saturated flow, the right-hand side of equation (11) becomes zero, leading to the Laplace equation for a uniform material. Let  $C(h)$  be defined as a function describing the rate of change of saturation with respect to the hydraulic head:

$$C(h) = \frac{\partial \theta_w}{\partial h} \quad (13)$$

then the right-hand term of equation (11) can be rewritten like this:

$$C(h) \frac{\partial h}{\partial t}$$

and Richards Equation in the head-based form looks like:

$$\text{div}(K \mathbf{grad}(h)) = C(h) \frac{\partial h}{\partial t} \quad (14)$$

For a 1-dimensional column, Richards Equation can be expressed in a mixed-form, which can be discretized in a finite difference approximation that ensures perfect mass balance (Celia et al., 1990).

$$\frac{\partial h}{\partial t} - \frac{\partial}{\partial z} \left( K(\theta) \left( \frac{\partial h}{\partial z} + \cos \gamma \right) \right) + s = 0 \quad (15)$$

where  $\gamma$  is the slope angle and  $s$  a source/sink term ( $\text{m}^3/\text{m}^2 \cdot \text{s}$ ), i.e. an external addition or removal of mass. For the application of equation (15), a *water retention curve* must be adopted, which relates  $\theta$  to  $h$ . The relationship between the water content  $\theta_w$  and the pressure head  $\psi$  (defined as matric potential when it assumes negative values) is known as water retention curve. It can be found under different names, including ‘soil-water characteristic curve’, ‘pressure head–water-content relationship’, ‘water content–matric potential curve’ and ‘capillary pressure–saturation curve’. The curve is unique for different types of soil and its knowledge is key in soil hydrology: in fact, it allows to predict the soil water storage and the available water supply for plants, quantity described by the so-called *field capacity*. Various models exist, which can describe the water retention curve with analytical formulations: some of these are mentioned in section 4.2.

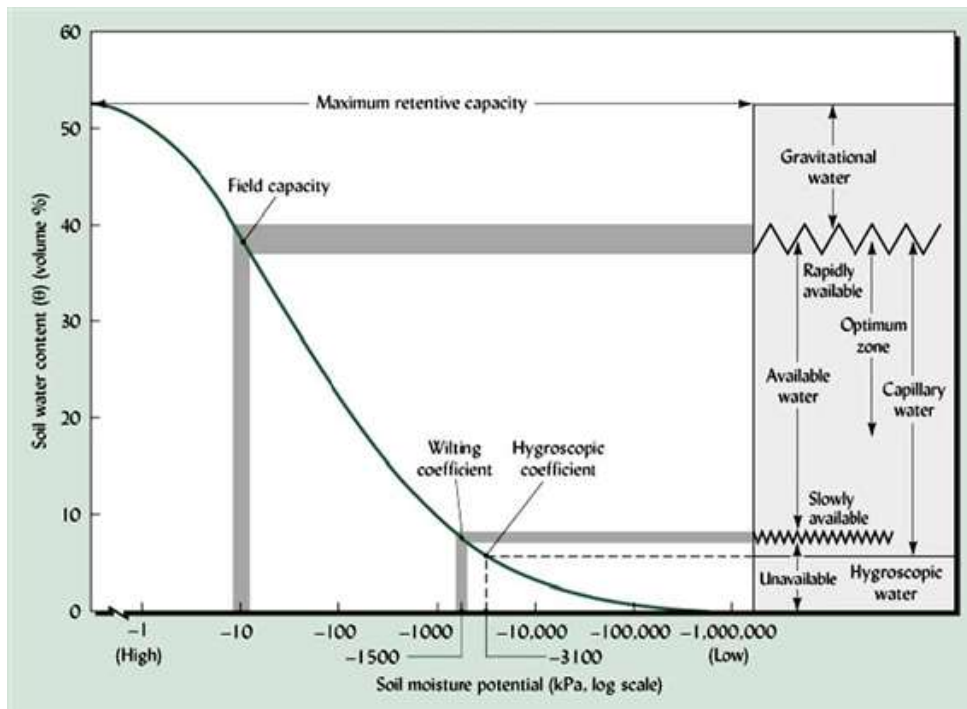


Figure 3-2: Characteristic curve relating moisture content to pressure head (Blaskó Lajos, 2008)

To produce the curve, the volumetric water content is plotted against the matric potential. When the potential is equal to zero, saturation conditions hold. For slightly lower values, capillary forces are the primary ones. A further decrease of  $\theta_w$  is accompanied by stronger bonds in the pellicular water, remaining in the smallest pores and around the soil grains at a radius smaller than  $1 \mu\text{m}$ .

The field capacity ( $\theta_{fc}$ ) can be described as the amount of soil moisture present in the soil after drainage of gravitational water, which typically occurs 2-3 days after the last rainfall or irrigation.  $\theta_{fc}$  is physically defined as the water content retained in the soil at -33 kPa/kg (or -0.33 bar) of hydraulic head. This definition is flexible, and the hydraulic head threshold can reach values like -10 kPa/kg, as indicated in Figure 3-2.

The *permanent wilting point* ( $\theta_{wp}$ ) coincides with the hydraulic head of -1500 kPa/kg (or -15 bar) and represents the water content at which “the plants growing in that soil are first reduced to a wilted condition from which they cannot recover in approximately saturated atmosphere without the addition of water to the soil” (Briggs et Shantz, 1912).

Figure 3-3 shows the phenomenon known as *hysteresis*, consisting in different wetting and drying curves. The *initial drainage curve* (IDC) results from the stepwise reduction of the matric potential from an initially saturated soil ( $\theta_s$ ). The *residual water content*  $\theta_r$  is reached when no more water can be drained. If a water input is provided at this point, with a stepwise matric potential increase up to 0, the curve follows the *main wetting curve* (MWC) and reaches the *satiated water content*  $\theta_o$ . A further reversal leads to the *main drainage curve* (MDC). Reversing the process in the wetting or drainage phase will always produce *scanning curves* between the MWC and the MDC.

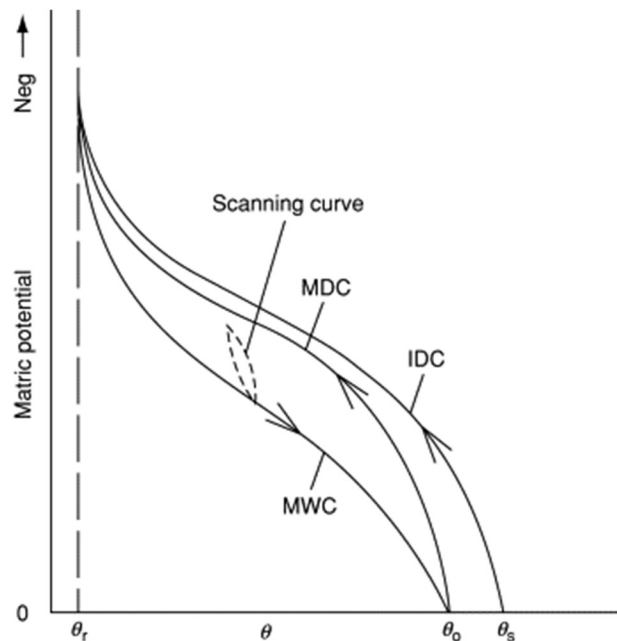


Figure 3-3: The initial drainage curve (IDC), the main wetting curve (MWC), the main drainage curve (MDC), and a scanning curve.  $\theta$  refers to the volumetric water content and the subscripts *r*, *o*, and *s*, to residual, satiated, and saturated (Dane, Lenhard, 2005)

As mentioned earlier, the soil-water characteristic curve depends greatly on the soil treated. In particular, it depends on two factors, which are the nature of the bonding and the porosity. In sand-like soils, the capillary forces govern the unsaturated zone, causing a fast release of most of the water at low absolute values of matric potential. Moving to clay-like soils, the adhesive and osmotic forces enhance a higher resistance to drainage. Finally, peaty soils usually display even more negative matric potential values for the same water content. An example of soil water characteristic curves is reported

in Figure 3-4: a big difference can be spotted between the behavior of a coarse-grained soil and a fine-grained one.

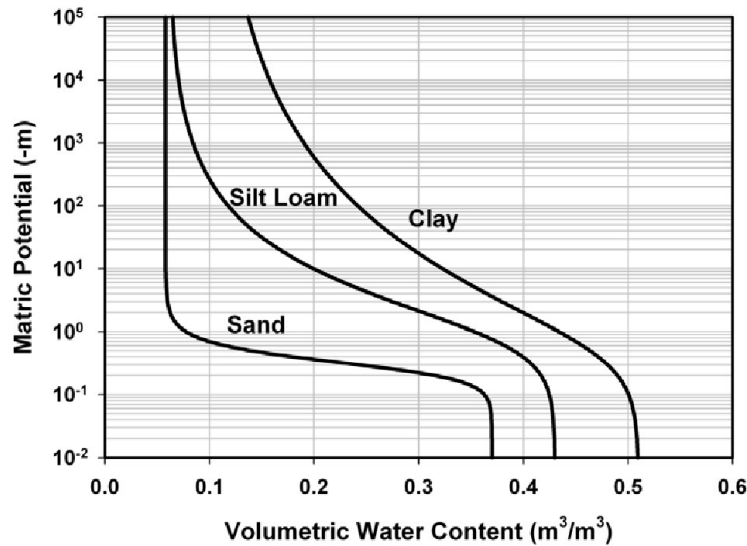


Figure 3-4: Typical soil water characteristic curves for soils of different texture (Tuller, Or, 2003)

### 3.2 Theory on thermal transfer in soil

Within the soil, heat mainly propagates in two ways: conduction and convection. Conduction is the phenomenon through which heat transfers in a continuous medium (solid or liquid) by internal molecular motion without any macroscopic movement. It is caused by the transfer of kinetic energy through numerous intermolecular collisions. In soil, it takes place between minerals, organic matter and water. Conduction is by far the predominant mechanism of heat transfer in soil (Koorevaar et al., 1983).

The second way of heat propagation is convection, the displacement of volumes of a medium in a liquid or gaseous phase moved by temperature gradients. In soil, the media through which convection occurs are the water and the air occupying the soil pores. In soils, free convection through water or air is usually negligible, except for scenarios with soil pores diameter larger than a few millimeters, enough to allow water and air fluxes to affect deeper layers' temperature (Martynov, 1959). Forced convection is the phenomenon through which air or water currents are forced to move by pressure gradients. It can be non-neglectable in the case of groundwater flow in very coarse sands, where it can increase the thermal conductivity by as much as 20% (Johansen, 1975).

Furthermore, water phase changes and the energy involved in such processes have a considerable influence on the ground temperature variations and on the heat transfer. This is due to the high value of the latent heat of vaporization for water (2264.705 kJ/kg). Whenever energy is supplied to the soil, liquid water reacts absorbing this energy and undergoing evaporation. When, instead, energy is being lost by the soil, vapor condensates, thus avoiding an immediate cooling of the ground. In both scenarios, soil moisture acts as a ground temperature (GT) stabilizer. As for heat transfer, the following can happen: in unsaturated strata, water moisture evaporation can lead to vapor diffusion and consequently to a possible condensation in different points. Water fusion and solidification are also responsible for latent heat fluxes in cold regions, even though they are less influential because of the latent heat of fusion for water equal to 333.55 kJ/kg.

Soil is characterized by two fundamental thermal properties. The first one is the volumetric heat capacity  $C$  ( $J/m^3 \cdot K$ ), related to the capability of a material to store heat. It is defined as the amount of heat absorbed by the material to raise the temperature of a unit volume of that material by  $1^\circ C$ . Heat capacity  $C$  is a linear function of the volumetric content  $\theta$  of the soil components, as can be read in the following:

$$C = \sum_i C_i \theta_i = \sum_i \rho_i c_i \theta_i \quad (16)$$

Some of the factors increasing  $C$  are the soil particles' density, soil compaction and moisture content. Andujar Marquez et al. (2016) propose typical values of  $C$  for common rocks and soils. Amongst these, they assign the values  $1.6 \text{ MJ/m}^3 \cdot K$  to dry clay/silt and  $3.4 \text{ MJ/m}^3 \cdot K$  to water-saturated clay/silt.

The second thermal property is the thermal conductivity  $\lambda$  ( $W/m \cdot K$ ), the ability of the medium to conduct heat. Fourier (1822) postulated that the total quantity of heat transfer  $\Phi$  ( $W$ ) flowing through a soil column from one point to another is directly proportional to the cross-section area  $A$  of soil and to the difference in temperature between the two points. On the other hand, it is inversely proportional to the distance between the points (along the direction  $s$ ). The direct proportionality factor is, indeed,  $\lambda$ . Such relations can be expressed in the formula:

$$\varphi = \frac{\Phi}{A} = \lambda \cdot \frac{\partial T}{\partial s} \quad (17)$$

where  $\varphi$  ( $W/m^2$ ) is the flux per unit area.

The thermal conductivity is not related in a linear way to the single heat conductivities of the soil components, even though this is the way it is currently computed in SNOWPACK, as explained in section 4.5.4.1. In reality, heat conduction takes place in an irregular way among the different media. The value of  $\lambda$  depends greatly on the relative position and distribution of the soil particles. These can be in contact with each other, well interconnected by the less conducting water or separated by the poorly conducting air.

Thermal properties can be determined indirectly by measuring the response of temperature to a heat input to a line source at a certain point (Taylor et Jackson, 1965). Some models have been developed to estimate  $\lambda$  and  $C$  of a soil based on the volume fractions of its constituents and the shape of its grains.

The thermal conductivity of soil depends on several factors: these are the texture and mineralogical composition, the porosity, the water content and the soil management (Yadav et Saxena, 1973). Any practice or process whose result is the compaction of the soil and a reduction of its porosity will have a significant impact on its thermal conductivity. The effect of water content on  $\lambda$  has received more attention than other factors (Riha et al., 1980).

Koorevaar et al. (1983) describe the evolution of  $\lambda$  with respect to the liquid water content (LWC) for a compacted sandy soil. In dry conditions, the  $\lambda$  is typically below 0.2 - 0.3 W/m·K, as conduction occurs only at the contact points between soil particles. During a moisture increase up to around 0.05, water forms films surrounding the soil particles, hence a slow growth of  $\lambda$ . Following, the additional water creates water bridges, very efficient in connecting separated soil particles, and  $\lambda$  starts to rise with a steeper slope. As the water content grows, the water bridges' cross-sectional area increases more slowly; consequently, also the  $\lambda$  slope continuously declines within the whole range 0.1 - 1 of soil moisture. A proof of the  $\lambda$  slope change is offered by the pairs of soil moisture -  $\lambda$  values found by Koorevaar et al. (1983): for LWC = 0.1,  $\lambda$  = 1.5 W/m·K; for LWC = 0.2,  $\lambda$  = 2.3 W/m·K; for LWC = 0.4,  $\lambda$  = 3.0 W/m·K. Clearly, the maximum  $\lambda$  is achieved at saturated conditions.

A study by Abu-Hamdeh et Reeder (2000) analyzed the thermal conductivity variations of four sieved and repacked soils: sand, sandy loam, loam and clay loam. The factors studied were bulk density, water content, salt concentration in solution and organic matter. In average, a 15% increase in bulk density made  $\lambda$  50% higher for all soils, thanks to the particle-contact enhancement. Moreover, it was observed that beyond a certain bulk density, higher values of moisture content increased  $\lambda$  less rapidly in the case

of clay loam and loam soils, and more rapidly in the case of sandy and sandy loam soils. The maximum  $\lambda$  was observed for sandy soil, with a value in accordance with literature values by Van Wijk (1963): 0.3 - 2.25 W/m·K. For the loamy soil too, the values found were in agreement with those reported by Ghauman et Lal (1985), relative to a maximum moisture of 0.20: 0.15 – 0.79 W/m·K. Tavman (1996) suggests that soils with smaller grain size, under the same overall porosity, require the presence of many more particles, which in turn cause more thermal resistance. Hence, a smaller thermal conductivity.

Regarding the two factors that were not assessed in this work (salt concentration in solution and organic matter), both provoked a net decrease of  $\lambda$ , as can be seen in detail in the cited study.

Table 3-1 proposed below shows some recurring values for thermal conductivity in various soils.

*Table 3-1: Values of thermal conductivity of three soil classes in function of humidity and density (Belarbi, 2013)*

Name of breed	Humidity, %	Density, kg/m <sup>3</sup>	Coefficient of heat conductivity, W/(m·°K)	
			at a positive temperature	in the frozen state
Sand	5	1200	0,47	0,6
	10	1200	0,72	0,92
	5	1400	0,66	0,8
	10	1400	1,0	1,95
	15	1400	1,16	1,57
	15	1600	1,45	1,86
	15	1800	1,8	2,2
	15	2000	2,2	2,56
Loamy sand	10	1200	0,44	0,52
	10	1400	0,84	0,8
	15	1600	1,1	1,28
	15	1800	1,38	1,52
	15	2000	1,63	1,74
Loams and clays	10	1400	0,51	0,79
	15	1400	0,65	0,98
	20	1400	0,76	1,09
	20	1600	1,02	1,3
	20	1800	1,1	1,4
	20	2000	1,44	1,7

The conduction of heat in dry soil is described by the diffusion equation:

$$\frac{\partial T}{\partial t} = \frac{\lambda}{C} \frac{\partial^2 T}{\partial s^2} \quad (18)$$

which is valid in conditions of uniform  $\lambda$  over space.

The term  $\lambda/C$  is related to the thermal diffusivity  $\alpha$  (m<sup>2</sup>/s), defined as  $\lambda/c$ , describing the speed at which temperature waves move through the soil or, in other words, the rate at which the soil warms up under

a given temperature gradient. The implementation of the diffusion equation (18) is described by Lehning et Bartelt (2002).

A word must be spent as well on ground temperature temporal fluctuations. GT is closely dependent on the air temperature: this implies the presence of GT fluctuations at a diurnal and at an annual scale. In both cases, the amplitude of the GT variation decreases exponentially with depth. Besides, a temporal shift in the curves is always found, affecting deeper layers with a certain delay. Plotting daily or weekly averaged temperatures shows a nearly sinusoidal annual wave. The magnitude of the temperature variation from maxima to minima greatly depends on the soil type: coarse soils will exhibit bigger oscillations. Some of the described characteristics are visible in Figure 3-5, relative to the soil thermal regime at an annual time scale.

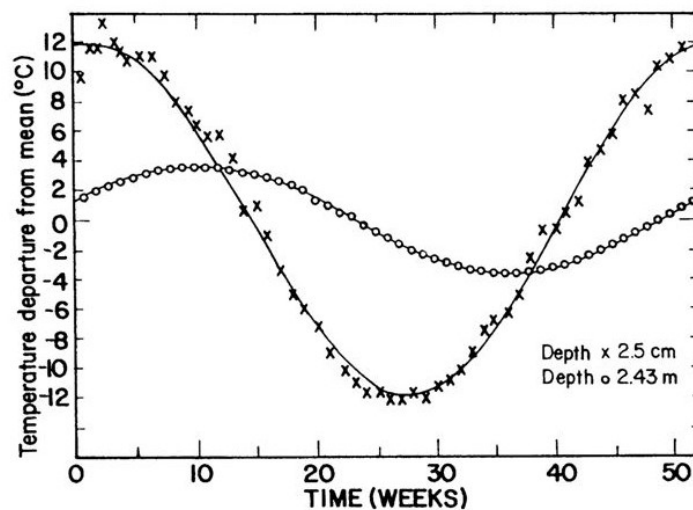


Figure 3-5: Annual temperature waves in the weekly averaged subsurface soil temperatures at two depths in a sandy loam soil (West, 1952)

### 3.3 Thermal boundary conditions and phase changes

An upper and a lower boundary condition are needed to solve the heat equation in the SNOWPACK model. The energy balance at the ground or snow surface is a complex process, indeed many factors play a role in it. Figure 3-6 illustrates the main components and mechanisms acting in modifying the snow or soil surface temperature in the SNOWPACK model. Radiation is the process by which energy emitted from a surface, propagates through electromagnetic waves and is absorbed by a receiving surface. It is normally divided in short wave (300 – 4000  $\mu\text{m}$ ) and long wave (4000 – 10000  $\mu\text{m}$ ) radiation.

99% of solar radiation reaches Earth as short wave and soil re-radiates it as long wave radiation. Radiation can be direct or scattered by the clouds, and once it reaches the surface it can be absorbed or reflected. The exchange of latent heat (amount of energy lost or gained during water phase changes) and sensible heat (energy required or released to vary the temperature of a substance with no phase change) is fundamental in controlling the surface temperature. Another key factor is the *geothermal heat flux*, used as a lower boundary condition: it is constant in time at a short time scale and always directed upwards, thanks to the Earth internal heat production.

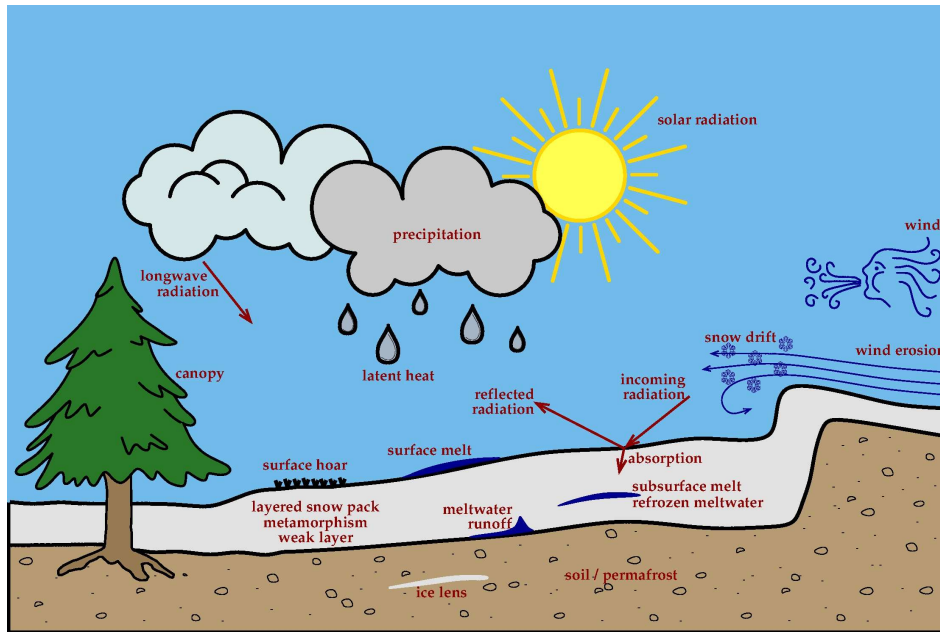


Figure 3-6: Relevant processes in the snow cover model SNOWPACK (SLF)

As mentioned before, radiation can be absorbed or reflected by the Earth surface. The fraction of the incident short wave radiation that is reflected is known as albedo. It can vary greatly depending on the material and its color. Literature reports a list of typical albedo values that have been proved valid.

Table 3-2: Typical values of albedo for natural surfaces (Nathan Cs, 2010)

Natural surface	Albedo	Natural surface	Albedo
Fresh snow	0.75 – 0.95	Dry silt loam soil (before cultivation)	0.23 – 0.28
Water	0.03 – 0.01	Dry silt loam soil (after cultivation)	0.15 – 0.18

Bare fields	0.12 – 0.25	Dry clay loam soil	0.18 – 0.22
Dark colored and rough soil surfaces	0.10 – 0.20	Sand (wet)	0.09 – 0.11
Light colored soil surfaces	0.40 – 0.50	Wet clay loam soil	0.11 – 0.13
Stubble fields	0.15 – 0.17	Wet ploughed fields	0.05 – 0.14
Sand (dry)	0.18 – 0.21	Forests	0.05 – 0.20
Dry sandy soil	0.25 – 0.45	Green grass	0.16 – 0.27
Dry clay soil	0.15 – 0.35	Dry grass	0.16 – 0.19

As illustrated, the values are not completely unambiguous, which is one of the reasons why soil albedo will be analyzed, among other parameters, in chapter 6. The lower the albedo is, the easier it will be for the body to gain heat. There are a series of factors affecting the albedo, among which seasonal and diurnal radiation changes, soil moisture (high moisture content, low albedo), color (more organic matter, lower albedo), surface roughness (fine-textured dry soils, high albedo).

According to Kirchhoff's law of thermal radiation (Kirchhoff, 1860), for an arbitrary body absorbing and emitting thermal radiation in thermodynamic equilibrium, the emissivity is equal to the absorptivity. A body's emissivity (usually indicated with  $\epsilon$ ) is the fraction of radiated energy from that body with respect to the radiated energy from a black body at the same temperature. It is function of the surface condition, temperature and radiation wavelength. To remedy the dependence on wavelength, total emissivity is defined as the resultant value of averaging the individual emissivity factors over the entire utilized radiation spectrum.

*Table 3-3: Typical values of emissivity for natural surfaces (An et Hemmati, 2017)*

Soil surface	Emissivity	Source
Soils, dark, wet to light, dry	0.9–0.98	Oke (1987)
Sand, wet	0.98	Van Wijk and Scholte Ubing (1963)
Sand, dry	0.95	Van Wijk and Scholte Ubing (1963)
Dark clay, wet	0.97	Van Wijk and Scholte Ubing (1963)
Dark clay, dry	0.95	Van Wijk and Scholte Ubing (1963)
Grass, green	0.96–0.98	Van Wijk and Scholte Ubing (1963)

## 4 SNOWPACK

### 4.1 Type of files and variables

SNOWPACK performs physical modeling of the various processes taking place in and between the soil, snow cover and atmosphere in order to simulate the evolution of the soil and the snow based on meteorological input data. SNOWPACK requires several kinds of information. First, the description of the place where the soil and snow column have to be simulated: name, latitude, longitude, elevation, slope; secondly, the time series of the various meteorological parameters (here referred to as *meteo* file); thirdly, the initial state of the various soil and snow layers (here referred to as *sno* file); lastly, the settings of the simulation keys (here referred to as *ini* file).

In the setup used, the *meteo* file must report a series of meteorological parameters, such as the air temperature, the relative humidity, the wind speed, the incoming or reflected short-wave radiation, the incoming long-wave radiation, the precipitation, the geothermal heat flux.

The *sno* file consists of a header and a block of lines describing the soil or snow layers' initial state and characteristics. The header contains multiple parameters which can be arbitrarily chosen; the most important ones are the number of soil and snow layers, the soil emissivity  $\epsilon$ , albedo  $\alpha$  and roughness length  $z_0$  (m), besides various canopy variables. The soil and snow layers are described by the following terms: thickness, initial temperature, initial volumetric fraction of ice, water, dry voids and solid part (respectively  $\theta_{ice}$ ,  $\theta_w$ ,  $\theta_v$ ,  $\theta_m$ ), density of dry compacted soil component  $\rho_m$  (kg/dm<sup>3</sup>), thermal conductivity of the dry soil  $\lambda_m$  (W/m·K), according to equation (25), specific heat capacity  $c_m$  of dry compacted soil component (J/kg·K), based on equation (28) and *classical grain radius*  $rg$  (mm) (Fierz et al., 2009). The setting of the volumetric fractions is meaningful only when the Bucket model is applied, as explained in section 4.2.

Finally, specific information about the site's pedology is often necessary to calibrate the *sno* parameters: this can regard the land use (grassland, bare rock, etc.) and the soil type. When Richards equation is implemented, SNOWPACK allows choosing between 14 soil classes, among which there are loam, sandy loam and silt loam, used in this study, and others varying from fine to coarse-grained soils.

It must be said that the wind and the meteorological measured data refer respectively to heights of 10 m and 2 m from the ground. However, in the *ini* file these values are both set, by mistake, to refer to a

6 m height. This error proved to affect only little the results, not changing the scientific conclusions which can be drawn from them.

#### 4.2 Richards equation in SNOWPACK

In section 3.1.2, it is enunciated that a water retention curve is the “tool” needed to use the Richards equation. Many of these soil-water characteristic curves have been proved valid in the last decades. Historically, two are at least worth mentioning: these are the one proposed by Campbell (1974) and the one introduced by Russo (1988). In SNOWPACK, the implemented water retention curve is the van Genuchten model (Van Genuchten, 1980):

$$\theta_w = \theta_r + (\theta_s - \theta_r) \frac{(1 + (\alpha|\psi|)^n)^{-m}}{Sc} \quad (19)$$

The parameters appearing in the water retention curve are  $\alpha > 0$  ( $m^{-1}$ ), related to the inverse of the *air entry suction*: this is the minimum matric suction required for the entry of air into the soil voids;  $n > 1$  (-), that is a measure of the pore-size distribution and  $m = 1 - \frac{1}{n}$  (-).  $Sc$  is a correction term that allows to take into account the air entry pressure, according to the approach by Ippish et al. (2006). Wever et al. (2015) point out that the residual water content in the water retention curve, in other words, the dry limit, is not comparable to the *water holding capacity*  $\theta_h$  described in section 4.3.

In SNOWPACK, in the implementation of Richards equation for the snow layers, the cited parameters are computed according to the equations presented by Wever et al. (2015). As for the soil layers, 14 available classes are identified in the SNOWPACK code. Such classes are responsible for the determination of the water retention capability by setting the van Genuchten values for the water retention curve. To this aim, the Rosetta soil classification and class mean hydraulic parameters are adopted (Schaap et al., 2001); the complete set of values is reported in Appendix A. Regarding the field capacity  $\theta_{fc}$ , the value is computed using the formulation proposed in Saxton et al. (1986) and the mean clay content for each soil class. In Table 4-1, an example for loam is presented.

Table 4-1: van Genuchten values relative to a loamy soil

$\theta_r$	$\theta_s$	$\alpha$	$n$	$K_{sat}$	Max pore size	$\theta_{fc}$
------------	------------	----------	-----	-----------	---------------	---------------

0.061	0.399	1.11	1.47	0.02947/(24·60·60)	0.005	0.262
-------	-------	------	------	--------------------	-------	-------

### 4.3 Bucket scheme in SNOWPACK

The Bucket scheme approximates the hydrological processes within the snow and soil layers. Setting enough layers, hence allowing them to be relatively thin, guarantees a more realistic simulation of the water transport and of its infiltration through the soil. In order to avoid quantitative issues with the modelled runoff, an unrealistic thickness of 25 m must be used to describe the soil layers in the *sno* file.

Percolating water occupies the pore space one layer at a time. As water begins to infiltrate and the uppermost layer gets filled, excess water moves to the layer beneath. Water does so when a limit is reached: this limit is the water holding capacity, defined as the minimum between the field capacity (function of  $rg$ ) and the pore space (depending on the mineral fraction). Likewise, lower layers are filled with water one after the other. The only layers which can undergo an upper water loss are the most superficial ones because of evaporation (up to 30-60 cm depending on the grain size) and water uptake by the vegetation roots. When the bottommost layer has reached its maximum water content, runoff starts being produced as the result of excess water.

The main disadvantage of this scheme is the impossibility to reproduce the volumetric water content, as gravity effect is partially neglected, with the only water losses being due to evapotranspiration. Moreover, below a certain depth, soil moisture is constant for the entire time series.

Following the implementation found in the master thesis by Hipp, the field capacity is calculated based on  $rg$ .

If  $rg < 17.0$

$$\theta_{fc} = \min \left( 0.95; \frac{0.32}{\sqrt{rg}} + 0.02 \right) \quad (20)$$

If  $rg < 60.8057$

$$\theta_{fc} = 0.0976114 - 0.002 \cdot (rg - 17) \quad (21)$$

Else

$$\theta_{fc} = 0.01 \quad (22)$$

Always ensuring that

$$\theta_{fc} \leq (1 - \theta_m) \quad (23)$$

The field capacity in function of  $rg$  is plotted in Figure 4-1.

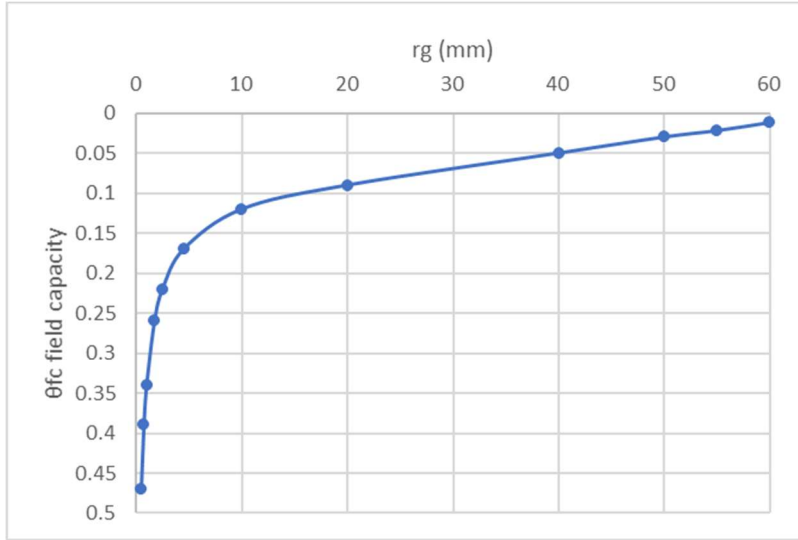


Figure 4-1: Field capacity in function of  $rg$ , when the Bucket model is applied

#### 4.4 Soil evaporation method

Two approaches exist to describe the latent heat exchange between atmosphere and bare soil: Evaporation Resistance (ER) and Relative Humidity (RH). When a snow cover is present, there is no differentiation. In order to describe the two main differences standing between the methods, it is necessary to introduce the bulk aerodynamic equation for computing latent heat exchange  $q_l$  ( $W/m^2$ ):

$$q_l = \beta \cdot (e_a - e_s) \quad (24)$$

where

$\beta$  = aerodynamic resistance (m/s)

$e_a$  = air vapor pressure (Pa)

$e_s$  is the vapor pressure at the surface or near the surface, according to the method being used. If the temperature of the topsoil layer is below 0 °C,  $e_s$  is taken as the surface vapor pressure in saturated conditions. If the temperature is above 0 °C,  $e_s$  can be defined in two possible ways: with ER, it is simply taken as the saturated vapor pressure in the uppermost layer, which corresponds to a depth of 1 cm in

these simulations. With RH, a reducing factor between 0 and 1 is applied to the last definition, making the overall  $e_s$  lower. This causes an overestimation of the negative vapor gradient from the atmosphere to the soil (causing excess condensation) and an underestimation of the positive vapor gradient from the soil to the atmosphere (causing insufficient evaporation).

The second difference lies in the heat exchange coefficient  $c$  (m/s) due to vapor exchange; this factor is at the numerator of the formula describing  $\beta$ . With RH it is defined as the inverse of an atmospheric resistance  $R_a$ ; with ER, an additional resistance  $R_{soil}$ , dependent on the relative humidity of the topsoil layer, is counted, used to reduce the heat exchange coefficient  $c$  in the case of evaporation. Such modification of  $c$  is only applied when  $e_s > e_a$  and the temperature of the topsoil element is  $\geq 0$  °C.

Concluding, when either method is applied in a discretized model, it is important to consider the difference between vapor pressure at the surface and in the middle of the topsoil layer. Besides, RH overestimates condensation even when the topsoil layer is saturated and the soil surface is warmer than the atmosphere.

Summarizing, the ER method has been introduced later as an alternative to the RH approach. It is based on the field capacity (Hurk et al., 2000) and its parameters were obtained by fitting experimental data. The main contrast from the RH method is that the surface vapor pressure is always assumed to be at saturation. This way, the unrealistic condensation resulting from the RH approach is avoided. A complete scheme of the calculations which define one or the other method is reported in Appendix B.

## 4.5 Other variables and phenomena

Although the sites analyzed are at medium-low altitudes, most of them are covered by a temporary snowpack in winter, for periods that range from days to weeks, or even months. The snow height considered by SNOWPACK during the simulations is generated from the observed precipitations.

### 4.5.1 Thermal boundary conditions

The thermal boundary condition at the soil top and bottom can be defined in two ways: one is by setting a fixed temperature, the other is called Neumann boundary condition. It consists in setting a certain

heat flux, which may be directed towards or from the soil boundaries. The Neumann condition is pursued, given the availability of means and data that guarantee the setting of such fluxes.

At the soil surface, SNOWPACK computes an energy balance equation whose result is a positive or negative net heat flux. At the soil bottom, a constant geothermal heat flux directed upwards is entered in the *ini* file. The information on geothermal heat fluxes for the sites analyzed in this work comes from a study published by Vedova et al. (1991). Making use of scattered data from boreholes, tunnels and lakes, his team was able to attempt drawing isolines of equal heat flow values in the whole alpine region. Some precious conclusions could be drawn from the work, in which the Swiss territory was divided into separate regions, as illustrated in Figure 4-2. Heat flow in the Upper Rhine Graben (1-2) is high ( $> 0.1 \text{ W/m}^2$ ), values in the Molasse Basin (3) are rather high ( $0.08 \text{ W/m}^2$ ), while heat flow in the Alps (4-5-6) is lower and varies widely ( $0.06\text{-}0.08 \text{ W/m}^2$ ) (Thimo, 2013).

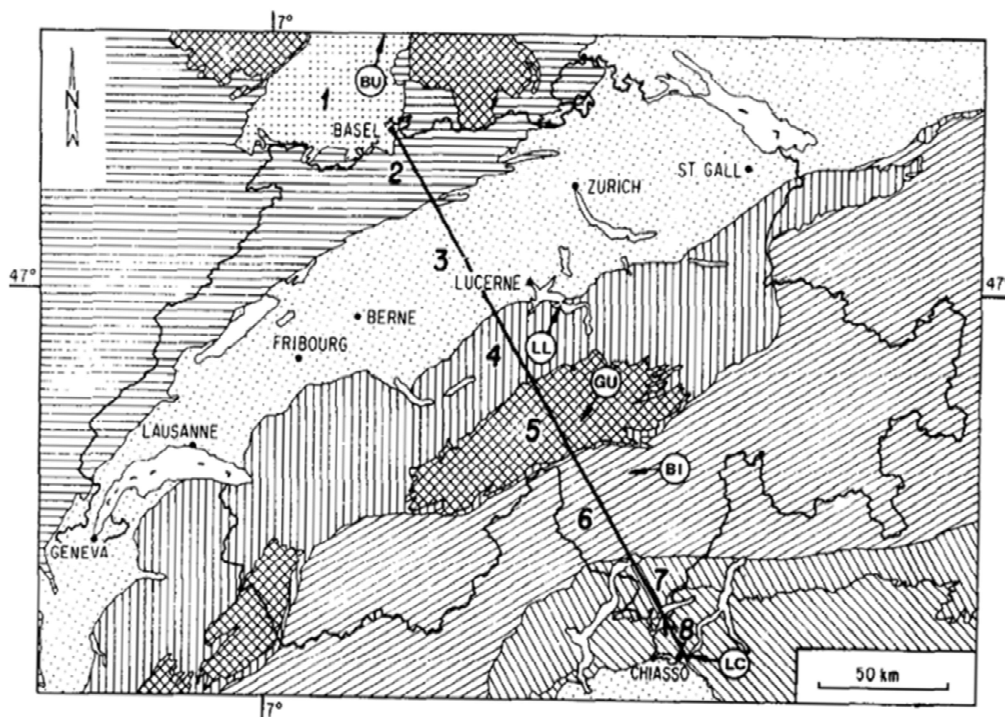


Figure 4-2: Swiss Geotraverse, crossing all the regions defined by differing geothermal heat fluxes (Vedova, 1991)

#### 4.5.2 Atmospheric stability correction

Various options are available in SNOWPACK to address the atmospheric stability correction for turbulent heat fluxes. The selection of an atmospheric stability correction is needed because a neutral boundary layer often overestimates heat fluxes and should hence be discarded when modelling turbulent sensible heat fluxes in stable conditions.

Numerous functions are available in literature: however, their applicability greatly depends on the chosen site where they are used. Schlögl et al. (2017) investigate six different stability corrections, among which two are particularly suitable for snow-free terrains: Michlmayr et al. (2008) derived from Stearns et Weidner (1993), and Holtslag et H. (1988). What differs among these parametrizations is the computation of the stability parameter  $\zeta$ , which means that this variable alone is responsible for most relevant information. According to the cited study, all the tested stability corrections perform well under low wind speeds and small temperature variations, with the one from Holtslag et H. (1988) showing optimum behavior in terms of Mean Arithmetic Mean (MAE) values on sensible heat fluxes.

#### 4.5.3 Roughness length

The roughness length ( $z_0$ ) is a mathematical tool to represent the roughness of any surface. It allows to approximate atmospheric turbulence and fluxes of various quantities near the surface. Its computation is based on the ratio between the frontal area of the average element (facing the wind) and its width. The closer the roughness length is to zero, the smoother the surface is. As values grow, they indicate bigger and bigger obstacles. High values imply weaker horizontal winds near the surface and a greater exchange with the atmosphere. A classification of  $z_0$  classes of interest for the current study is reported in Table 4-2.

*Table 4-2: Terrain classification due to Davenport and quoted by Wieringa (1960)*

class		Roughness length (m)	Landscape features
No.	Name		
1	Sea	0.0002	Open water, tidal flat, snow with fetch above 3 km
2	Smooth	0.005	Featureless land, ice

3	Open	0.03	Flat terrain with grass or very low vegetation, airport runway
4	Roughly open	0.10	Cultivated area, low crops, obstacles of height H separated by at least 20 H

#### 4.5.4 Thermal parameters

It must be made clear that it is not the objective of this work to measure and determine the soil thermal characteristics of one specific site. In fact, the goal is to evaluate the goodness of the implementation of SNOWPACK in the simulation of ground temperature (GT), volumetric liquid water content (LWC), evapotranspiration (ET) and runoff. Since, however, the thermal properties of the soil play a considerable role in the determination of ground temperatures, an appreciable part of the sensitivity analysis is dedicated to them.

##### 4.5.4.1 Thermal conductivity

The computation of the soil matrix thermal conductivity  $\lambda_{bulk}$  (W/m·K) is calculated in SNOWPACK with a weighted average that sums the conductivity of each medium in the following way:

$$\lambda_{bulk} = \lambda_m + (\lambda_w \cdot \theta_w) + (\lambda_{ice} \cdot \theta_{ice}) \quad (25)$$

where:

$\lambda_m$  is the thermal conductivity of the dry soil (provided as input parameter);

$\lambda_w$  is the thermal conductivity of water, computed following Hipp's master thesis:

$$\lambda_w = 0.11455 + 1.6318 \cdot 10^{-3} \cdot T \quad (26)$$

$\lambda_{ice}$  is the thermal conductivity of ice:

$$\lambda_{ice} = 0.4685 + \frac{488.19}{T} \quad (27)$$

where the temperature is in K.

The limit of equation (25) is the little importance assigned to the water content. In fact, assuming a soil temperature of 20 °C,  $\lambda_w$  becomes equal to 0.59 W/m·K. This means that from unsaturated to fully

saturated conditions,  $\lambda_{bulk}$  will increase by a maximum of 0.59 W/m·K, excluding the presence of ice. It is true that the soil thermal conductivity dependence on the water content depends in turn on the soil density, and results can vary to some extent based on this. However, the vast majority of literature studies reveal that  $\lambda_{bulk}$  is highly influenced by the LWC, causing values to easily rise by 1 W/m·K from dry to saturated conditions. The reason behind the thermal conductivity enhancement operated by water is the creation of water bridges, very efficient in connecting separated soil particles.

Another inconsistency identified is the high  $\lambda_m$  necessary to simulate the measured GT. In chapter 6, it is demonstrated how a value around 1.4 W/m·K seems to well simulate the slope of the GT-depth curves. Independently from the contribution brought by water, which for LWC < 0.5 is not so influential, such value appears much higher than any proposed by scientific studies on the topic.

These two considerations suggest that, on the one hand, high values of  $\lambda_m$  are needed to compensate for the low contribution that water can provide to  $\lambda_{bulk}$ ; on the other hand, the heat transport module coded in SNOWPACK requires high thermal conductivities to represent the evolution of temperatures in depth correctly.

A universal, correct equation for computing the matrix thermal conductivity does not exist, because different forms would be needed each time the soil type, the porosity or the water content change. It is also because of this that a simplified linear formulation is currently used in SNOWPACK. A more complex version exists in the model, but it can be applied when ice is widely present in the soil, which is not the case in this work. Studies on the formulation of  $\lambda_{bulk}$  began in 1949 with Kersten (1949), whose parametrization was followed and modified by Johansen (1975). Later, Farouki (1982) compiled thermal conductivity research from seven authors: Kersten, Johansen, Mickley, Gemant, De Vries, Van Rooyen, and McGaw. Each researcher had come up with his own method for computing  $\lambda_{bulk}$  in fine-grained and coarse-grained soils. The grouping of the studies demonstrated a significant variability among the results. Duarte et al. (2016) partially explained the reasons behind this, affirming that most historic research had been done in frozen regions, and the same formulas could not be simply transferred to tropical or temperate climates.

#### 4.5.4.2 Heat capacity

SNOWPACK's computation of the heat capacity  $c$  (J/kg·K) consists of a weighted average of the specific heat capacities of each medium, among which  $c_m$  is the one defined by the user (relative to the dry compacted soil).

$$c = \frac{(\rho_{air} \cdot \theta_{air} \cdot c_{air}) + (\rho_{ice} \cdot \theta_{ice} \cdot c_{ice}) + (\rho_w \cdot \theta_w \cdot c_w) + (\rho_m \cdot \theta_m \cdot c_m)}{\rho_{bulk}} \quad (28)$$

where:

$\rho_{air} = 1.1 \text{ kg/m}^3$  (using the ideal gas law),  $\rho_{ice} = 917 \text{ kg/m}^3$ ,  $\rho_w = 1000 \text{ kg/m}^3$  (at 0 °C);

$c_{air} = 1004.67 \text{ J/kg}\cdot\text{K}$ ,  $c_{ice} = 2100 \text{ J/kg}\cdot\text{K}$ ,  $c_w = 4190 \text{ J/kg}\cdot\text{K}$  (at 0 °C);

$$\rho_{bulk} = (\rho_{ice} \cdot \theta_{ice}) + (\rho_w \cdot \theta_w) + (\rho_m \cdot \theta_m) \quad (29)$$

This formulation is physically correct, contrary to the one for thermal conductivity, leaving less space for discussions and reformulations. The literature values for  $C$  reported in section 3.2 for a fine-grained soil are consistent with the best ones for  $c_m$  obtained in Payerne throughout the sensitivity analysis.

#### 4.5.5 Canopy

The canopy module was initially developed to be implemented in conifer forests (Rutter et al., 2009). This first version considered trunks and leaves as a single body. The updated second version came with the introduction of a two-layer canopy module, useful to separate the lower part consisting of trunks from the upper one made of branches and leaves (Gouttevin et al., 2015).

In SNOWPACK *sno* file header, it is possible for the user to set some of the main parameters relative to canopy. The first one is the canopy height, whose values can range from a few tens of centimeters for grass and bushes to several meters for trees. Then there is the *Leaf Area Index* (LAI), a dimensionless quantity defined as the one-sided green leaf area per unit ground surface area ( $\text{m}^2/\text{m}^2$ ) in broadleaf canopies (Watson, 1947). Its values can be lower than 1 for sparse low vegetation and greater than 5 - 6 for forests. Next, the *Direct Throughfall* (DT), defined as the proportion (unitless) of the precipitation that reaches the ground surface when certain vegetation is present. This is a quantity which normally varies a lot with time, because of its dependence on the moisture content within the vegetation, as well as on the canopy height and LAI, which will be, in our case, studied separately. Low values (< 0.6) are

normally associated with forests, where the trees' action is much more effective. High values ( $> 0.8$ ) describe a short vegetation cover such as grass. Values close to 1 would ignore canopy's action in retaining precipitation. The last selectable parameter of the *sno* file header is the canopy albedo, which can be given two different values, whether it's referred to dry or wet conditions.

From the code itself, other parameters can be modified. Among these the root depth, a variable that is decisive from the perspective of the soil moisture uptake by the plant roots. The deeper the roots, the greater the plant's capability to extract water from the soil and make it subject to transpiration. According to the fraction of roots, transpiration is partitioned between the different soil layers. Root water uptake is limited to the reachable water in each layer, defined by the field capacity and the wilting point. These two are solely dependent on the soil type, with  $\theta_{wp} = 0.17 \cdot \theta_{fc}$ .

Following, a few other variables are presented: the Canopy Basal Area, which refers to the density of trunks (stems in our case) on the ground; the Biomass Heat Capacity, equal to 2400 J/kg·K for needles and to 800 J/kg·K for grass; the Biomass Density, which can be set to about 900 kg/m<sup>3</sup> to represent grass; the Trunk Fraction Height, which defines the fraction of the overall canopy height that consists of trunks (it is only considered when a two-layer canopy module is applied). Finally, the friction generated by the presence of canopy is simulated by a roughness length set equal to 10% of the canopy height.

## 5 DATA AND ANALYSIS TOOLS

### 5.1 Origin of the data

The meteorological data are obtained from the MeteoSwiss automatic monitoring network and also from *SwissSMEX* in the station of Rietholzbach. The soil information is offered by the joint project *SwissSMEX (Swiss Soil Moisture EX-periment)*, initiated by ETH\_Zurich, Agroscope ART and MeteoSwiss in 2008 to investigate soil moisture evolution at sites with different land cover types. The soil information includes a set of temperatures and soil moisture measurements taken at various depths. These go from 5 cm up to 150 cm for some stations and sometimes multiple sets of measurements are available (up to four in the case of soil moisture).

Finally, the DEM required to use Alpine3D are provided by SwissTOPO and are accessible online for research purposes. The land cover is the CORINE data set from the European project Copernicus.

In chapter 7, the results obtained in chapter 6 are tested in ten new sites equipped with meteorological stations and soil measuring tools. A map of these sites is reported in Figure 5-1, while the sites' geography and main characteristics are listed in Table 5-1. As can be seen, most places are located in the Swiss Plateau, with the exception of Magadino Cadenazzo (Ticino) and Sion (Valais). Furthermore, all except Plaffeien lie at altitudes below 800 m.

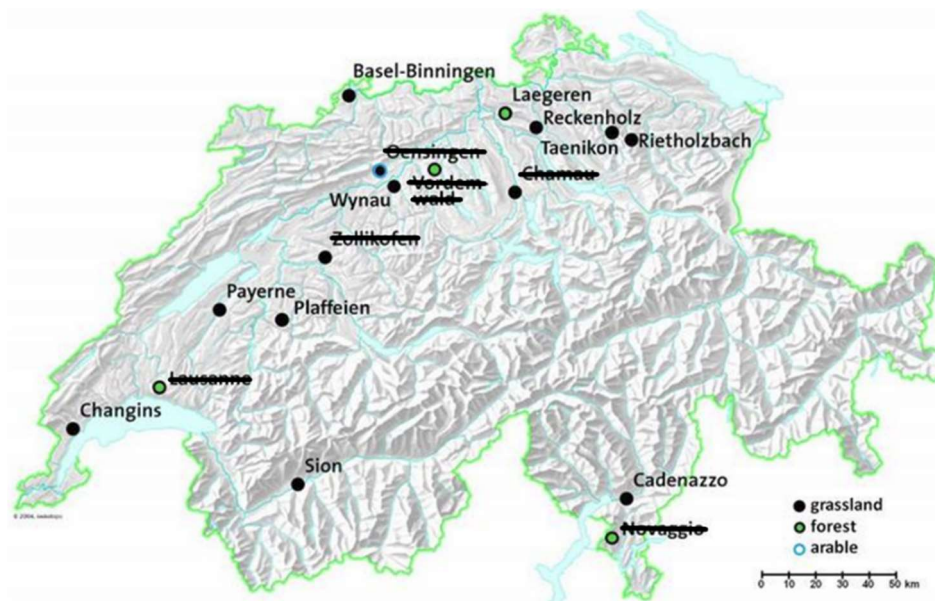


Figure 5-1: Location of SwissSMEX stations for soil monitoring (<https://iac.ethz.ch>)

Reported in Appendix C, a table can be found, indicating the duration of each site's simulations and the availability of meteorological data for each station.

Figure 5-2 and Figure 5-3 illustrate two of the several stations whose data are used in the present study.



*Figure 5-2: Payerne station for soil monitoring (<https://iac.ethz.ch>)*



*Figure 5-3: Plaffeien station for soil monitoring (<https://iac.ethz.ch>)*

Table 5-1: Geographical and physical data of the stations analyzed in chapter 7

ID	Name	Latitude	Longitude	Elevation (m a.s.l.)	Land Use	Soil	Geothermal heat flux (W/m <sup>2</sup> )	Remarks
BAS	BASEL	47.54103	7.58356	316	grassland	loam	0.10	
BER	BERN	46.99074	7.46400	552	grassland	loam	0.08	
CHN/C GI	NYON CHANGINS	46.40104	6.22773	455	grassland	loam	0.08	
LAG/N ABLAE	LAEGERN	47.47824	8.36437	688	grassland	clay	0.08	Shallow soil
MAG/ CAD	MAGADINO CADENAZZO	46.16003	8.93366	203	grassland	silt loam	0.06	Groundwater in 70 cm
PAY	PAYERNE	46.81158	6.94242	490	grassland	loam	0.08	Cambisol, Molasse
PLA/P LF	PLAFFEIEN	46.74771	7.26626	1042	grassland	sandy loam	0.08	
REC	RECKENHOLZ	47.42769	8.51794	443	grassland	loam	0.08	
RIE/R HB	RIETHOLZBAC H / ZURICH AFFOLTERN	47.38043	8.99340	755	grassland	loam	0.08	Cambisol
SIO	SION	46.21864	7.33021	482	grassland	sandy loam	0.06	
TAE	TAENIKON	47.47987	8.90487	539	grassland	loam	0.08	
WYN	WYNAU	47.25501	7.78746	422	grassland	silt loam	0.08	

## 5.2 Output processing

The primary tool to analyze, compare and visualize the data was a MATLAB script, here summarized.

### DATA PLOTS:

Measured and modelled data (ground temperature and soil moisture) are plotted against time. When more than one set of measurements is available, multiple sets are plotted, so long as they do not show evident errors or temporal gaps. Together with the liquid water content (LWC), also the ice volumetric content is reproduced, since it can be held accountable for sudden drops in the modelled LWC.

### AVERAGE GROUND TEMPERATURE COMPARISON:

The chosen time resolution to assess the modelling of ground temperature (GT), LWC and evapotranspiration (ET) is seasonal. Being the timeseries quite long (from 7 to 9 years), the results are presented under the form of average values referring to a 3-month long time scale. Lower time resolution, e.g. from sub-daily to weekly cycles, is not evaluated.

Average GT across the whole time series are computed and plotted for both input and output. A “season filter” is created to split each set of data into seasonal 4 sets. Average GT relative to each season are computed and plotted, for both measured and modelled data, taking into consideration the whole time series. The same is done at a monthly level. Average air temperatures are computed and plotted, in order to roughly validate the correctness of the near-surface GT measurements.

It must be specified that the seasons are selected by grouping the twelve calendar months into four 3-month periods based on similar temperatures. Therefore, so-called meteorological seasons (relative to the northern hemisphere) are adopted: for instance, the meteorological winter begins on December 1<sup>st</sup> and includes the months of December, January, and February.

Another way to visually compare measured and modelled GT is through scatter plots. Every point's x-coordinate represents the measured GT and the y-coordinate the modelled one. The closer the points are to the drawn bisector having a slope equal to 1, the better the simulation. For each season a different color is assigned; the scatter plots are realized for all depths.

### GROUND TEMPERATURE PERFORMANCE MEASURES:

Five statistical parameters are computed. These are the Mean Absolute Error (MAE), the Mean Squared Error (MSE), the Root-Mean-Square Error (RMSE), the Nash-Sutcliffe Efficiency (NSE) and the Kling-Gupta Efficiency (KGE). The RMSE is computed this way:

$$RMSE = \sqrt{\frac{\sum_{i=1}^n (e_i)^2}{n}} \quad (30)$$

where  $n$  is the total number of data,  $e_i$  represents the deviation between the measured and the modelled GT at the timestep  $i$ .

MAE, MSE and RMSE summarize performance in a way that disregards the direction of over- or under-prediction. They are all dimensional indices and their best values are zero.

The RMSE index is a widely used measure of precision; one of its features is that it tends to emphasize larger differences in a series, whereas lower ones are virtually neglected: in other words, it is very sensitive to outliers. The RMSE was chosen to evaluate the reproduction of GT, being the most accurate and most utilized in other scientific studies.

The indexes NSE and KGE are ideal to describe river discharge data, as well as water quality constituents such as sediment, nitrogen, and phosphorus loading. Because they highlight the mean characteristics of a phenomenon, hence they are not suited for the analysis of GT, they are not utilized here.

#### LIQUID WATER CONTENT:

The same approach is used for LWC, apart from the scatter plots, which are not realized in this case. As it is common to dispose of multiple sets of measured LWC, more than one is illustrated, if characterized by realistic values.

With respect to the LWC, only the RMSE is computed, relative to depths greater than 25 cm. In fact, above this depth, the soil moisture magnitude varies enormously in brief time windows, making any analysis extremely difficult and with little physical basis.

#### RUNOFF:

The modelled runoff is plotted against time, together with its total average. The values are in  $\text{kg/m}^2 \cdot 3\text{h}$ . There are no sites among the ones studied, for which runoff measurements coming from soil lysimeters are available; hence the absence of a set of measured data to compare the modelled with. This can be

done only at a watershed scale thanks to the application of Alpine3D and the comparison of its output with the measured river discharge.

#### EVAPOTRANSPIRATION:

This section is only implemented for Payerne, Bern and Rietholzbach, where ET data are available. The variables of interest are Evaporation from the soil, Evaporation from the canopy, Transpiration from the canopy, and Total Evapotranspiration. In Payerne and Bern, the measured ET is only available as daily value. To make the data comparable, the four said modelled variables are turned daily, by summing the values produced by SNOWPACK every 3 h. These are later plotted separately and together, aiming to illustrate the quantitative composition of the total evapotranspiration, made up of the three different phenomena. In Rietholzbach, instead, the measured ET is available every hour. So, it is summed over a time windows of 3 h to make it comparable to the modelled data.

Afterwards, measured and modelled ET are plotted, followed by a representation of the difference between the two (measured – modelled), its moving average (window length = 15 days) and its total average.

In order to understand the dependence of the ET modelling accuracy on the season, a season filter is applied. Similarly to what is done with GT and LWC, both measured and modelled ET are divided according to the season and averaged (across multiple years) for each season. The result allows to assess when the matching is done correctly and when a gap exists.

For ET, the adopted statistical index is the RMSE. It is computed referring to each of the four seasons, the reason being the great variety of accuracy obtainable by the model according to the period of the year.

#### RUNOFF + EVAPOTRANSPIRATION:

Finally, a mass balance verification is executed: three modelled cumulative quantities are weighted over the whole timeseries: runoff, ET and total precipitation (PSUM). The aim is to verify the coincidence between runoff + ET and total precipitation.

## 6 RESULTS - PAYERNE SENSITIVITY ANALYSIS

The purpose of this sensitivity analysis is to assess the influence of a series of parameters on ground temperature (GT), evapotranspiration (ET), soil moisture (LWC) and produced runoff. Extreme values for each parameter are tested and compared between each other, in order to magnify the effects on the quantities under study. Besides, the output data are visually and analytically placed side by side with the measurements, a precious tool that helps to identify a set of parameters able to represent at best the reality, hence validating SNOWPACK's parametrization.

The station of Payerne is selected for this analysis because of the availability of many data: OSWR, OLWR, ET measurements, as well as the possibility to run Alpine3D over the catchment where Payerne is located. Moreover, being characterized by a loamy soil, the same ideal set of parameters can be transferred and applied without further changes to the other sites where the soil is of type loam. The simulation is run over a 9-year period, from August 2008 to October 2017.

Among the available atmospheric stability corrections, three are tested: Neutral, Michlmayr and Holtslag. The option Neutral, as expected, shows unacceptable predictions of GT. The formulas by Michlmayr and Holtslag are then compared, exhibiting extremely similar results for both GT and ET. Therefore, the parameterization proposed by Michlmayr is chosen for all the simulations because of its previous adoption in other related studies.

This sensitivity analysis is first conducted without the canopy module (sections 6.1 and 6.2) in order to restrict the analysis to the infiltration models, the evaporation methods and the soil parameters, isolating these factors from possible ambiguities derived from the implementation of canopy. With this being said, the quantity ET only consists of soil evaporation in sections 6.1 and 6.2, while in section 6.4 it is the result of summing soil evaporation and canopy evapotranspiration.

LWC is not assessed in the Bucket simulations because of the unrealistic patterns produced, as explained in section 4.3. An example of the constant LWC reproduction below a certain depth for the whole time series is offered by Figure 6-1.

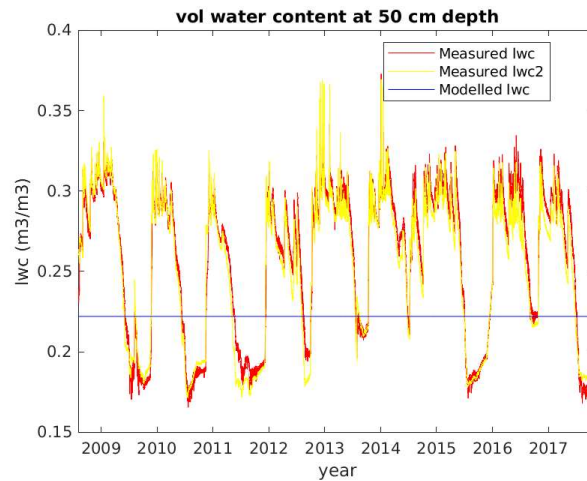


Figure 6-1: Soil moisture vs time, modelled and measured. Bucket, ER. Depth: 50 cm

## 6.1 Bucket model

The initial parametrization, reference for all tests in this section, is the following one:  $rg$ : 2.5 mm ; Specific heat capacity  $c_m$ : 1400 J/kg·K ; Thermal conductivity  $\lambda_m$ : 1.4 W/m·K ; Solid fraction: 0.55 ; Density  $\rho_m$ : 2600 kg/dm<sup>3</sup> ; Roughness length  $z_0$ : 0.02 m ; Soil albedo: 0.17 ; Soil emissivity: 0.98 .

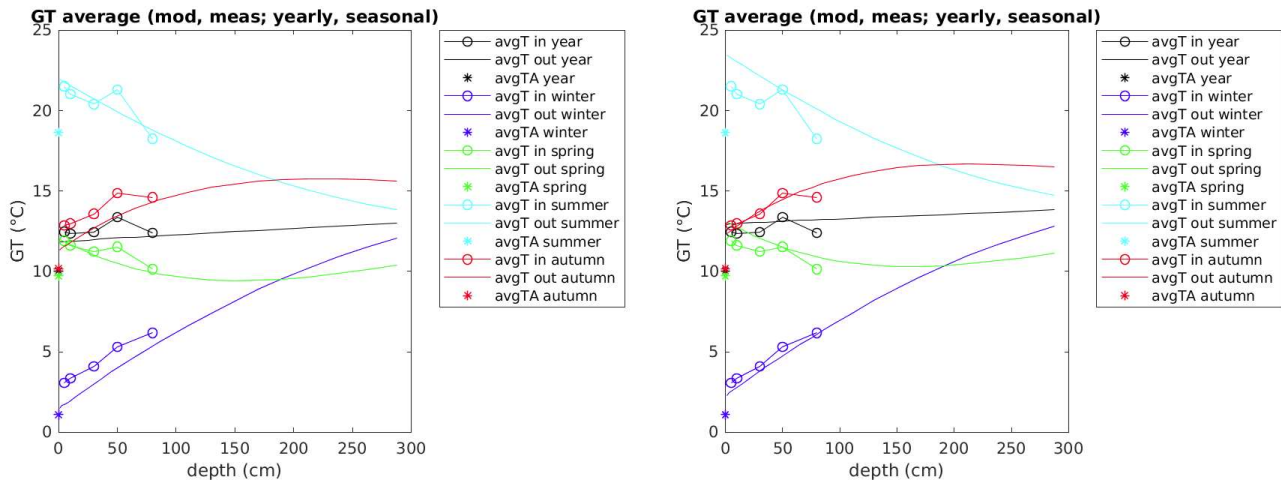
### SOIL EVAPORATION METHOD

As a first step, the two soil evaporation approaches described in section 4.4 are compared:

- Evaporation resistance (ER)
- Relative humidity (RH)

The graphic tool used to compare different configurations consists of plotting seasonal and yearly average GT against the soil depth. Modelled data always appear with a continuous line, while measurements are characterized by lines interrupted by various symbols. Average air temperatures are also plotted, in order to roughly validate the correctness of the GT measurements.

With ER, the GT is generally lower than with RH, specifically: 1.5 °C lower in summer, 1 °C lower in the other seasons. As pictured in Figures 6-2, this allows ER to produce a very good match between April and September. On the other hand, RH reproduces well the GT from November to March.

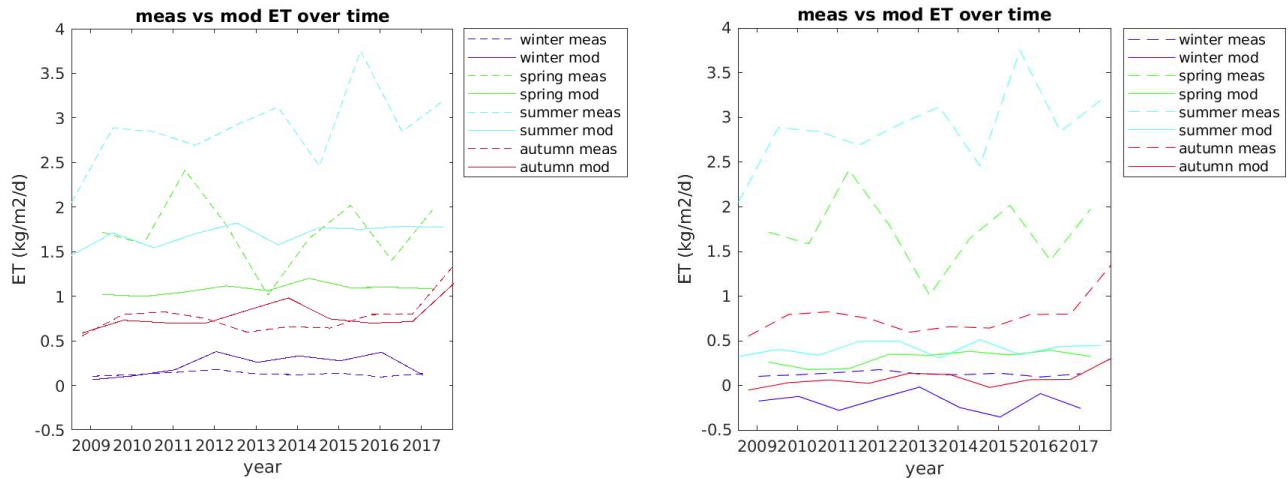


Figures 6-2: Seasonal and yearly average GT vs depth, modelled and measured. Soil evaporation methods: ER (left panel), RH (right panel)

The choice of the evaporation method has a considerable influence on the Evapotranspiration (ET). This quantity, as for now, is made up of the soil evaporation only, as canopy is absent.

The analytical variable used to study ET variations is the average difference between measured and modelled ET throughout the whole time series. High absolute values of difference in ET imply a poor ET modelling, while the closer they get to zero, the better. Moreover, positive values stand for an underestimation of ET, while negative values indicate an overestimation of it.

The difference in ET is equal to 0.444 kg/m<sup>2</sup>·d (ER) and to 1.245 kg/m<sup>2</sup>·d (RH). Figures 6-3 make it possible to visualize the ET average, computed for each season of the whole time series, both measured and modelled.



Figures 6-3: Seasonal average ET vs time, modelled and measured. Soil evaporation methods: ER (left panel), RH (right panel)

At first glance, ER better predicts the ET of the site. Despite its value of difference in ET is far from zero, the modelled results are close to the measurements, especially in winter and autumn. On the contrary, RH fails in reproducing the ET in all seasons. Spring and summer see extremely low values; in winter the net balance shows condensation phenomena to be predominant, as highlighted in section 4.4 to be one of the biggest issues of the RH method. Given this fact, further sensitivity analysis on ET with the RH method will not be reported from here on.

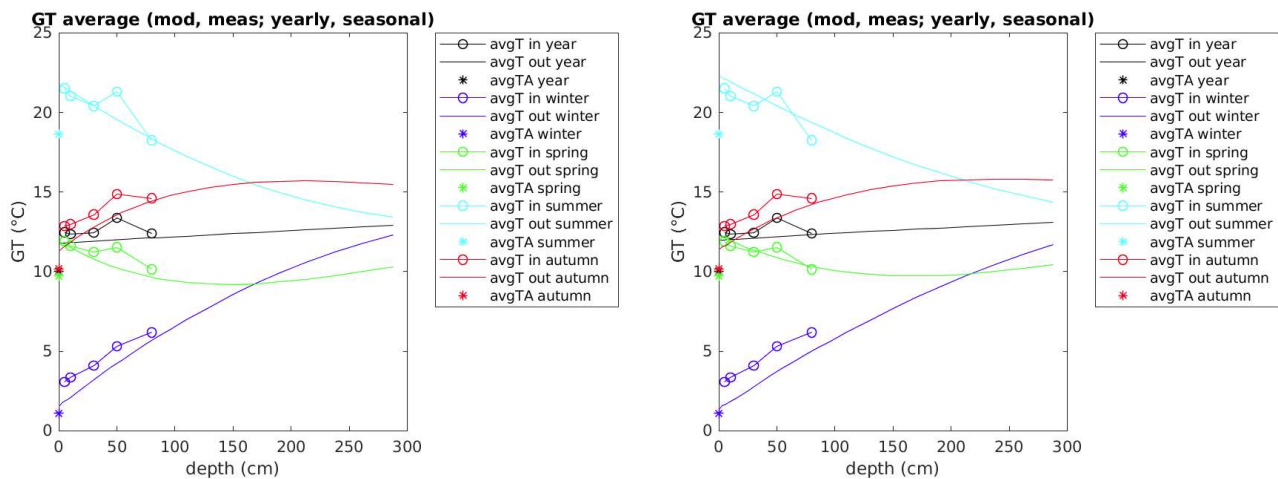
The reason behind the GT differences lies in the ET gap between the two evaporation methods. More water evaporating from the soil, thus a greater latent heat flux  $q_l$  directed upwards, involves a heat loss for the soil in all seasons.

Regarding runoff, the average value throughout the time series is analyzed to make comparative evaluations. The absence of a lysimeter in the station of Payerne, as well as in the others, does not allow to compare the modelled results to measurements. The application of the model Alpine3D to validate the runoff calculated by SNOWPACK will be presented in section 7.4. As for now, what is done is a mere evaluation of the sensitivity of a series of parameters on the runoff output.

The average runoff is equal to  $0.149 \text{ kg/m}^2\cdot 3\text{h}$  (ER) and to  $0.249 \text{ kg/m}^2\cdot 3\text{h}$  (RH): the gap between the two values has its origins in the low ET obtained with RH, thus allowing more water to contribute to the runoff.

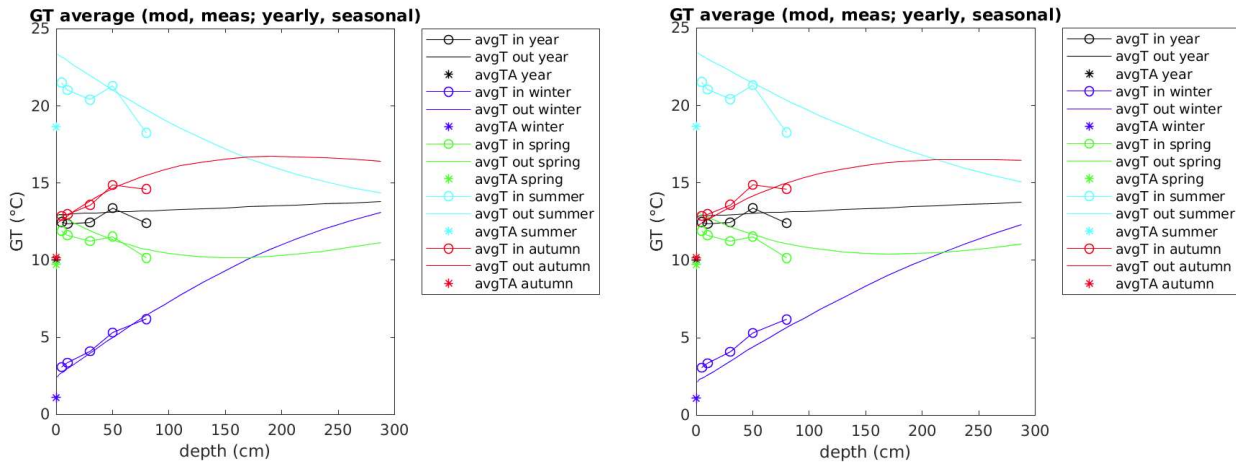
## RG

The second parameter that is found to have a considerable impact on GT and ET is  $rg$ , because of its unique role in representing the soil type. Growing different values are tested: 0.5; 0.75; 1; 1.75; 2.5; 4.5; 10; 40; 50; 55; 60; 100. The first simulations shown below are run with the ER method. To analyze the consequences of a change in  $rg$  on GT, two extreme cases are taken. The first is  $rg = 0.5$  which, with a  $\theta_{fc}$  of 0.47, represents a typical clay soil. The second one is  $rg = 40$ , which simulates a gravel soil with a  $\theta_{fc}$  of 0.05. The effect of  $rg$  is not the same on all seasons. Referring to an 80 cm depth, its increase brings lower GT in winter (-0.6 °C), but higher GT in spring (+0.4 °C) and summer (+1 °C), while it does not have any effect in autumn. The influence of  $rg$  is increasingly observable with depth. Figures 6-4 report the average GT with the two different  $rg$  values.



Figures 6-4: Seasonal and yearly average GT vs depth, modelled and measured.  $rg$ :  
0.5 mm, clay (left panel), 40 mm, gravel (right panel)

The second set of simulations is run with the RH method. The first  $rg$  value is here taken equal to 0.75 because  $rg = 0.5$  produces runoff and ET that are not consistent with the results coming from higher  $rg$  values.  $rg = 0.75$ , with a  $\theta_{fc}$  of 0.39, represents a typical sandy clay soil. The second value,  $rg = 40$ , simulates a gravel soil with a  $\theta_{fc}$  of 0.05.  $rg$ 's effect varies according to the season, as visible in Figures 6-5. Referring to an 80 cm depth, its increase brings lower GT in autumn (-0.5 °C) and winter (-0.7 °C), but higher GT in spring (+0.4 °C) and summer (+0.6 °C). In the same way as with ER, the influence of  $rg$  is increasingly observable with depth.



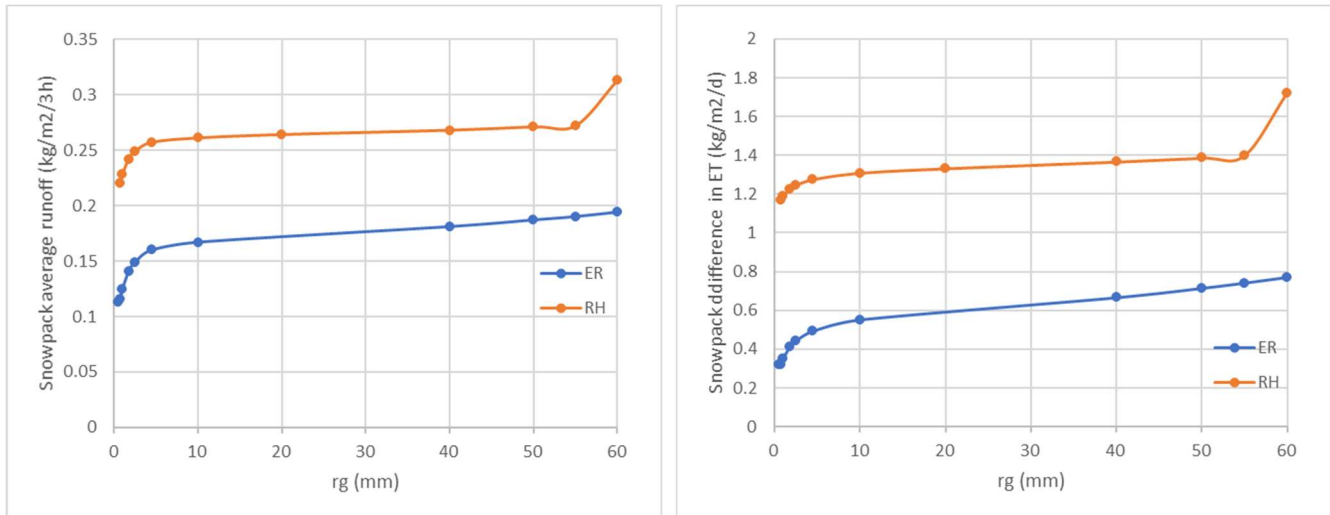
Figures 6-5: Seasonal and yearly average GT vs depth, modelled and measured.  $rg$ : 0.75 mm, sandy clay (left panel), 40 mm, gravel (right panel)

The grain size acts in two ways on the GT. The first one has to do with the soil heat resistance, the second one with the ET. The first way, which is more influential, can be explained in these terms: high values, simulating loose soils, cause the soil to heat up more easily in the warmer months and to cool down more in the colder ones. Finer soils, as expected, apply a greater heat resistance to the temperature variation of the air and ground surface. Secondly, increases in  $rg$  cause a general decrease in the modelled ET throughout the year (especially with the ER method). As already explained, a lower ET leads to higher temperatures. In summer these two effects sum up; in winter they play against each other, but the change in gradient proves to be predominant, causing a GT decrease. Overall, ER and RH simulations react similarly to  $rg$  variations.

Figures 6-6 show the response of the average runoff and the difference in ET to  $rg$  variations. Two comments must be done on low and high  $rg$  values. The very fine soil types described by values smaller than 2 mm encounter a problem in the water infiltration modelling realized by SNOWPACK. Being the soil overall depth equal to 25 m, the time needed for all the layers to fill with water is high. As a result, the runoff appears absent for months (or even years for  $rg = 0.5$ ). This happens because the field capacity is high, and water is not released easily enough to the lower layers. Secondly, the sudden increase of runoff for  $rg$  values higher than 55 mm occurring with the RH method deserves further investigation, because clearly unrealistic. Finally, two clarifications on the curves: in the right-hand

graph, the difference in ET is plotted, meaning that low values correspond to high modelled ET and vice versa. Secondly, the unit of measure: runoff is displayed in  $\text{kg/m}^2\cdot 3\text{h}$ , while ET in  $\text{kg/m}^2\cdot \text{d}$ . Hence, to compare the values, runoff must be multiplied by 8. If this is done, it can be noticed how the water mass balance is well respected.

The right-hand figure shows that only with ER and low values of  $r_g$  it is possible to minimize the difference in ET. Increasing  $r_g$  produces worse simulations in terms of ET.



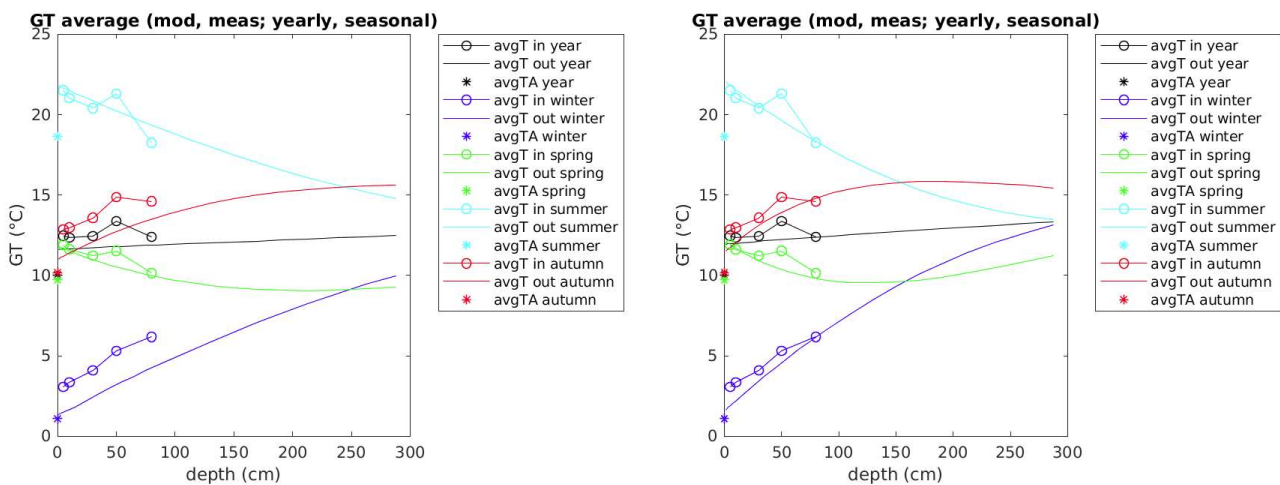
*Figures 6-6: Modelled runoff (left panel) and difference in ET (right panel) trends with the two soil evaporation methods ER and RH*

The following sensitivity tests are realized with the ER method, because of two arguments: first, the ET is much better simulated by ER, whereas RH makes the ET practically null if considered in average along the year. Secondly, although for the topsoil layers the RMSE value for GT prediction is smaller by 0.1 – 0.3 with RH, the RMSE value at 80 cm is considerably lower for ER (0.82) compared to the one for RH (1.28). The more accurate results at such depth (as well as at 30 cm), thus for a bigger portion of soil, are considered in the choice of the evaporation method to be adopted.

## SPECIFIC HEAT CAPACITY

The following values for specific heat capacity  $c_m$  (J/kg·K) are tested: 500; 1000; 1400 (initial); 1800; 2300. The minimum (500) and maximum (2300) values are visually and analytically compared (Figures 6-7), in order to highlight the GT sensitivity to  $c_m$  changes.

Associated to a  $c_m$  increase, two main effects can be spotted: one is the variation in surface GT, more evident in winter (+0.4 °C) and autumn (+0.6 °C). The second one, more significant, is the change in GT gradient. This can be quantified through the changes in GT at 80 cm depth: an appreciable increase for winter (+1.8 °C) and autumn (+1.3 °C) and a decrease for summer (-1 °C).



Figures 6-7: Seasonal and yearly average GT vs depth, modelled and measured.  $c_m$ : 500 J/kg·K (left panel), 2300 J/kg·K (right panel)

Analyzing the modelled GT next to the measurements, neither of the two reported values for  $c_m$  is realistic. The former is too low: in fact, the soil is not able to store enough heat, causing the deep soil layers to warm up excessively in summer. On the other hand, the latter value (2300) produces the opposite behavior. Too much geothermal heat is stored by the soil layers in winter and autumn, causing them to reach too high temperatures.

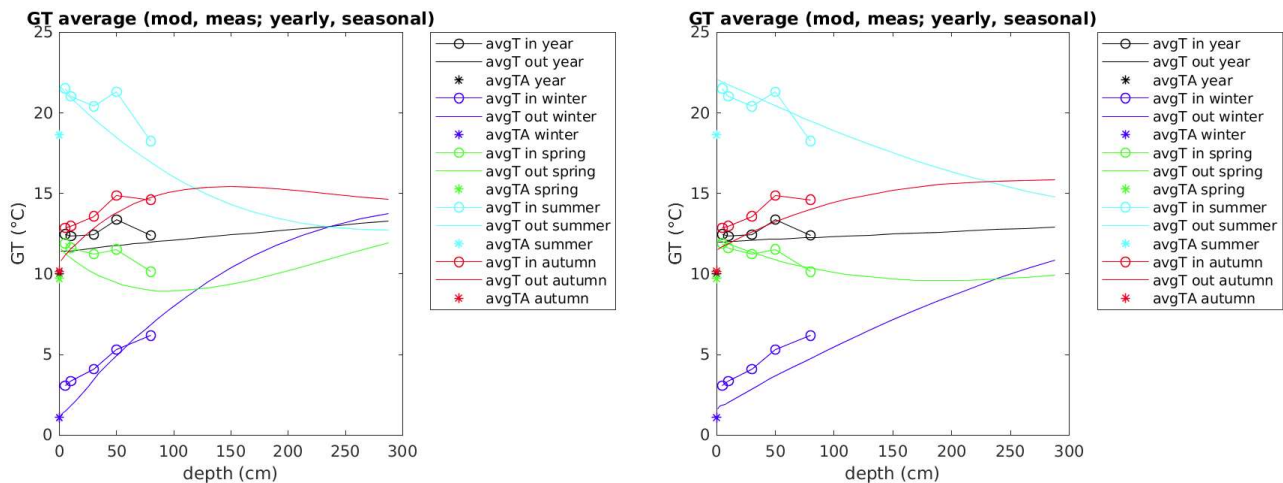
An intermediate value between these two extremes is the most appropriate to reproduce correctly the shape of the GT-depth curves. A visual comparison suggests that any value between 1000 and 1800 is acceptable. It can be said that  $c_m$  affects in a relevant way neither the runoff nor the ET.

The values in the cited range are compared to the ones proposed by Andujar Marquez et al. (2016) for heat capacity  $C$  in fine-grained soils: the authors assign the values  $1.6 \text{ MJ/m}^3 \cdot \text{K}$  to dry clay/silt and  $3.4 \text{ MJ/m}^3 \cdot \text{K}$  to water-saturated clay/silt. If transformed into specific heat capacity  $c$  ( $\text{J/kg} \cdot \text{K}$ ) and then to dry compacted soil heat capacity  $c_m$  ( $\text{J/kg} \cdot \text{K}$ ), the values are consistent with each other.

## THERMAL CONDUCTIVITY

The following values for thermal conductivity  $\lambda_m$  ( $\text{W/m} \cdot \text{K}$ ) are tested: 0.5; 1; 1.4 (initial); 1.8; 2.3. The minimum (0.5) and maximum (2.3) values are compared (Figures 6-8), in order to highlight the GT sensitivity to  $\lambda_m$  changes.

Analogously to  $c_m$ ,  $\lambda_m$  affects the surface GT and above all the GT gradient. Increasing  $\lambda_m$  brings about higher surface GT for all seasons, especially spring, summer (+0.7 °C) and autumn (+0.5 °C). As for the GT gradient, the GT at 80 cm depth varies as follows: it diminishes in winter (-2.0 °C) and autumn (-0.7 °C) and it grows in spring (+1.3 °C) and summer (+2.6 °C).



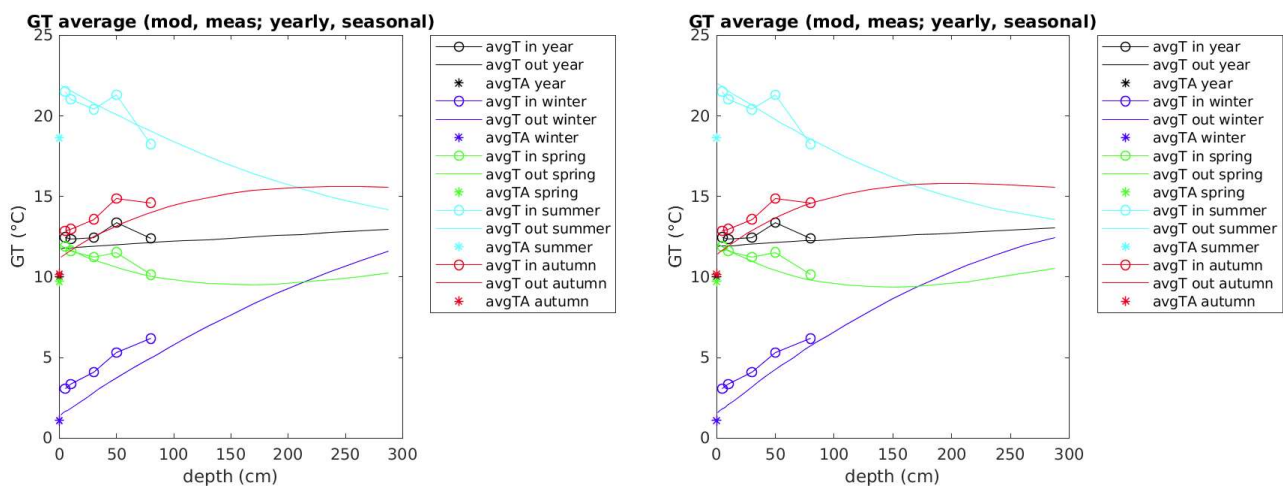
Figures 6-8: Seasonal and yearly average GT vs depth, modelled and measured.  $\lambda_m$ :  
 0.5  $\text{W/m} \cdot \text{K}$  (left panel), 2.3  $\text{W/m} \cdot \text{K}$  (right panel)

The action of the  $\lambda_m$  can be observed from the graphs. A conductivity as low as 0.5 is clearly unable to transmit into depth the influence of the air temperature. The result, in depth, is very low summer GT and very high winter ones. On the other hand, a value like 2.3 is responsible for elevated heat transmission, leading summer GT to very high values. A value between 1.4 and 1.8 could reproduce

correctly the shape of the GT-depth curves. Like for  $c_m$ ,  $\lambda_m$  's effect on runoff and ET is negligible, if compared to the influence of  $rg$  on these two quantities. As explained in section 4.5.4.1, the  $\lambda_m$  values here obtained are hardly comparable to the ones found in literature. This is due on one hand to the fact that literature values refer to the bulk thermal conductivity, whereas SNOWPACK requires as input the thermal conductivity of the dry compacted soil. On the other hand, even if bulk values were to be compared, this model would still need much greater values to produce a good fitting with the observed data.

### SOLID FRACTION

Porosity is here studied, by changing the value initially assigned to the solid fraction. Three values are tested: 0.40; 0.55 (initial); 0.70. The lowest and highest are represented below, in Figures 6-9.



Figures 6-9: Seasonal and yearly average GT vs depth, modelled and measured.

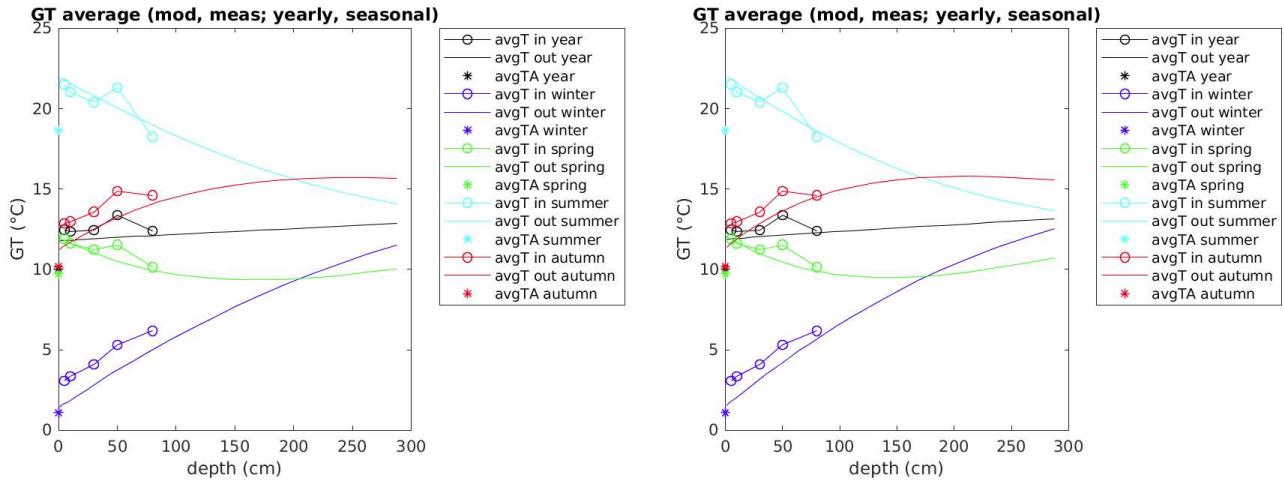
Solid fraction: 0.40 (left panel), 0.70 (right panel)

From the figures, the solid fraction does not affect GT as much as the previous parameters do. Increasing the solid fraction to 0.70, the GT gradients grow, especially in summer and winter. This can be due to the smaller quantity of water that, infiltrating, can contribute to the heat transfer.

The GT gradients are better simulated by a solid fraction close to 0.55 (porosity = 0.45), which is the one associated with loam in literature. ET and runoff do not undergo any variation.

## DENSITY

Density  $\rho_m$  (kg/dm<sup>3</sup>) of the dry compacted soil is analyzed, by testing the values: 2000; 2600 (initial); 3200. Results from the lowest and highest are represented below, in Figures 6-10.



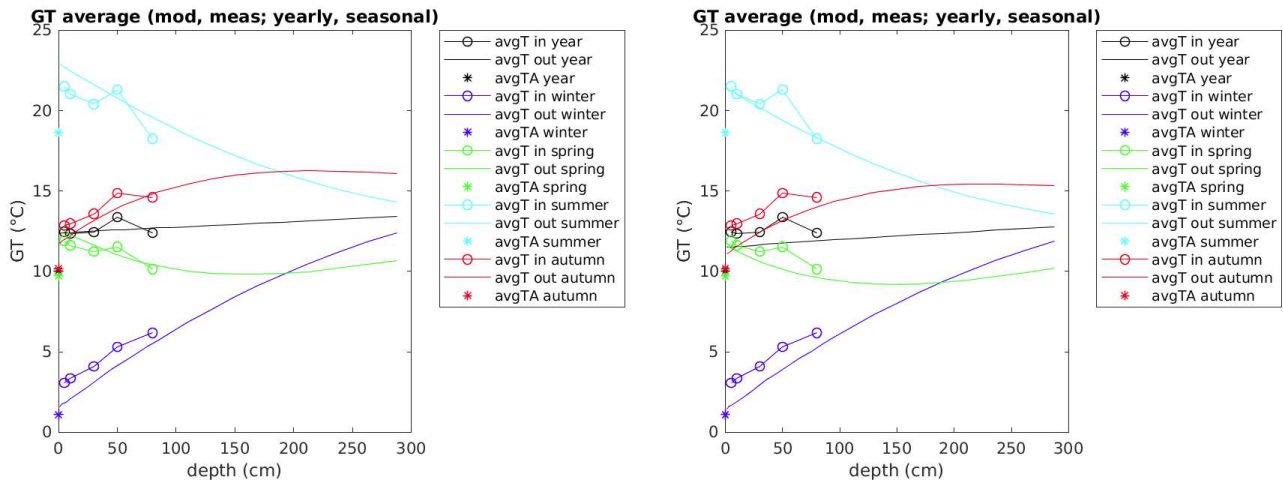
Figures 6-10: Seasonal and yearly average GT vs depth, modelled and measured.

Dry compacted density: 2000 kg/dm<sup>3</sup> (left panel), 3200 kg/dm<sup>3</sup> (right panel)

Higher density causes a bigger GT gradient, which can be due to the increase in specific heat capacity. The slope of the GT curve is better simulated by 2600, which is also a more physical value for the soil under study, based on the bulk density values listed by Joint Technical Committee (2016), who assign a bulk density of 1430 kg/dm<sup>3</sup> to loamy soils. The ET and runoff do not prove affected by density changes.

## ROUGHNESS LENGTH

The soil roughness length  $z_0$  (m) is evaluated, through the following values: 0.005; 0.02 (initial); 0.05. Average GT relative to the lowest and highest values are displayed in Figures 6-11.



Figures 6-11: Seasonal and yearly average GT vs depth, modelled and measured.  
 Roughness length: 0.005 m (left panel), 0.05 m (right panel)

As  $z_0$  increases from 0.005 to 0.05, temperatures get lower by 1 °C in autumn and spring and by 2 °C in summer. Higher turbulent fluxes associated with a  $z_0$  increase, lead to heat dissipation and lower temperatures in the warm months of the year.

The original value of 0.02 m represents a good compromise to well represent all the seasons and provides the best RMSE. It must be reminded that these simulations do not include any canopy, so the value 0.02 m, associated in literature to “flat terrain with grass or very low vegetation” (see Table 4-2), is chosen also to mimic the presence of a low grass cover.

The main goal of the  $z_0$  tests is to verify the applicability of different roughness lengths to simulate the presence of canopy and its effect on ET. The modelled ET is affected only little by  $z_0$ : in fact, modelled ET decreases by 0.05 kg/m<sup>2</sup>·d when passing from 0.005 m to 0.05 m. Although apparently small, this variation in ET is of the same order of magnitude as the one obtained after the introduction of canopy in section 6.4. This is a satisfying result, which allows to possibly neglect the implementation of a canopy module when the vegetation is sufficiently low. Further investigations can be realized on the role of roughness length as a mathematical tool to account for low canopy presence.

## SOIL ALBEDO

To select the correct value for soil albedo, the first approach is to evaluate the Outgoing Short Wave Radiation (OSWR). The modelled values are compared to the field dataset and their difference is computed. When the average difference reaches the value of zero, a realistic soil albedo is being used. By following this method, the value 0.21 is identified. However, as visible in Figure 6-12, the gap between measured and observed OSWR can easily reach the order of 100 W/m<sup>2</sup>, while the OSWR absolute values range between 50 and 200 W/m<sup>2</sup>. These high variations imply a low certainty on the measures and on the correctness of the simulation. For this reason, more importance is assigned to the typical albedo values displayed in Table 3-2 and the soil albedo is set to 0.17. This new value produces an average difference between measured and modelled OSWR of only 5.8 W/m<sup>2</sup>, a small amount if compared to the high mentioned variations.

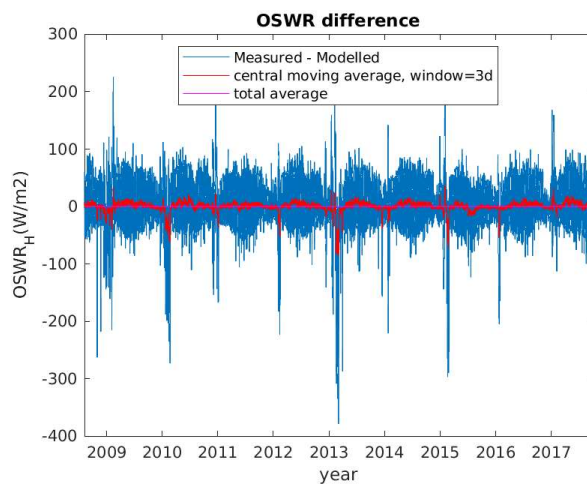


*Figure 6-12: Difference between measured and modelled OSWR and its average. Soil albedo: 0.21*

In conclusion, 0.21 simulates slightly better GT in summer, but overall the RMSE is the same as with 0.17. Runoff and ET modelled values are affected very little by the soil albedo compared to the effect of the first factors analyzed in this section.

## 6.2 Richards equation

Richards equation is the infiltration model utilized for the simulations present in this section. A sensitivity analysis is carried out, structured in the same way as in section 6.1, with the addition of an

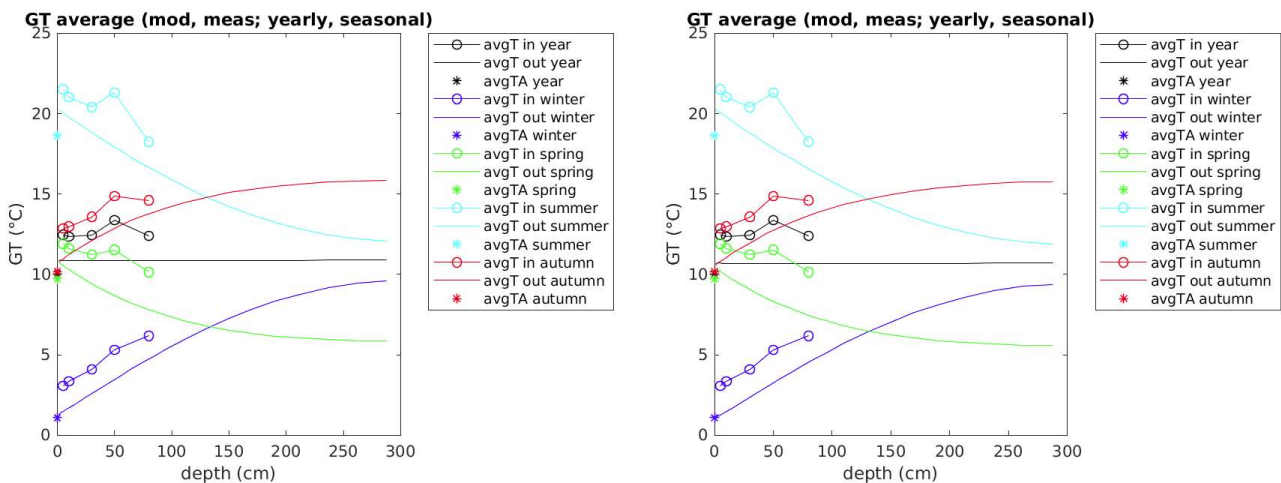
evaluation of the liquid water content reproduction. When the results are similar or equivalent to the ones obtained with the Bucket model, reference will be made to them, without reporting further figures or numbers. The initial parametrization, reference for all tests in this section, is the following one: Soil type: loam ; Specific heat capacity  $c_m$ : 1400 J/kg·K ; Thermal conductivity  $\lambda_m$ : 1.4 W/m·K ; Solid fraction: 0.55 ; Density  $\rho_m$ : 2600 kg/dm<sup>3</sup> ; Roughness length  $z_0$ : 0.02 m ; Soil albedo: 0.17 ; Soil emissivity: 0.98 .

## SOIL EVAPORATION METHOD

As a first step, the two soil evaporation approaches described in section 4.4 are compared:

- Evaporation Resistance (ER)
- Relative Humidity (RH)

Figures 6-13 show moderate GT changes, even though when looking at the RMSE at 80 cm, the better modelling is produced with ER, which has an RMSE = 1.72 against the RMSE = 1.97 of RH. In fact, GT is slightly higher with ER than with RH.

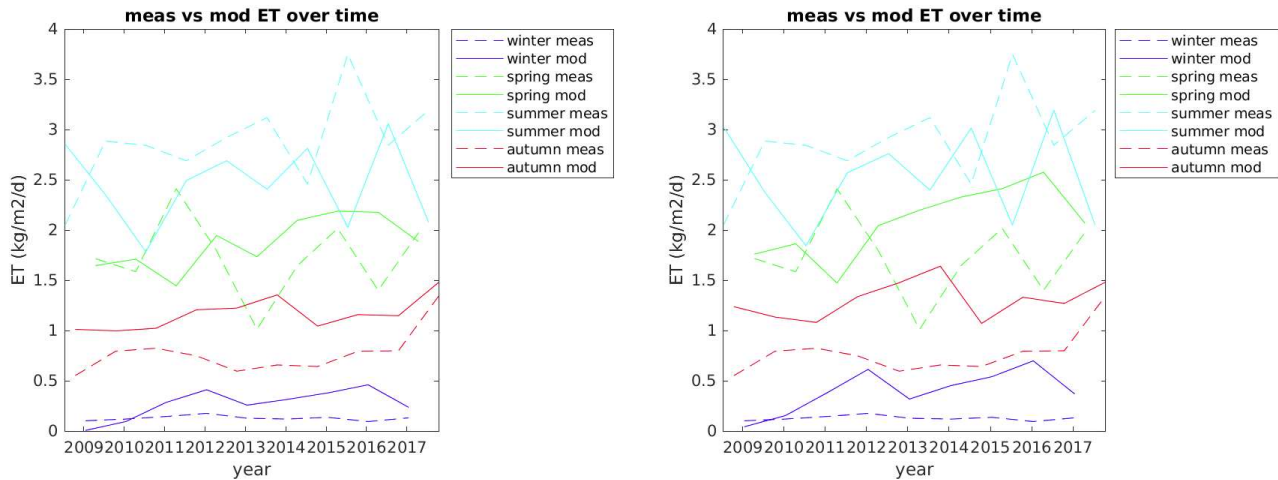


*Figures 6-13: Seasonal and yearly average GT vs depth, modelled and measured. Soil evaporation methods: ER (left panel), RH (right panel)*

In this section, canopy is not present within SNOWPACK simulations. Nonetheless, the modelled ET brought by the soil only is higher than the measurements in all seasons except for summer, both with ER and RH (Figures 6-14). RH overestimates ET more than what ER does, while in summer they

reproduce almost the same values. The average difference between the measured and the simulated ET over the historical series is  $-0.043 \text{ kg/m}^2\cdot\text{d}$  with ER and  $-0.181 \text{ kg/m}^2\cdot\text{d}$  with RH.

This behavior is completely different than what is observed with the Bucket model. In fact, the rapid infiltration and consequent drying out seen for RH in section 6.1 does not occur at all with the Richards equation, which is able to maintain the top layers humid enough to simulate ET with the correct order of magnitude.



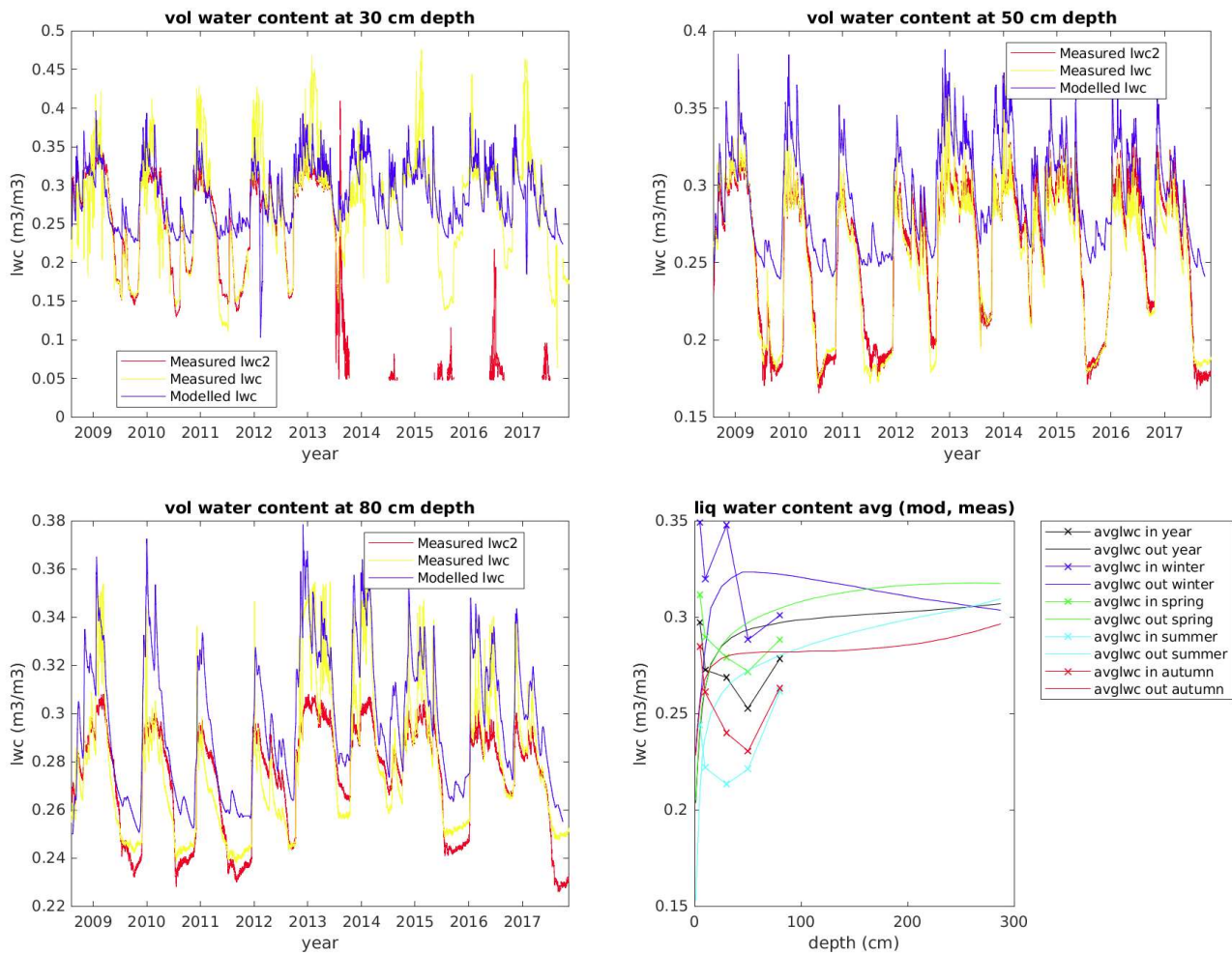
*Figures 6-14: Seasonal average ET vs time, modelled and measured. Soil evaporation methods: ER (left panel), RH (right panel)*

Once more, ET and GT are related. With the ER method, ET is overestimated less than with RH; consequently, the temperatures appear slightly higher and closer to the measurements.

As far as the runoff goes, its average value is lightly higher with ER ( $0.076 \text{ kg/m}^2\cdot 3\text{h}$ ) than with RH ( $0.061 \text{ kg/m}^2\cdot 3\text{h}$ ). The difference in the two quantities is exactly equal to the difference existing in ET, which is coherent from a water mass balance point of view.

Assessing soil moisture, its reproduction with ER and RH is practically the same, with RMSE differing by a maximum of 0.006 at 50 cm. In Figures 6-15 below, some plots relative to the ER method are reported. The first three figures show the LWC trend at different depths over the historic series, comparing measured and modelled data. The fourth figure proposes the average values separated by season. As can be seen from the plots, there are two sensors measuring soil moisture in the station of Payerne.

The two data sets are not completely consistent with one another, leading to remarkable uncertainty on these measures.



Figures 6-15: Soil moisture vs time, modelled and measured. Depth: 30 cm (top left panel), 50 cm (top right panel), 80 cm (bottom left panel). Seasonal and yearly average soil moisture vs depth, modelled and measured (bottom right panel)

At 30 cm, the modelled LWC is less stretched than the measurements. At 50 cm and 80 cm, the general trend sees the modelled LWC higher both in summer and winter months. In the bottom-right figure, the input LWC is the one represented in yellow in the other plots.

The main tool to evaluate LWC modelling is the RMSE. Its values, for ER, are: 0.06 (30 cm), 0.05 (50 cm), 0.02 (80 cm). They are the proof of a good match between modelled and measured data.

## SOIL TYPE

Out of the 14 soil classes available in the SNOWPACK code, 5 are tested here, chosen based on their differing field capacity. They are reported in Table 6-1, together with the values of  $\theta_{fc}$  and  $\theta_s$  found in the Rosetta soil classification.

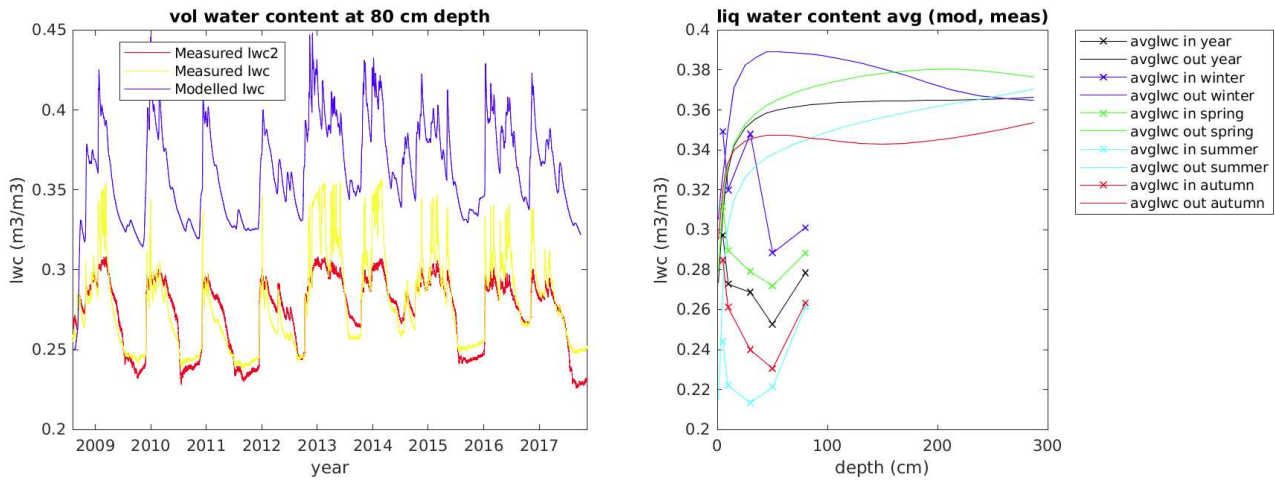
*Table 6-1: The tested soil types, reported with their characteristics and results*

Soil type	Silty clay	Loam	Sandy loam	Loamy sand	Sand
$\theta_{fc}$	0.452	0.262	0.205	0.171	0.132
$\theta_s$	0.481	0.399	0.387	0.390	0.375
Runoff (kg/m <sup>2</sup> ·3h)	0.077	0.076	0.106	0.137	0.218
Difference in ET (kg/m <sup>2</sup> ·d)	-0.069	-0.043	0.011	0.214	0.813

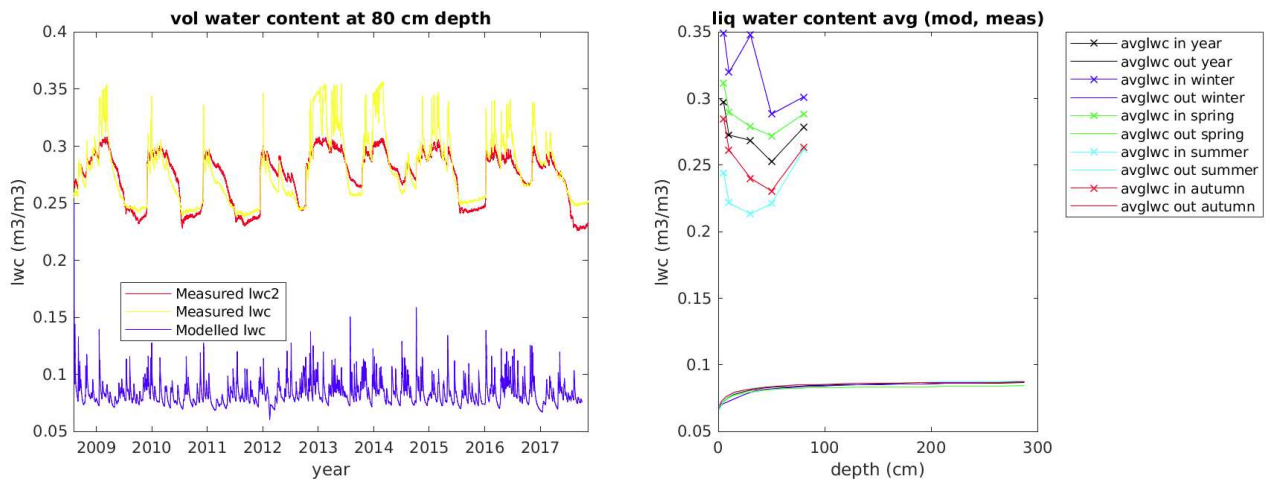
The effect on GT is modest: the comparison between the finest and the loosest of the 5 soil types only shows a small difference in summer. With silty clay, the RMSE at 80 cm is equal to 1.70, while for sand it is equal to 1.83. This gap is quite small, considering the remarkable difference in grain size and field capacity between the two soil types. Since from the average GT plots almost no difference can be spotted, such plots are not reported here.

It has been said how the soil type loam overestimates the ET. Silty clay, having a higher  $\theta_{fc}$ , has an even more pronounced effect. Sandy loam, with a very close  $\theta_{fc}$ , behaves like loam. On the other hand, sand produces an ET modelling extremely low for summer and spring seasons, due to the low value of field capacity. In turn, the runoff consequently appears much increased.

A further demonstration of the consequences of the soil type choice with its relative field capacity comes from the analysis of the liquid water content. Simulating the soil as silty clay, the modelled LWC overestimates the measurements by a considerable quantity, as shown in Figures 6-16. The RMSE is equal to 0.10 for depths from 30 to 80 cm. The opposite scenario is a sandy soil, for which the LWC is greatly underestimated, as revealed by both Figures 6-17. Here, the RMSE is as high as 0.20.



Figures 6-16: Silty clay. Soil moisture vs time, modelled and measured, depth: 80 cm (left panel). Seasonal and yearly average soil moisture vs depth, modelled and measured (right panel)



Figures 6-17: Sand. Soil moisture vs time, modelled and measured, depth: 80 cm (left panel). Seasonal and yearly average soil moisture vs depth, modelled and measured (right panel)

Interesting observations can be made with respect to the soil moisture sensitivity to most parameters' variations. Changes in the evaporation method or, as it will be exposed in section 6.4, in the canopy parameters' values, which in turn affect significantly the ET, do not bring relevant modifications to the LWC. Average variations are always in the order of thousandths, on an LWC scale from 0 to 1, sometimes

reaching 0.01. On the contrary, the oscillations observed in both measured and modelled LWC data reach values such as 0.1 - 0.2. The soil type selection is found to be the only variable capable of bringing a bigger change onto LWC, in the order of hundredths. Higher LWC variations are observed in the superficial layers rather than in deep ones, due to the more direct influence that water losses by evaporation can have on the water content in this zone. From a water dynamics point of view, this limited effect on LWC can be explained with runoff: in a simulated soil where the ET is lower than in another one, the net water surplus does not accumulate in the soil pores; instead, it moves down the soil column and accelerates the rate at which runoff is produced.

### **SPECIFIC HEAT CAPACITY**

The same values tested with Bucket are tried here, leading to the same conclusions. An intermediate value between 1000 J/kg·K and 1400 J/kg·K is acceptable, because suitable to reproduce correctly the shape of the measurements curve. The latter is chosen because of its good RMSE (0.15 - 0.3 better than with 1000). It can be said that  $c_m$  affects in a relevant way neither the runoff nor the ET, while it does not affect at all the LWC.

### **THERMAL CONDUCTIVITY**

The same values compared in the Bucket section are tested here, driving to equivalent conclusions. Both 1.4 W/m·K and 1.8 W/m·K provide a good shape, from a visual and statistical comparison. As for  $c_m$ , the effect of  $\lambda_m$  on runoff and ET is negligible, if compared to the influence of  $rg$  on these two quantities. With respect to LWC, conductivity changes create no influence.

### **SOLID FRACTION**

Changes in solid fraction, therefore in porosity, have absolutely no influence on any output parameter. In fact, as reported in Table 4-1, once a soil type is selected, all the van Genuchten values for the water retention curve are automatically imposed by SNOWPACK. Among these, there is  $\theta_s$  (saturated water content). The soil fraction is computed solely in function of this value.

## DENSITY

The same values tested with the Bucket model are compared here, and the same considerations can be developed.  $2600 \text{ kg/dm}^3$  is chosen as value for the dry compacted soil density, because of its capacity to well simulate the slope of the GT curve and its physical basis. ET, runoff and LWC do not prove affected by density changes.

## ROUGHNESS LENGTH

Four roughness length  $z_0$  (m) values are tested: 0.002; 0.005; 0.02 (initial); 0.05. Referring to Table 4-2 by Davenport, the best results as far as GT simulation are here obtained with values from the category “smooth”, precisely 0.002 and 0.005 m: these refer to a featureless land or ice. On the other hand, the set of measurements comes from a real scenario characterized by a grass coverage (category “open”: values like 0.02 and 0.05 m). It is clearly erroneous to rely on unrealistic and low  $z_0$  values for a good GT fitting.

As already noticed in the Bucket model simulations, low values (0.002 in this case) lead to a big increase in GT in the period that goes from April to September, with a peak increase of  $1 \text{ }^\circ\text{C}$  in the summer months (with respect to the simulations run with  $z_0 = 0.02 \text{ m}$ ). No variations are observed in LWC.

## SOIL ALBEDO

The average difference between modelled and observed OSWR is almost the same as with Bucket. Following the same reasoning, the value of 0.17 is confirmed, as in the Bucket simulations. Setting 0.21 produces slightly lower GT, making the overall RMSE worse by up to 0.2. Runoff, ET and LWC are not affected by albedo changes.

## 6.3 Discussion

With both infiltration models, the best modelling is achieved with the Evaporation Resistance method, able to reproduce in a realistic way GT and ET. When possible, parameters' values are chosen based on literature studies; in the remaining cases, they are identified through a visual analysis of the results

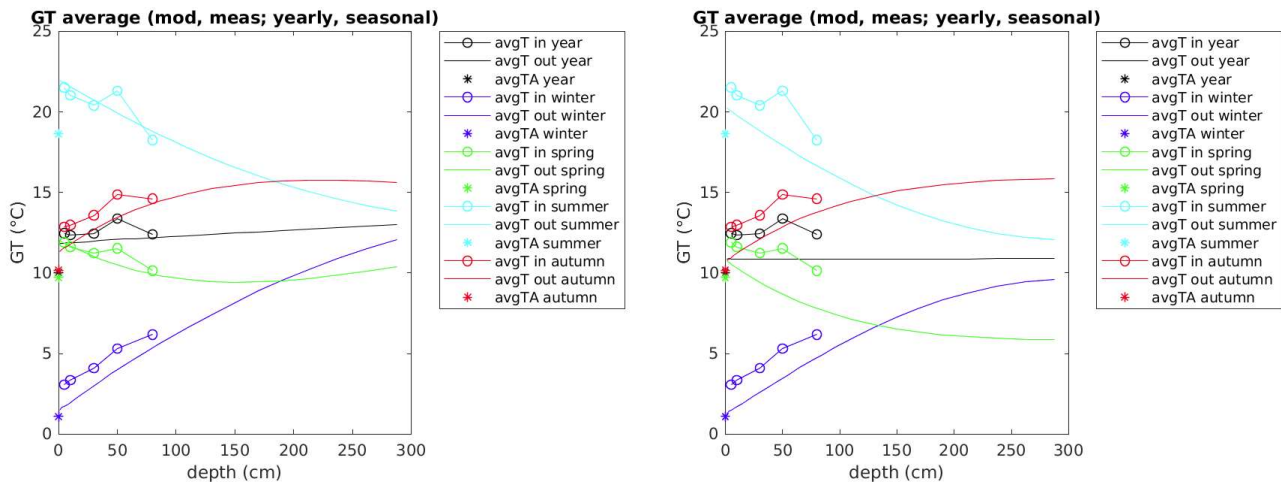
produced by the model together with the measurements. Regarding the thermal parameters, one must rely on the range of values proposed in the analysis, since it is hard to select the best absolute values of  $\lambda_m$  and  $c_m$ . In fact, the efficiency in simulating GT varies greatly according to the season. Besides, being the surface GT very dependent on the soil evaporation method, the selection of one or the other method can lead to a different choice of best values of  $\lambda_m$  and  $c_m$ .

The final soil parametrization obtained after the sensitivity analysis is summarized in Table 6-2. It is valid for both infiltration models and relative to the Evaporation Resistance method.

Table 6-2: Final soil parametrization

$rg$ (mm)	$c_m$ (J/kg·K)	$\lambda_m$ (W/m·K)	porosity	density (kg/dm <sup>3</sup> )	$z_o$ (m)	albedo
2.5	1400	1.4	0.45	2600	0.02	0.17

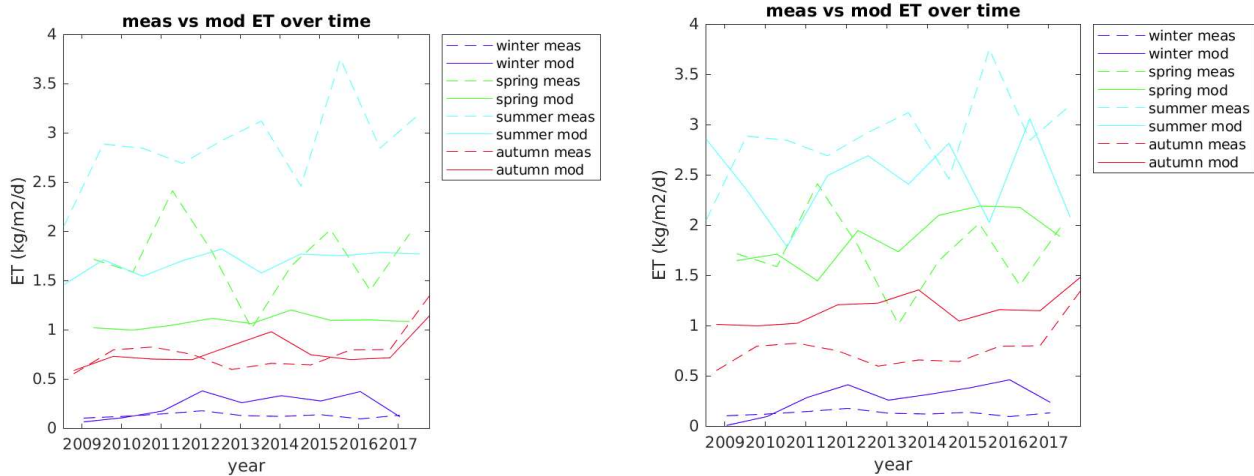
The choice of the water infiltration model greatly impacts SNOWPACK’s output for all the four studied quantities. GT, for instance, is simulated remarkably better with the use of the Bucket model, with which the difference between observed and modelled data is reduced. This is particularly true in the warmer months (summer in primis, spring and partially autumn) and to a less extent in winter and autumn. On the other hand, Richards tends to underestimate GT by no less than 1-2 °C in all seasons, as displayed in Figures 6-18.



Figures 6-18: Seasonal and yearly average GT vs depth, modelled and measured.

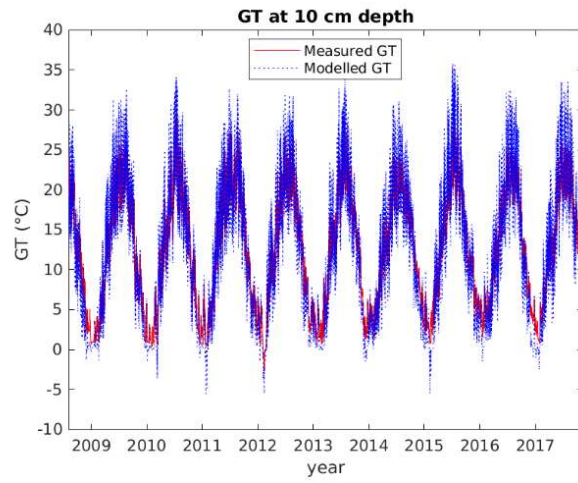
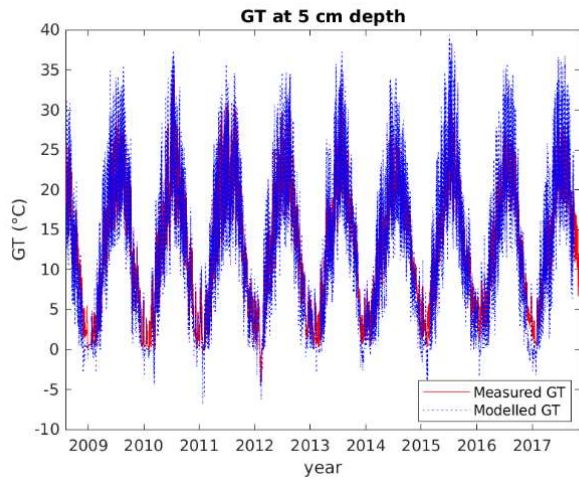
Final soil parametrization with: Bucket, ER (left panel), Richards, ER (right panel)

Having to respect the soil water mass balance, ET and runoff are mathematically complementary. It is found that they both depend largely on the infiltration model. Richards equation is the most physically based tool to describe soil water dynamics, hence a more accurate ET is simulated with it. The simple Bucket model highly underestimates the real ET, reaching only about 68% of it. In Figures 6-19 the average ET produced by the two models in each season is represented.

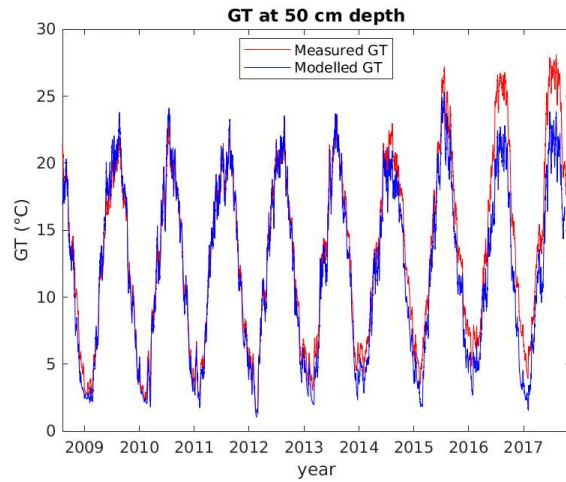
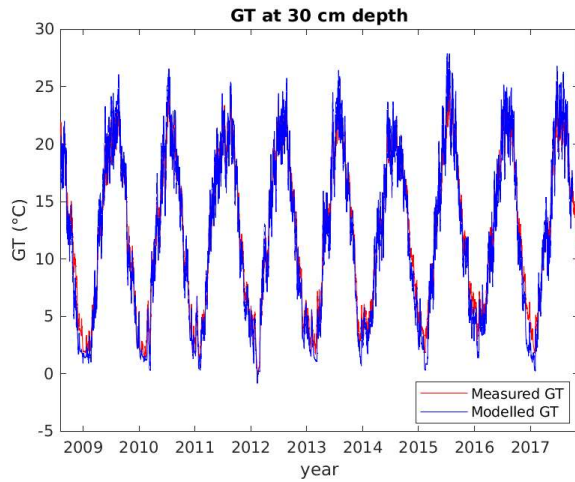


*Figures 6-19: Seasonal average ET vs time, modelled and measured. Final soil parametrization with: Bucket, ER (left panel), Richards, ER (right panel)*

The entire time series of modelled and measured GT is presented, for each depth, from Figures 6-20 to Figure 6-22. The plots refer to the configuration with the Bucket model and the ER method, proven to be the best setting for GT reproduction. The soil parametrization is the one exposed in Table 6-2. From these graphs, the satisfying fitting obtained in spring and summer and the underestimation of GT occurring in autumn and winter can be observed. Annual and monthly variations are overall well captured. The anomalous GT increase measured at 50 cm depth in the last three years is associated to the gradient change seen in the average measured GT of Figures 6-18.



Figures 6-20: Modelled and measured GT vs time. Depth: 5 cm (left panel), 10 cm (right panel)



Figures 6-21: Modelled and measured GT vs time. Depth: 30 cm (left panel), 50 cm (right panel)

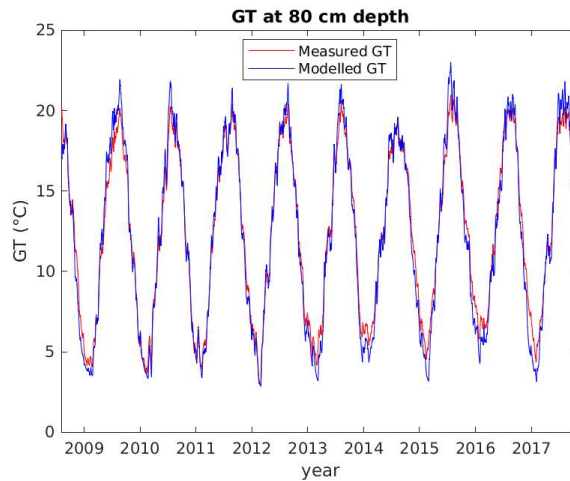


Figure 6-22: Modelled and measured GT vs time. Depth: 80 cm

## 6.4 Canopy module

So far, all simulations described have been run without the canopy module. This section aims at assessing the sensitivity of GT, ET and LWC to variations in the parameters describing the vegetation. In order to synthesize this analysis, the results coming from simulations run with different configurations (infiltration model, soil evaporation method) are put together. The goal is to understand, in general, which canopy parameters affect the most the model output and to quantify this influence.

### 6.4.1 Canopy module implementation

The analysis begins with the comparison between a no canopy scenario and one where canopy is included. The one-layer canopy module is implemented due to the nature of the vegetation, which corresponds to low grass in all sites. The two-layer canopy module is not suitable here, because developed for forest systems. The results are in some cases divided by configuration and by season because for many quantities the sensitivity depends a lot on the season the focus lies upon. The values reported in Table 6-3 refer to GT changes at 80 cm depth. Such quantity is considered representative because the GT-depth curves shift in their entirety, while GT gradients remain constant.

As canopy is here introduced, its parameters are set to values that are supposed to simulate grass. These are: canopy height = 0.5 m; canopy leaf area index (LAI) = 1.5; canopy direct throughfall (DT) = 0.6; canopy albedo = 0.25; root depth = 0.2 m.

Table 6-3: Effect of canopy implementation on GT at 80 cm depth

Effect of canopy introduction on GT	Winter	Spring	Summer	Autumn
Bucket, ER	-0.4 °C	-1.2 °C	-1.2 °C	-1.0 °C
Bucket, RH	-0.1 °C	-0.7 °C	-0.4 °C	-0.3 °C
Richards, ER	-0.4 °C	-1.0 °C	-1.3 °C	-1.0 °C
Richards, RH	-0.4 °C	-1.0 °C	-1.1 °C	-1.0 °C

In all scenarios, a GT decrease occurs for all seasons. Results from the first, third and fourth configuration are consistent with one another, pointing spring, summer and autumn as the most affected seasons. Only Bucket RH temperatures have a significantly lower dependence on the presence of canopy. This overall reduction of GT makes the prediction worse for the Bucket, ER configuration (RMSE at 80 cm = 1.33) and much worse for the Richards ones, which were already marked by low GT modelling. On the contrary, such decrease benefits Bucket, RH, which has however been identified as an unrealistic configuration.

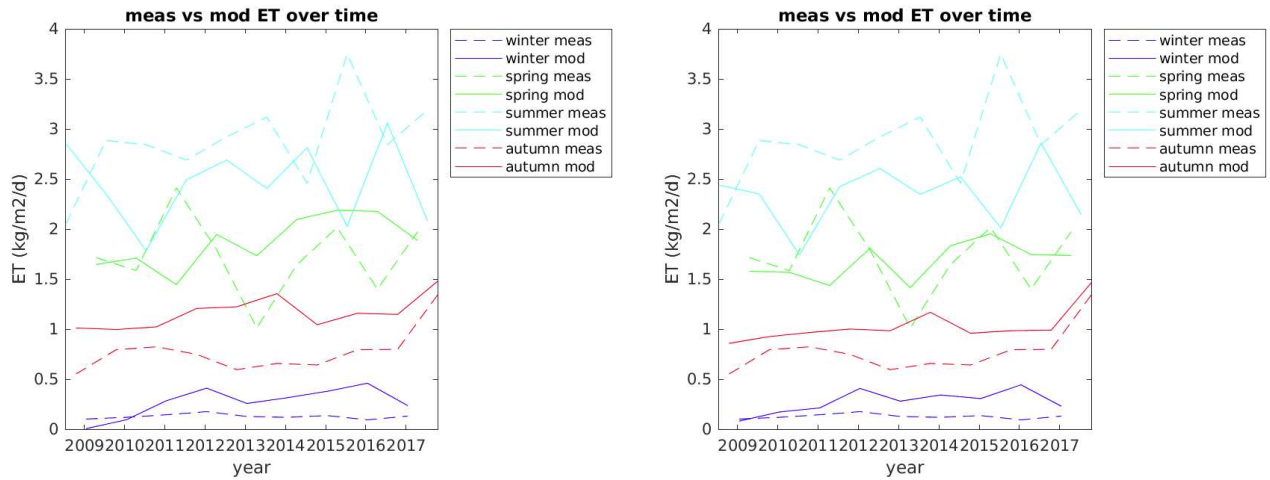
Regarding ET, canopy's effect is not the same for ER and RH: statistics are reported in Table 6-4. With the Bucket model, modelled ET sees an increase in spring and mostly summer, bringing closer modelled and measured data. However, with the Richards equation, introducing canopy lowers the ET, especially in spring, summer and autumn. This makes the fitting better for spring and autumn but worse for summer, making the last column's values difficult to interpret.

Table 6-4: Effect of canopy implementation on average difference in ET

Difference in ET (kg/m <sup>2</sup> ·d)	No canopy	With canopy	Change in difference in ET
Bucket, ER	0.44	0.39	-0.05
Bucket, RH	1.24	1.09	-0.15
Richards, ER	-0.04	0.06	+0.10

Richards, RH	-0.18	-0.06	+0.12
--------------	-------	-------	-------

Figures 6-23 show the drastic reduction in modelled ET when canopy is added. The plot refers to the Richards, ER configuration.



Figures 6-23: Seasonal average ET vs time, modelled and measured. Richards, ER.

Canopy OFF (left panel), ON (right panel)

LWC is not affected by the implementation of canopy. Anticipating the results of further simulations, it can be said that none, among the studied parameters, has a significant influence on the modelled LWC at depths equal to and below 30 cm. The observed variations in LWC are of the order of thousandths on a scale where 1 represents saturation. Compared to other significant results, this one can be considered negligible for the current study.

Here the sensitivity analysis on the canopy parameters begins, and two remarks must be made. The first one regards some issues encountered while testing different sets of parameters. GT anomalies were obtained in various simulations: GT would suddenly be modelled with extremely high and unrealistic values, exceeding measurements by up to 10 °C. The latent heat  $q_l$  and the sensible heat  $q_s$  leaving the soil in summertime would decrease from peaks of 300 W/m<sup>2</sup> to peaks of 100 W/m<sup>2</sup> and 20 W/m<sup>2</sup> respectively. This behavior was found with all the four configurations, both with one and two-layer canopy. It was not possible to associate it to a specific set of values. However, it was noted that low canopy heights (< 0.5 m) and high values of Direct Throughfall (> 0.7) were often the cause of such

anomalies. For this reason, canopy height simulations were limited to values above the initial one of 0.5 m. The reason behind this issue was found to be related to the variables describing the atmospheric stability, which go under the name of  $psi_m$  and  $psi_s$  in the SNOWPACK code. Further investigation is necessary if the canopy module wants to be implemented in the modelling of grassland.

All the next comparisons will exclude the configuration Richards, RH because of its high similarity in results to Richards, ER. Besides, the results on ET with Bucket, RH will be neglected because of their very low and unrealistic values.

#### 6.4.2 Canopy height

The first of the parameters to be checked is the canopy height. This varies from the original value of 0.5 m to 0.9 m. These are values that correspond to the ones normally associated with grass; if bushes or trees were to be modelled, higher values of canopy height would be needed. Besides, the use of the two-layer canopy model would be suggested. Table 6-5 shows that increasing height produces lower GT and that such effect is more visible in the warm months of the year. Again, the GT gradients remain quite constant.

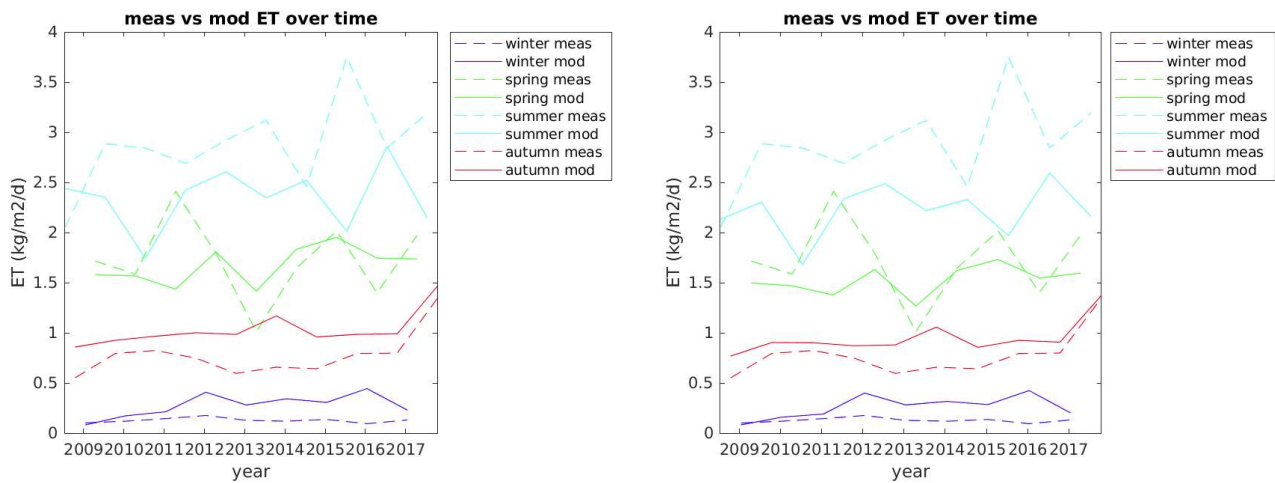
*Table 6-5: Effect of canopy height change (from 0.5 m to 0.9 m) on GT at 80 cm depth*

Effect of increasing canopy height on GT	Winter	Spring	Summer	Autumn
Bucket, ER	-0.1 °C	-0.4 °C	-0.4 °C	-0.3 °C
Bucket, RH	-0.1 °C	-0.5 °C	-0.5 °C	-0.4 °C
Richards, ER	-0.1 °C	-0.3 °C	-0.3 °C	-0.2 °C

This time, ET changes are consistent between the different configurations: a decrease in ET is observed, more evident with Richards than with Bucket (Table 6-6) and more pronounced in the warm months of the year. Figures 6-24 show this behavior relative to the configuration Richards, ER.

Table 6-6: Effect of canopy height change (from 0.5 m to 0.9 m) on average difference in ET

Difference in ET (kg/m <sup>2</sup> ·d)	Height = 0.5 m	Height = 0.9 m	Change in difference in ET
Bucket, ER	0.39	0.44	+0.05
Richards, ER	0.06	0.15	+0.09



Figures 6-24: Seasonal average ET vs time, modelled and measured. Richards, ER.  
Canopy height: 0.50 m (left panel), 0.90 m (right panel)

SNOWPACK computes the evapotranspiration as three components: Canopy Evaporation, Canopy Transpiration, Soil Evaporation. These are averaged throughout the whole timeseries and transferred to tables presented for each canopy parameter.

With the described canopy height change, the overall ET passes from 1.33 kg/m<sup>2</sup>·d to 1.25 kg/m<sup>2</sup>·d (Richards, ER). The quantity showing a reduction is the Soil Evaporation, as displayed in Table 6-7. This can be due to a greater shading created by higher vegetation; a similar behavior has been noticed assessing roughness length increases in sections 6.1 and 6.2.

*Table 6-7: Partitioning of ET before and after canopy height change (from 0.5 to 0.9 m)*

Richards, ER: partitioning of ET (kg/m <sup>2</sup> ·d)	Canopy Evaporation	Canopy Transpiration	Soil Evaporation
Canopy height 0.5 m	0.11	0.21	1.01
Canopy height 0.9 m	0.11	0.22	0.92

#### 6.4.3 Canopy Leaf Area Index

Following, the influence of the Leaf Area Index is assessed. The tested values go from 1 to 4, a range that is coherent with the tested canopy heights (Byrne et al., 2007). As indicated in Table 6-8, the LAI effect on GT is more marked in summer, and secondly in spring and autumn. Here as well, variations in LAI cause a shift of the GT-depth curves and not a change in gradient.

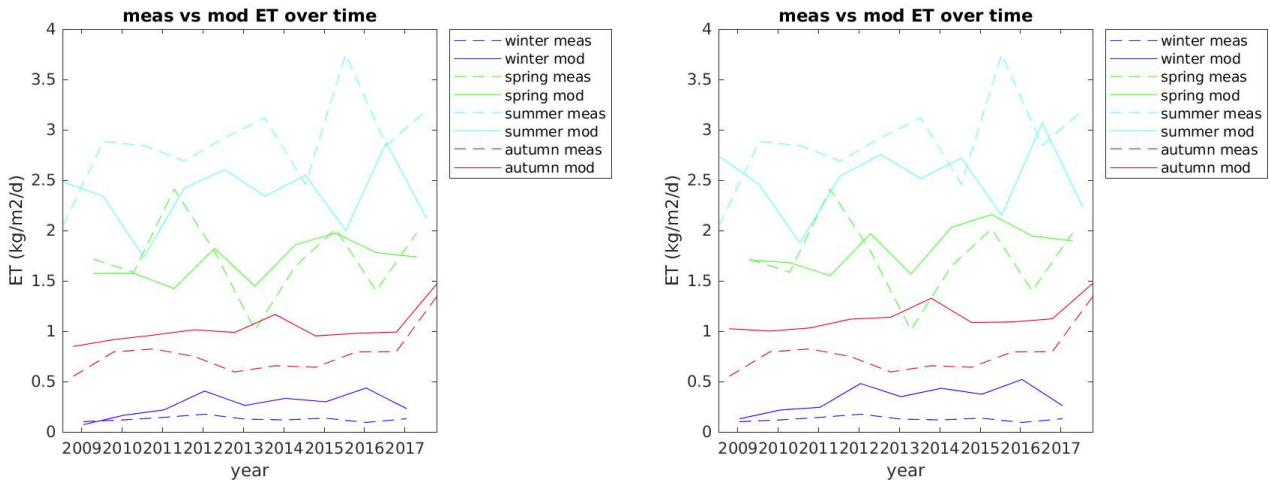
*Table 6-8: Effect of canopy LAI change (from 1 to 4) on GT at 80 cm depth*

Effect of increasing LAI on GT	Winter	Spring	Summer	Autumn
Bucket, ER	-0.1 °C	-0.5 °C	-0.8 °C	-0.5 °C
Bucket, RH	-0.1 °C	-0.5 °C	-0.8 °C	-0.5 °C
Richards, ER	-0.1 °C	-0.3 °C	-0.5 °C	-0.3 °C

Going from a low LAI of 1 to a high value like 4, ET increases substantially for both configurations (Table 6-9). The behavior is more visible in summer, then in spring and finally in autumn, as illustrated in Figures 6-25 (Richards, ER). The rise in ET is directly related to the decrease in temperatures, especially in those seasons where ET is higher, such as summer. These results confirm the theory under which a greater loss of latent heat under the form of evapotranspiration provokes significant lowering in GT at all depths.

Table 6-9: Effect of canopy LAI change (from 1 to 4) on average difference in ET

Difference in ET (kg/m <sup>2</sup> ·d)	LAI 1	LAI 4	Change in difference in ET
Bucket, ER	0.44	0.17	-0.27
Richards, ER	0.06	-0.06	-0.12



Figures 6-25: Seasonal average ET vs time, modelled and measured. Richards, ER. Canopy LAI: 1 (left panel), 4 (right panel)

The overall ET goes from 1.33 kg/m<sup>2</sup>·d to 1.46 kg/m<sup>2</sup>·d (Richards, ER). As expected from a leaf area increase, evaporation and most of all transpiration by canopy increase substantially. Differently, evaporation from the soil decreases, as illustrated in Table 6-10. This might be due to a lack of soil moisture in the most superficial layers, following the absorption of more water by the vegetation.

Table 6-10: Partitioning of ET before and after canopy LAI change (from 1 to 4)

Richards, ER: Partitioning of ET (kg/m <sup>2</sup> ·d)	Canopy Evaporation	Canopy Transpiration	Soil Evaporation
LAI 1	0.08	0.13	1.12
LAI 4	0.17	0.51	0.78

#### 6.4.4 Canopy Direct Throughfall

Next, the effect of Direct Throughfall (DT) is evaluated. The range of tested values goes from 0.45 to 0.90, a relatively wide one, considering that DT should be limited to values above 0.6 - 0.7 if only grass cover were considered (Corbett et Crouse, 1968). These authors also suggest that a realistic value for grass is DT = 0.85. However, this one could not be implemented systematically because of GT anomalies that were generated with high values of DT.

As displayed in Table 6-11, increasing the DT produces a significant increase of GT, more evident with Bucket and in the warmest months, with a peak in summer. Once more, the GT at every depth are shifted, without gradient variations.

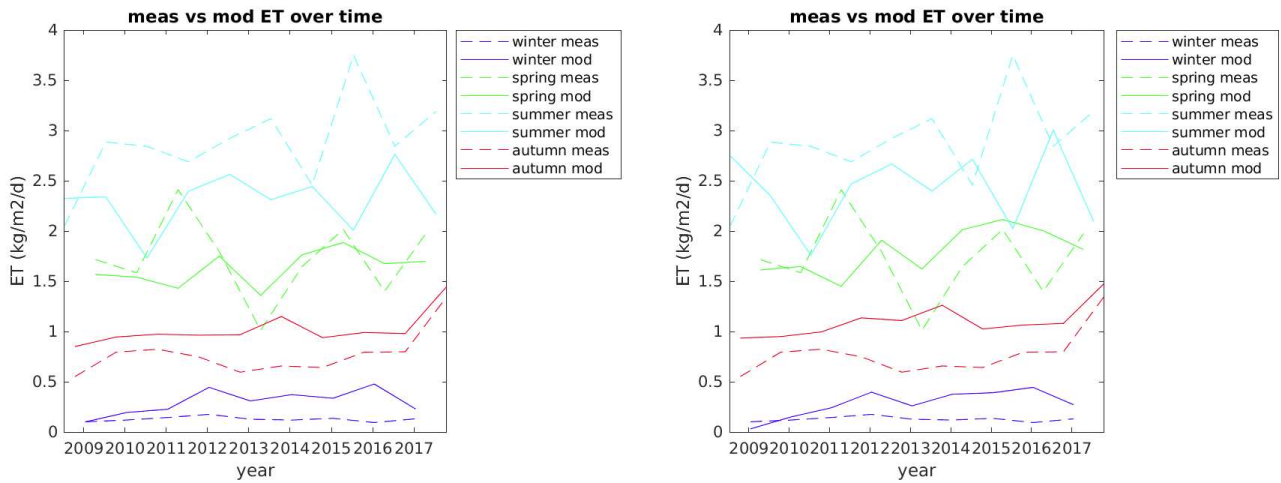
*Table 6-11: Effect of canopy DT change (from 0.45 to 0.90) on GT at 80 cm depth*

Effect of increasing DT on GT	Winter	Spring	Summer	Autumn
Bucket, ER	+0.6 °C	+1.8 °C	+2.5 °C	+1.7 °C
Bucket, RH	+0.6 °C	+1.9 °C	+2.8 °C	+1.9 °C
Richards, ER	+0.6 °C	+1.4 °C	+2.0 °C	+1.5 °C

Assessing ET, it is possible to assist to an increase in spring, followed by a slight one in summer and autumn. The plots showing such variations are found in Figures 6-26 (Richards, ER). With Bucket, this effect is negligible, as indicated by the constant difference in ET (Table 6-12).

*Table 6-12: Effect of canopy DT change (from 0.45 to 0.90) on average difference in ET*

Difference in ET (kg/m <sup>2</sup> ·d)	DT 0.45	DT 0.90	Change in difference in ET
Bucket, ER	0.38	0.39	+0.01
Richards, ER	0.08	0.00	-0.08



Figures 6-26: Seasonal average ET vs time, modelled and measured. Richards, ER. Canopy DT: 0.45 (left panel), 0.90 (right panel)

When DT is increased, the overall ET grows from 1.31 kg/m<sup>2</sup>·d to 1.40 kg/m<sup>2</sup>·d (Richards, ER). Within such growth, there is a remarkable decrease of evaporation and transpiration from canopy, probably associated with its reduced capability of retaining water. On the contrary, soil evaporation undergoes an increase, as shown in Table 6-13.

Table 6-13: Partitioning of ET before and after canopy DT change (from 1 to 4)

Richards, ER: Partitioning of ET (kg/m <sup>2</sup> ·d)	Canopy Evaporation	Canopy Transpiration	Soil Evaporation
DT 0.45	0.12	0.28	0.91
DT 0.90	0.05	0.05	1.30

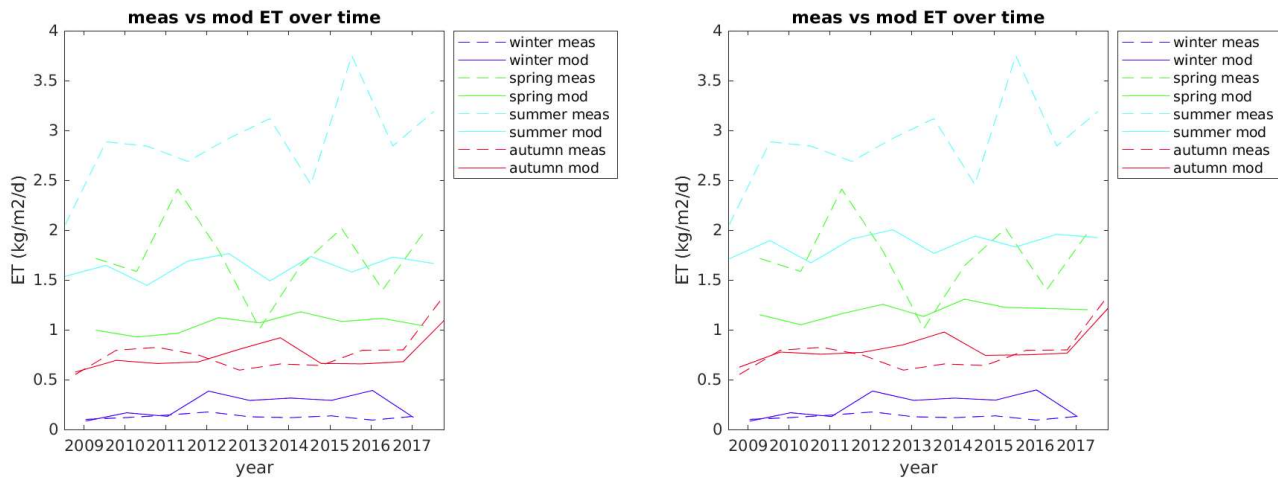
#### 6.4.5 Canopy root depth

Then, the influence of the root depth is studied. This variable is decisive from the perspective of the soil moisture uptake by the plant roots. The tested root depth values go from 0.05 m to 0.90 m. As expected, an ET increase is observed for both configurations (see Table 6-14 and Figures 6-27). It is more evident with the Bucket model than with the Richards one. With Richards, moisture is continuously re-distributed through the soil, but not in Bucket. Thus, in Richards, if moisture is sucked from the surface,

it will be replenished. If canopy transpiration acts via roots, sucking moisture from deeper layers, this will make little difference in Richards, but a lot in Bucket. The ET increase is also more visible in summer than in other months of the year, due to the fact that in summer the topsoil layers tend to be dry. If the roots reach higher depths, they encounter much more moisture. In winter, on the other hand, the moisture distribution is more homogeneous with respect to depth.

*Table 6-14: Effect of root depth change (from 0.05 m to 0.90 m) on average difference in ET*

Difference in ET (kg/m <sup>2</sup> ·d)	Root depth 0.05	Root depth 0.90	Change in difference in ET
Bucket, ER	1.16	1.07	-0.09
Richards, ER	0.08	0.05	-0.03



*Figures 6-27: Seasonal average ET vs time, modelled and measured. Richards, ER. Root depth: 0.05 m (left panel), 0.90 m (right panel)*

An increment of the root depth only affects the canopy transpiration. This phenomenon, in fact, gains from a rise of the roots' expansion. The values are reported in Table 6-15.

*Table 6-15: Partitioning of ET before and after root depth change (from 0.05 m to 0.90 m)*

Richards, ER: Partitioning of ET (kg/m <sup>2</sup> ·d)	Canopy Evaporation	Canopy Transpiration	Soil Evaporation
Root depth 0.05 m	0.11	0.18	1.03
Root depth 0.9 m	0.11	0.22	1.02

As far as GT goes, the observed variations are in the order of hundredths of degrees.

#### 6.4.6 Other canopy parameters

Finally, some remarks are done with respect to a series of parameters that so far have not been addressed. The first is the Canopy Albedo: literature studies set this variable to around 0.25. The value 0.15 is tested, provoking an ET increase of only 0.02 kg/m<sup>2</sup>·d on average. Secondly, the Biomass Heat Capacity: two different values (2400 J/kg·K, relative to needles, and 800, relative to grass) are compared and no significant dependence on this parameter is found. Last, the Trunk Fraction Height, which has no effect on these simulations because run with the one-layer canopy module.

It is noted that the introduction of canopy, together with every parameter variation which contributes to its increased effect, causes a ground temperature reduction. This GT change is rather high when canopy is introduced, because of its low Direct Throughfall value (0.65). Likewise, a GT reduction reaching 2.5 °C is observed when DT is decreased from 0.90 to 0.45, which represents a very wide range of values, overcoming the ones suitable for grass.

Introducing canopy can have a double effect on ET, whether the infiltration model is Bucket or Richards. In the first case, ET increases slightly and in the second one, it is reduced. In most occasions, a GT decrease comes with an increase in evapotranspiration: as previously said, greater losses of latent heat provoke a cooling of the soil, not only at superficial layers. This mechanism takes place with LAI and DT changes, with the first of the two causing the greatest ET increase among all parameters. No GT variation

accompanies the ET increase when a root depth change occurs. Increasing the canopy height surprisingly produces a reduction in ET, due to the smaller amount of soil evaporation.

The current version of the canopy module is limited in the sense that the effect of canopy is constant throughout the year, i.e. the grass has always the same height, the same Leaf Area Index, and Direct Throughfall, parameters that would normally vary significantly with time. This is clearly a rough approximation, which leaves room for future improvement.

Furthermore, the parameters' values' selection was affected by the anomalies encountered when testing, for instance, low canopy heights and high DT, a suitable parametrization to simulate low vegetation opposing little resistance to moisture capture by the soil. Further investigation is needed to fix the code, avoid the resulting overestimation of GT and be able to use the one-layer canopy module to model grassland in a realistic way.

## 7 RESULTS – VALIDATION

The stations used in this study are located in low altitude areas, ranging from the 203 m of Magadino Cadenazzo to the 1042 m of Plaffeien, with the majority being around 500 m a.s.l.

All can be identified with a mesic soil temperature regime, meaning that the mean annual soil temperature stands between 8 °C and 15 °C, and the difference between mean summer and mean winter temperatures is more than 5 °C.

All, except for Laegern, are characterized by very low grassland vegetation and open fields, i.e. with no obstacles around them, apart from a fence shorter than 1 m at a few meters distance. Only Laegern is located in a forest, where solar radiation is obstructed by the high vegetation. Because of problems encountered with the SNOWPACK simulation on this site, it is excluded from the study.

The purpose of this section is to validate the results obtained for Payerne in ten new soils having equal or very similar characteristics. Six of them are also described as loam: for them, the same *sno* file as Payerne is applied. For the remaining four, the same *sno* file is used, but with different grain size. This is done in Richards by setting the right soil type (silt loam or sandy loam), and in Bucket by adjusting *rg* in order to yield the same field capacity as with the soil class imposed in Richards (according to the formulas presented in section 4.3).

The mentioned *sno* file has the following values: Specific heat capacity  $c_m$ : 1400 J/kg·K ; Thermal conductivity  $\lambda_m$ : 1.4 W/m·K ; Solid fraction: 0.55 ; Density  $\rho_m$ : 2600 kg/dm<sup>3</sup> ; Roughness length  $z_0$ : 0.02 m ; Soil albedo: 0.17 .

Nevertheless, all the simulations greatly distinguish themselves from the others because of the implementation of local meteorological data to each SNOWPACK simulation.

All simulations are run without canopy because of two reasons: one is the high variability in the results following canopy parameters' changes; the other is the impossibility to simulate the real grass conditions, with a low canopy height and a high DT, due to the found ground temperature (GT) anomalies. Nevertheless, the used roughness length equal to 0.02 m, linked to "Flat terrain with grass or very low vegetation" (Table 4-2), partly mimics the presence of a low vegetation cover.

Concerning the soil evaporation method, Evaporation Resistance is chosen. This preference is due to the fact that with the Bucket model and Relative Humidity, the evapotranspiration (ET) prediction is

erroneous, and with it also the GT values. As for Richards, RH slightly overestimates the observed ET, thus ER is kept, also to have a comparison between Bucket and Richards results under the same other conditions.

## 7.1 Ground temperature

SNOWPACK simulations are run with the Bucket and the Richards equation infiltration models in eleven sites, including Payerne. The results on GT are reported under the form of tables showing RMSE values for each depth (Table 7-1 and Table 7-2). The complete set of figures with seasonal average GT, measured and modelled, is found in Appendix D (from Figures 0-1 to Figures 0-12).

Each station offers at least one dataset of field measurements to be compared to the SNOWPACK output. Many stations are equipped with more than one GT measuring system. However, the second and third sets of measurements frequently offer the same values as the first set, or they consist of two depths only, or even they have measurements at differing depths that are deeply inconsistent with one another. For these reasons only one set is kept, which must show monotonic temperature values, with respect to depth, in the summer and winter seasons. The right set is chosen also by looking at the measured average air temperature (TA in the plots), which must be consistent with the observed GT.

First, the Bucket model simulations are analyzed. In few of the loamy and silt loam sites (Reckenholz, Rietholzbach, Wynau), the fitting resembles the one in Payerne: temperatures are underestimated in winter and autumn, while they are better simulated in spring and summer. In Nyon Changins, Taenikon and Magadino Cadenazzo, the simulated GT are closer to the measured ones in winter and autumn, whereas they overcome them in spring and summer. In the sandy loam sites of Plaffeien and Sion, the simulated GT appear much higher than the observed ones, except for winter, where the fitting is good. The only exception is Basel, where the modelled-measured bias is surprisingly minimized, and only in summer a slight overestimation of less than 1 °C occurs. The measurements coming from the station in Bern present very high variations between consecutive depths, which make it hard to understand what the real thermal regime is. Consequently, the GT modelling in Bern is given less importance than in the other stations, where GT field data at different depths are coherent with each other.

Four plots are reported below, illustrating what has been said, relative to the sites of Taenikon, Basel (Figure 7-1), Rietholzbach, and Sion (Figures 7-2).

The main criticality is the wrong shape of the GT-depth curve in autumn: in all sites, including Payerne, the temperature gradient in the soil is too high. This can be due to either a higher specific heat capacity or a lower thermal conductivity (or both factors) than in reality. The issue lies in the impossibility of modifying such thermal parameters without negatively affecting the GT-depth gradient of the other seasons, in particular winter and summer. This is clearly illustrated in Figures 6-7 and Figures 6-8 in the sensitivity analysis of section 6.1.

In some of the tested locations, this problem also exists for the modelling of winter temperatures: this is particularly evident in Reckenholz and Rietholzbach, but is also present, to a less extent, in Nyon Changins, Magadino Cadenazzo, Wynau and Sion. Here, reducing  $c_m$  or increasing  $\lambda_m$  would make the fitting better for winter and autumn, but worse for spring and summer.

However, in some sites, like Reckenholz, the gradient of the GT-depth curves is modelled incorrectly for the whole year, except maybe for spring. This means that, despite being classified as loam, Reckenholz soil is much different from the one in Payerne in terms of thermal parameters. Hence, not only there can be issues in representing the GT-depth curve gradient limited to one or two seasons, but there can be soils which need a completely different thermal parametrization. This is partially due to the allocation of just one soil type to the entire soil column, which may not be representative of the reality.

With this being said, low RMSE values relative to the problematic seasons in the listed sites must be read carefully, considering the possibility of a wrong simulation of the GT gradient as the cause of an apparently good fitting. The reported figures help in identifying such phenomena.

On a different topic, the GT variations visible on multi-annual plots are satisfactorily reproduced, with most significant increases and decreases at the annual and monthly scale being well captured.

All the considerations done so far are also valid for the simulations run with Richards, ER. In fact, the same criticalities affecting the modelling of the GT-depth curve in autumn and sometimes in winter remain. Furthermore, there is a general underestimation of GT in all seasons, as in Payerne, ranging from 1 °C to 2 °C. Only the sandy loam soils of Plaffeien and Sion appear more adequately simulated. This better fitting could mean that the soil parametrization obtained for loam applies better to sandy loam soils when Richards equation is used.

Table 7-1 and Table 7-2 report the RMSE values for each depth, respectively for a Bucket, ER and a Richards, ER configuration. All loamy soils are put together, followed by the silt loam and the sandy loam ones.

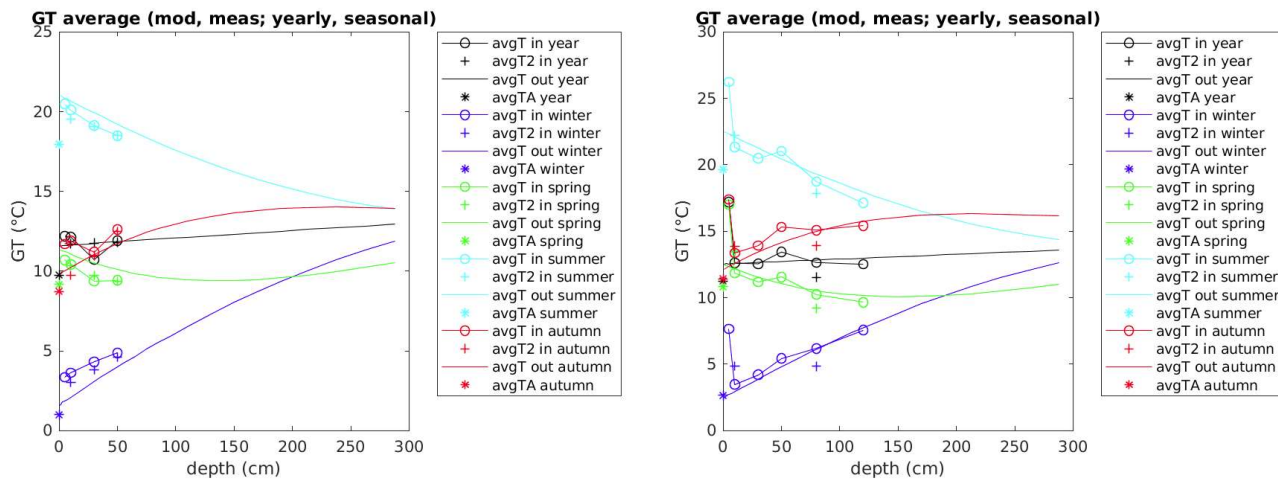
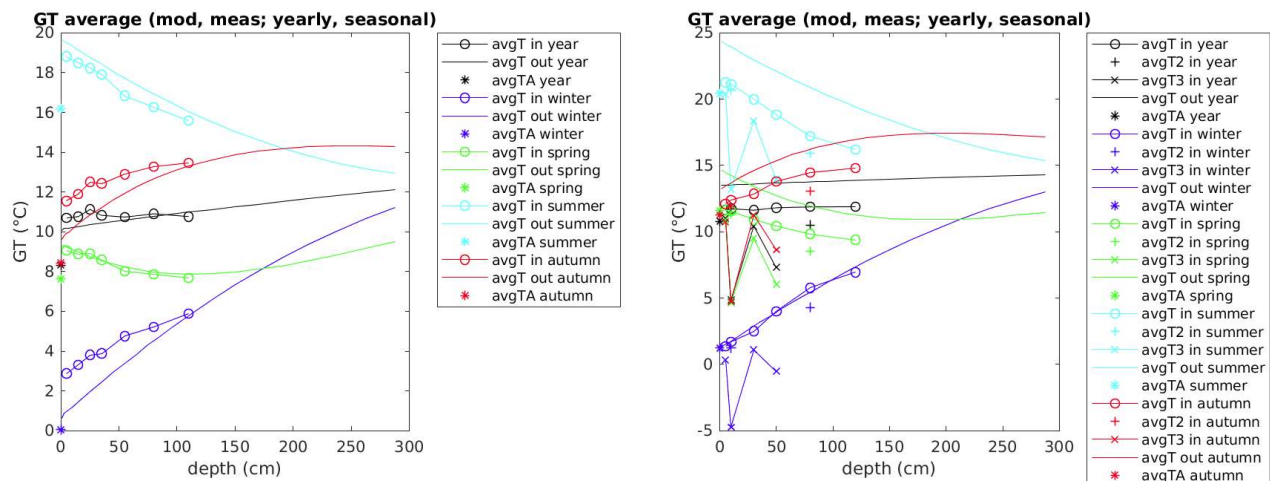


Figure 7-1: Seasonal and yearly average GT vs depth, modelled and measured. Bucket, ER. Taenikon (left panel), Basel (right panel)



Figures 7-2: Seasonal and yearly average GT vs depth, modelled and measured. Bucket, ER. Rietholzbach (left panel), Sion (right panel)

Table 7-1: RMSE values on ground temperature, at different depths, for the 11 studied sites. The starred values stand for values that are less representative than the others because of bias in the measurement.

RMSE, Bucket ER		5 cm	10 cm	30 cm	50 cm	80 cm	120 cm	150 cm
loam	PAY	2.9	2.5	1.2	2.0*	0.8		
	BAS		2.5	1.2	1.5*	0.6	0.7	
	BER	3.2*	3.6*	1.9*	2.5*	0.4*	4.0*	
	CGI	3.6	3.1	1.9	1.7	1.4		
	REC		2.6	1.3	1.0	0.8		1.1
	TAE	3.4	3.0	1.3	1.2			
	RHB	3.6	2.5 (15cm)	2.0 (25cm)	1.7 (35cm)	1.6 (55cm)	1.2	1.2 (110cm)
silt loam	MAG	3.4	2.8	1.6	1.3	1.0		
	WYN	3.0	2.5	1.2	0.9			
sandy loam	PLA	3.1	2.8		2.4		2.8	
	SIO	4.0	3.4	2.5	2.4	2.4	2.3	

*Table 7-2: RMSE values on ground temperature, at different depths, for the 11 studied sites. The starred values stand for values that are less representative than the others because of bias in the measurement.*

RMSE, Richards ER		5 cm	10 cm	30 cm	50 cm	80 cm	120 cm	150 cm
loam	PAY	2.8	2.4	1.8	3.0*	1.7		
	BAS		2.2	1.4	2.4*	1.4	1.3	
	BER	3.0*	4.0*	2.5*	3.6*	1.0*	5.3*	
	CGI	2.9	2.5	1.6	1.3	1.1		
	REC		2.2	1.5	1.4	1.5		1.8
	TAE	3.0	2.7	1.5	1.5			

	RHB	3.1	2.5 (15cm)	2.3 (25cm)	2.1 (35cm)	2.0 (55cm)	1.9	2.2 (110cm)	
silt	MAG	3.0	2.6	1.9	1.7	1.5			
loam	WYN	2.9	2.6	1.7	1.7				
sandy	PLA	2.6	2.3		1.7		2.0		
loam	SIO	3.0	2.5	1.4	1.3	1.5	1.5		

## 7.2 Evapotranspiration

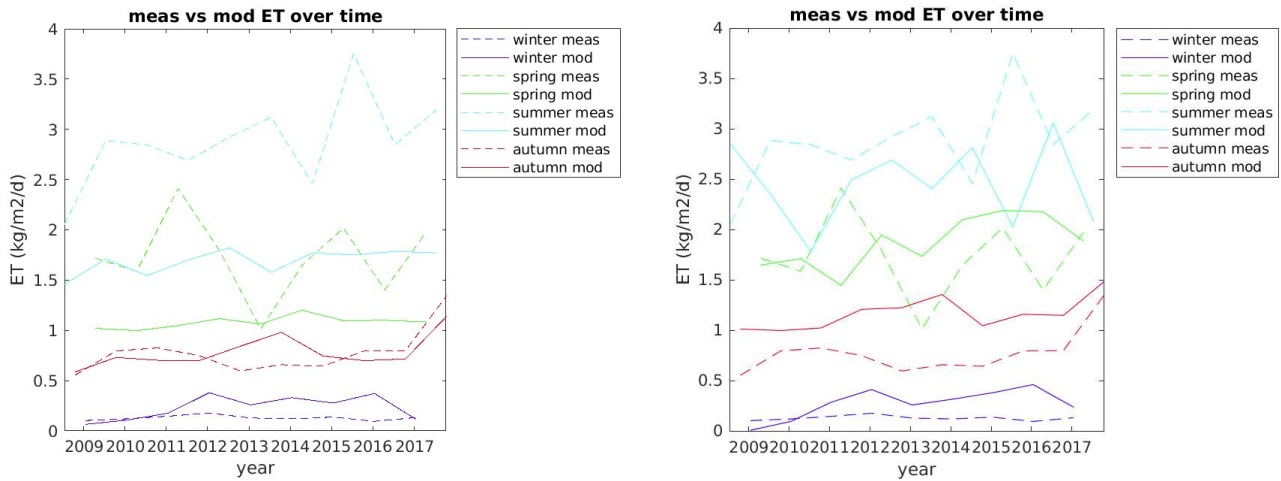
ET measurements are only available for three stations: Payerne, Bern and Rietholzbach. The first two lie at a reciprocal distance of about 20 km and are both at an altitude of about 500 m. The third one, instead, is located in the north-east area of the country, at 800 m a.s.l.

With the Bucket model (left-hand side of Figures 7-3, Figures 7-4, Figures 7-5), only winter and autumn are modelled satisfactorily in Payerne and Bern, but not in Rietholzbach. All three stations share a bad, because too low, modelling of ET in spring and summer.

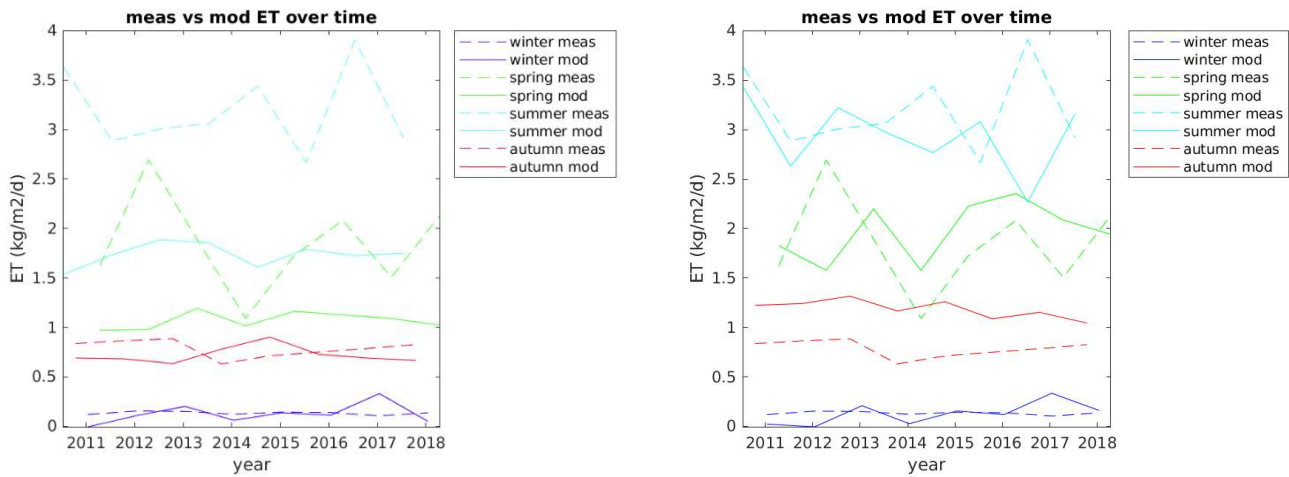
The configuration Richards, ER (right-hand side of Figures 7-3, Figures 7-4, Figures 7-5) leads to the best modelling of ET. The results from Payerne and Bern show many similarities because, for both, spring and autumn ET is overestimated by few tenths of  $\text{kg}/\text{m}^2\text{-d}$ , while summer ET is underestimated also by few tenths of  $\text{kg}/\text{m}^2\text{-d}$  (Figures 7-3 and Figures 7-4). Likewise, Rietholzbach produces an underestimation of ET in summer by the same quantity as the other two stations. However, in the other seasons, ET is underestimated, making this behavior different from the first two sites (Figures 7-5). The continuous underestimation of ET in Rietholzbach over the whole year causes the average difference in ET to be higher than for Payerne and Bern, where higher and lower modelling compensate each other (Table 7-3).

Nonetheless, looking at the RMSE values reported for the configuration Richards, ER in Table 7-4, it can be derived that the modelling in Rietholzbach is the best one for all seasons except for winter. Moreover, the modelled ET clearly respects the measured ET seasonal trend, with its highs and lows.

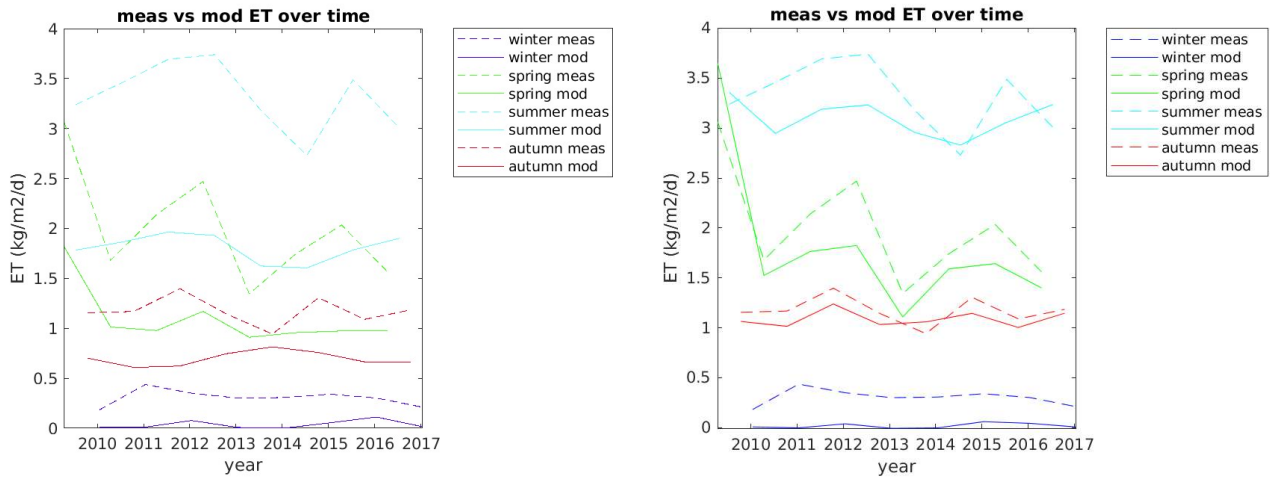
A confirmation of the interaction between GT and ET is derived from a comparison between the observed datasets of Payerne and Rietholzbach, leaving out Bern for its variable GT measurements. Evaluating season by season, the higher GT measured in Payerne (up to 3 °C more in summertime) than in Rietholzbach are always accompanied by a proportionally lower ET in all seasons.



Figures 7-3: Payerne. Seasonal average ET vs time, modelled and measured. Infiltration model: Bucket, ER (left panel), Richards, ER (right panel)



Figures 7-4: Bern. Seasonal average ET vs time, modelled and measured. Infiltration model: Bucket, ER (left panel), Richards, ER (right panel)



Figures 7-5: Rietholzbach. Seasonal average ET vs time, modelled and measured. Infiltration model: Bucket, ER (left panel), Richards, ER (right panel)

Table 7-3: Difference in ET with Bucket, ER and Richards, ER, for the three sites

Difference in ET (kg/m <sup>2</sup> ·d)	Payerne	Bern	Rietholzbach
Bucket, ER	0.44	0.56	0.80
Richards, ER	-0.04	-0.07	0.21

Table 7-4: RMSE values on ET, with Richards, ER, for the three sites and for each season

RMSE, Richards, ER	Payerne	Bern	Rietholzbach
Winter	0.20	0.11	0.30
Spring	0.51	0.54	0.37
Summer	0.84	0.67	0.42
Autumn	0.43	0.41	0.15

### 7.3 Soil moisture

To assess soil moisture, or liquid water content (LWC), SNOWPACK simulations are run with the Richards equation infiltration model in eleven sites, including Payerne. The Bucket model, as previously explained, is not able to offer a good LWC representation because of the simple physics behind it. Measurements at 5 cm and 10 cm are neglected from any comparison because of the higher atmospheric and biological disruption that affects these depths, making the data highly variable and the indicated soil type hardly corresponding to the real one.

After a few test simulations, it was noticed that the saturated water content  $\theta_s$  derived from the selection of a soil type was often a limit to the modelling of the LWC. In fact, being set for loam to 0.399, it prevented an accurate simulation of soil moisture, whose measurements often exceeded this value. Therefore, it was raised to 0.45, a common value for loamy soils used in all the simulations with the Bucket model seen so far. This way, modelled LWC increased when there were the conditions to do so, and it did not in those cases where it was not initially limited by  $\theta_s$ . This change did not alter significantly the GT and ET modelling, whose results have been updated accordingly to this variable's change all the same. As well as for loam, also the classes silt loam and sandy loam were modified, bringing the  $\theta_s$  to a value higher by 0.05.

Modelled ice content is plotted together with soil moisture, even though measurements of this quantity are not available. Simulating a certain ice content in the soil pores leads to evident drops in the modelled LWC, for reasons of water mass balance. Sporadic ice content is modelled at 30 cm depth, while it is absent more deeply. At 5 and 10 cm it is common to see frequent ice layers during the cold season. When such modelling is compared to the actual LWC data, the sudden, sharp drops do not appear in the same way. Near the surface these have a smaller magnitude, while at 30 cm they do not exist at all, meaning that there is a general overestimation of ground freezing. This is expected, given the widespread underestimation of GT in all seasons, including winter.

In general, soil moisture is well simulated at an annual and monthly scale. Averaging statistical results between multiple depths, seven of the eleven sites present RMSE values below a threshold of 0.05: these are Payerne, Bern, Nyon Changins, Reckenholz, Taenikon, Wynau and Rietholzbach. The remaining four sites have RMSE values between 0.07 and 0.09. The complete set of RMSE values is reported in

Table 7-5, where values in yellow depict measurements that are likely biased, given their difference from the ones taken at consecutive depths.

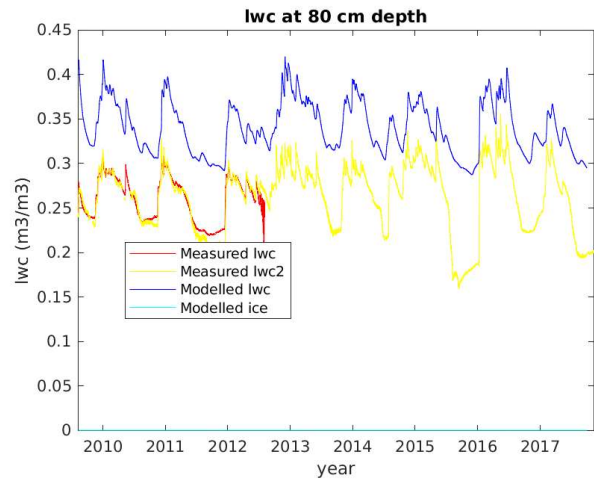
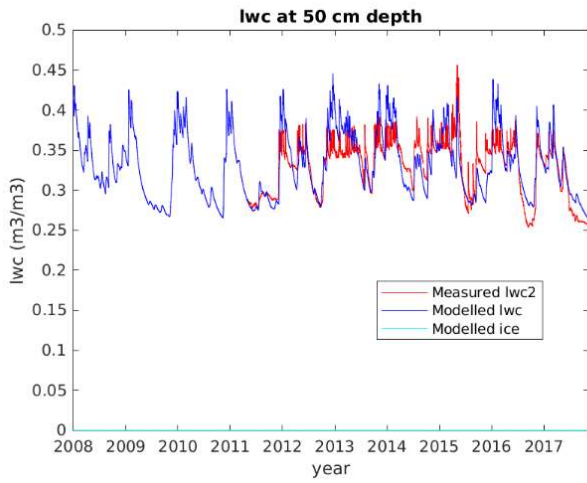
Among the simulations realized for the eleven sites, a better modelling at lower or higher depths cannot be observed as a common trend.

A limit of the RMSE statistics is that it cannot highlight whether the modelled LWC has a bias. Analyzing accuracy separately, the situation is not at all uniform; in fact, four sites (Bern, Reckenholz, Magadino Cadenazzo, Plaffeien) are characterized by an underestimation of soil moisture. Three are defined by an overestimation of it (Payerne, Basel, Taenikon). Then, Nyon Changins, Wynau have both lower and higher modelling, while Rietholzbach and Sion show adequate results.

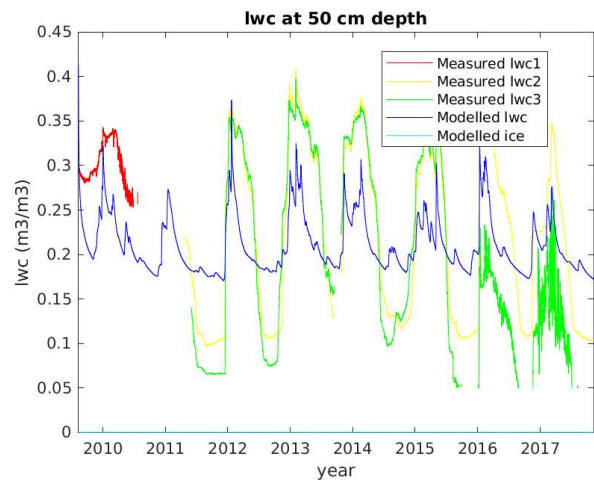
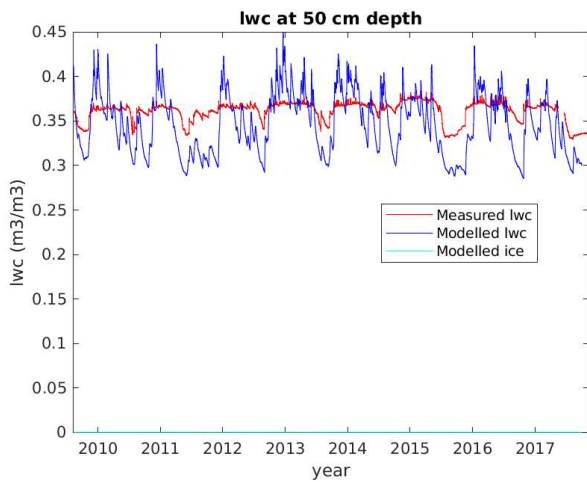
In most cases, variations are well reproduced by the model, as visible in Figures 7-6 relative to Nyon Changins ad Basel. There are however a few cases where the measurements appear relatively constant and the modelling is not able to reproduce such trends, such as in Bern (Figures 7-7, left-hand side) and Rietholzbach. This might be due to a superficial water table not reproducible by the model. The opposite can happen as well (see Sion, Figures 7-7, right-hand side), that is highly variable field data (perhaps wrong) and more stable modelling.

Regarding the three soil types being simulated, it is difficult to assess general behaviors related to the soil type choice, because of the small sample for silt loam and sandy loam (two sites each). It can be said that Magadino Cadenazzo (silt loam) and Plaffeien (sandy loam) are marked by an evident underestimation of LWC, whereas Wynau (silt loam) has good accuracy and Sion (sandy loam) is affected by the high LWC oscillations already discussed.

A summary of LWC data, both modelled and measured, for all the eleven sites, is available under the form of average seasonal values from Figures 0-13 to Figures 0-18 in Appendix E.



Figures 7-6: Soil moisture vs time, modelled and measured. Nyon Changins, depth: 50 cm (left panel); Basel, depth: 80 cm (right panel)



Figures 7-7: Soil moisture vs time, modelled and measured. Bern, depth: 50 cm (left panel); Sion, depth: 50 cm (right panel)

*Table 7-5: RMSE values on soil moisture, at different depths, for the 11 studied sites. The starred values stand for values that are less representative than the others because of bias in the measurement.*

RMSE		Depth				
Soil type	Site	30 cm	50 cm	80 cm	120 cm	150 cm
loam	PAY	0.06	0.05	0.02		
	BAS	0.04	0.07	0.08	0.08	
	BER	0.04*	0.03	0.03	0.04	
	CGI	0.03	0.02	0.05		
	REC	0.06	0.05	0.09*		0.02
	TAE	0.06	0.04			
	RHB	0.07 (35 cm)	0.03 (55 cm)	0.03	0.02 (110 cm)	
silt loam	MAG	0.05	0.11			
	WYN	0.03	0.05			
sandy loam	PLA	0.11	0.12	0.07	0.05	
	SIO	0.08	0.09	0.09		

#### 7.4 Runoff

This section's target is to validate the produced runoff at the Payerne station with actual river discharge data from the river Broye. This is done by applying the distributed version of SNOWPACK, Alpine3D, a three-dimensional, physically based, snow cover and earth surface model. It is run in the Broye catchment (Figure 7-8), where Payerne is located, for a 14-month period, precisely from August 2012 to September 2013. Alpine3D is able to compute, over an entire hydrographic catchment, the integral

of the runoffs produced by each soil column, which can be compared to the river discharge. A considerable spatial approximation is realized: the soil characteristics are the same everywhere: one unique *sno* file with the values obtained from the sensitivity analysis of chapter 6 is applied everywhere. The most relevant values are reported in Table 7-6.

*Table 7-6: Soil parametrization used in Alpine3D simulations*

$c_m$ (J/kg·K)	$\lambda_m$ (W/m·K)	porosity	density (kg/dm <sup>3</sup> )	$z_0$ (m)	albedo
1400	1.4	0.45	2600	0.02	0.17

Furthermore, no routing scheme is applied for two reasons: imposing one would imply losing some information and, since the analysis treats cumulative values, the results would not change significantly.

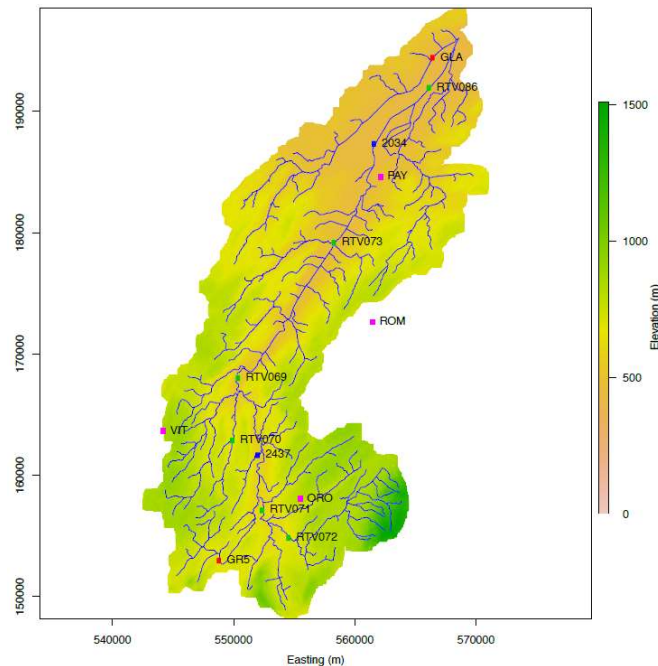


*Figure 7-8: Map of the Broye catchment, equipped with coordinates and elevation (Michel, 2018)*

The Alpine3D simulations are run with both water infiltration models, respectively five with Bucket and one with Richards. The difference between the simulations lies in the *rg* value, which is selected based on the consequent field capacity  $\theta_{fc}$ . The five resulting  $\theta_{fc}$  for the Bucket simulations, reported in Table 7-7, are associated in literature with the following soil types: in order, silty clay, loam, sandy loam, loamy

sand, sand. It cannot be said, however, that by changing  $rg$  a totally different soil is modelled, as other parameters remain unchanged. Table 7-7 here below also displays the Alpine3D results in terms of cumulative runoff, comparable with the cumulative discharge and the cumulative precipitation over the catchment for the same time window.

*Table 7-7: Description of the six simulations' setup and results*

Model	Bucket					Richards
$rg$ (mm) or soil type	0.8	1.8	3.0	4.5	8.0	loam
$\theta_{fc}$	0.38	0.26	0.20	0.17	0.13	0.26
Runoff (m <sup>3</sup> )	125030	138140	140970	143020	145600	116320
Discharge (m <sup>3</sup> )	96348					
Rainfall (m <sup>3</sup> )	193020					

In spite of the spatial standardization of the soil characteristics, the simulated runoff has the same order of magnitude of the river discharge. The simulated runoff increases with higher  $rg$  values, due to the decreasing capability of retaining moisture and leaving it subject to evaporation.

A good variety of  $rg$  values is tested for Bucket, and with all of them the runoff is overestimated. Besides, considering artificial areas as well, such as towns and roads (with land covers like concrete and asphalt), would increase the simulated runoff further. This means that, even if a proper spatial soil description were to be applied, the runoff would still be too high. Such high runoff values can be explained with the analysis of ET developed in section 6.1: ET was found to be underestimated with the Bucket model when compared to field data. Being this quantity strictly related to the runoff by a soil water mass balance, it is plausible that underestimating ET causes a wrong, overestimated modelled runoff.

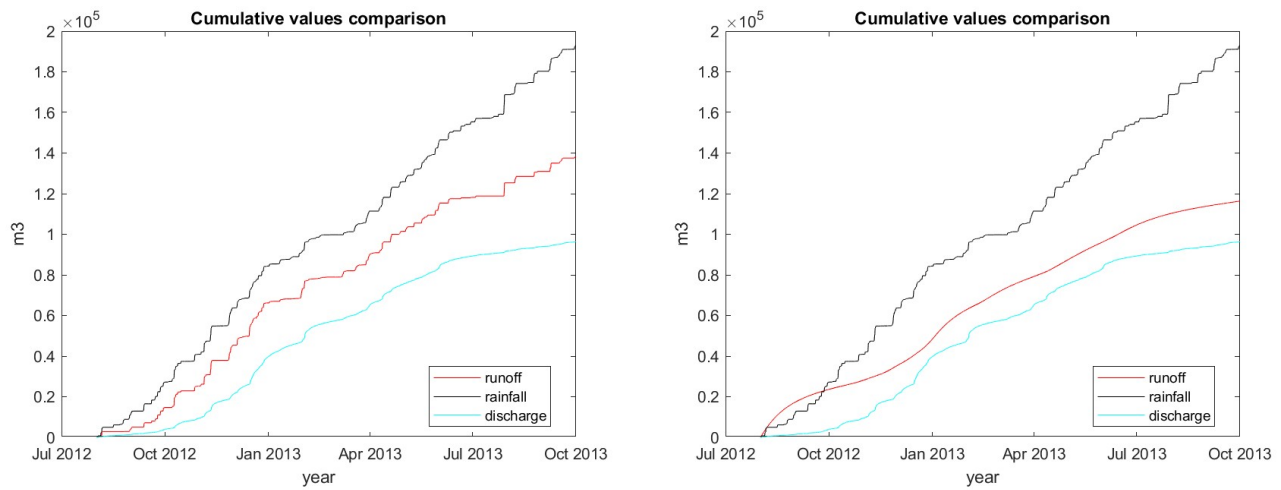
On the other hand, Richards reduces the bias between runoff and discharge more than any Bucket simulation. This is physically consistent with the aforementioned argument on ET: in fact, the average difference between measured and modelled ET with Richards over a nine-year period was found to be close to zero, precisely  $-0.04 \text{ kg/m}^2\cdot\text{d}$ .

Figures 7-9 illustrate the results of two Alpine3D simulations, with the runoff overestimation being clearly visible. The first plot is relative to a Bucket configuration with  $rg = 1.8$  mm (whose  $\theta_{fc}$  is associated with a loamy soil), whereas the second one is the Richards configuration (loamy soil). Figures 7-10 show cumulative graphs produced with SNOWPACK, over the same time window used for the Alpine3D simulations and relative to the same two configurations previously described. The gap between measured and modelled ET can be observed. For the Richards configuration, ET is slightly overestimated, meaning that the Alpine3D runoff could be even higher.

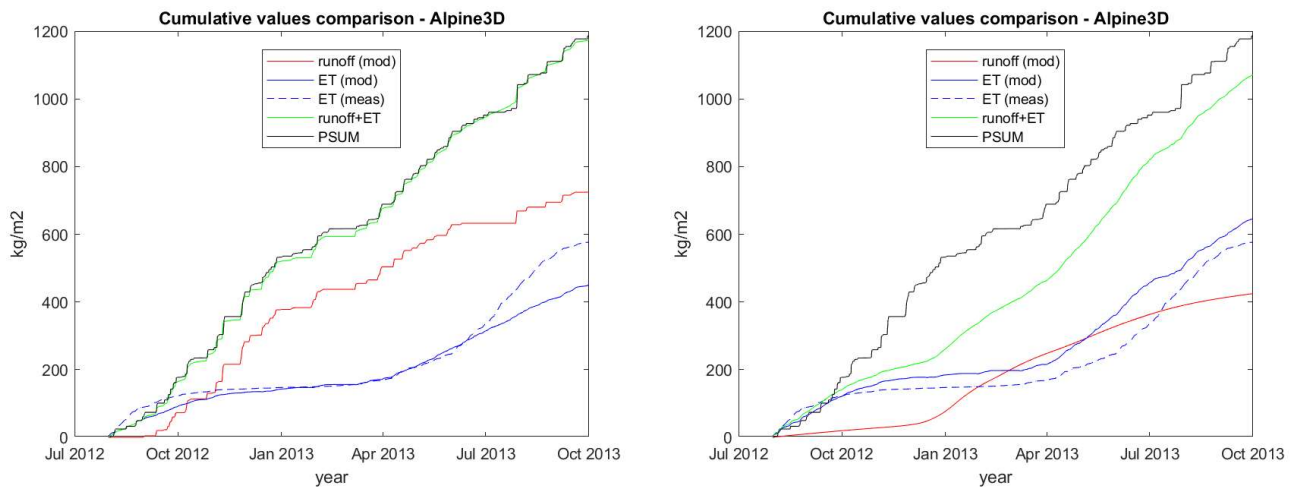
Some further notes can be made with respect to the reported graphs. First, the ratio runoff/precipitation is not constant passing from SNOWPACK to Alpine3D simulations, because of the use of data coming from multiple rain gauge stations spread over the Broye catchment. Secondly, the sum of cumulative runoff and ET does not match exactly with the cumulative precipitation. This phenomenon can be assessed looking at Figures 7-11, which display the same cumulative values for a nine-year time length. The existing gap is in part due to the initial conditions of the simulated soil column, whose water content is set equal to about half of the saturation one. Therefore, the soil needs some time to fill with water and start producing runoff, hence the straight horizontal line characterizing the initial phase of the runoff curve in both Figures 7-11. This phenomenon is more influential with low  $rg$  values and finer soil types, and it can be easily solved by setting the initial soil column to saturated conditions. If this can explain the little gap present in the Bucket simulation, which indeed disappears when looking merely at the years 2012-2013 and omitting the initial phase, it is not enough to explain the gap within the Richards simulation. In this case, the gap is continuously increasing from the first year 2009 to the last one 2017. As a matter of fact, when zooming at the 2012-2013 period, the gap appears larger and larger with time, with the smallest gradient of the runoff + ET curve from November to January. This can be explained with the fact that a fraction of winter precipitation falls as snow, not producing any immediate runoff, if not only in springtime. However, further investigation is needed to identify the reason for this increasing bias when Richards model is applied.

Lastly, the shape of the runoff curve changes a lot from Bucket to Richards, as pictured in Figures 7-12. Bucket produces a discrete graph, depicted by high values. On the other hand, Richards produces a continuous runoff output, marked by seasonal trends. The same characteristics can be observed from the cumulative plots presented in Figures 7-9 and Figures 7-10. Finally, the non-cumulative runoff produced by Alpine3D with the Bucket model and with Richards equation is compared to the non-

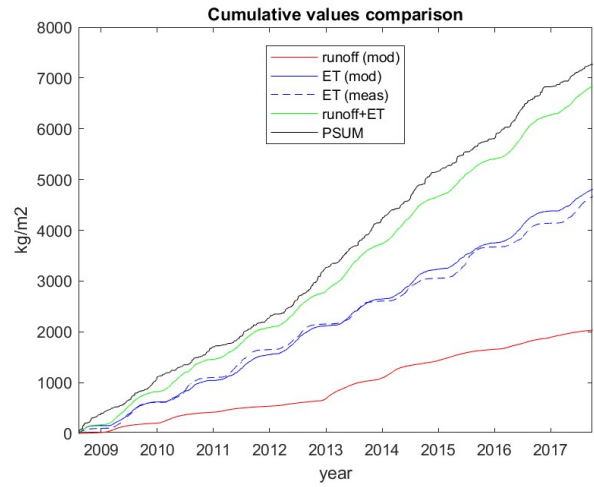
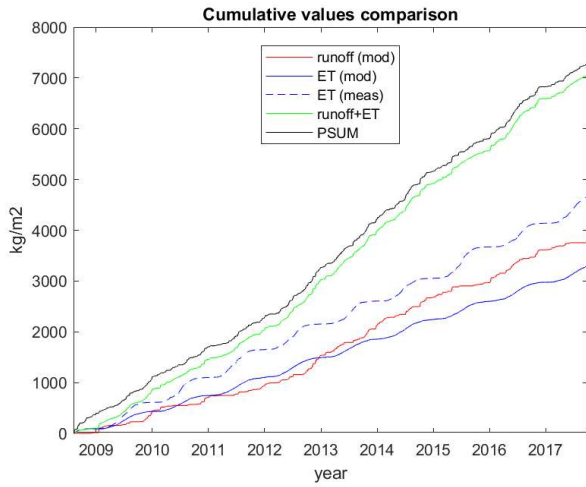
cumulative river discharge (Figures 7-13). At first sight, the scale between the two models is very different. With Bucket, high runoff production alternates with periods of absent runoff. With Richards instead, the runoff has the same order of magnitude as the discharge, but it appears far too smooth to represent accurately the discharge and to be used in a hydrological model.



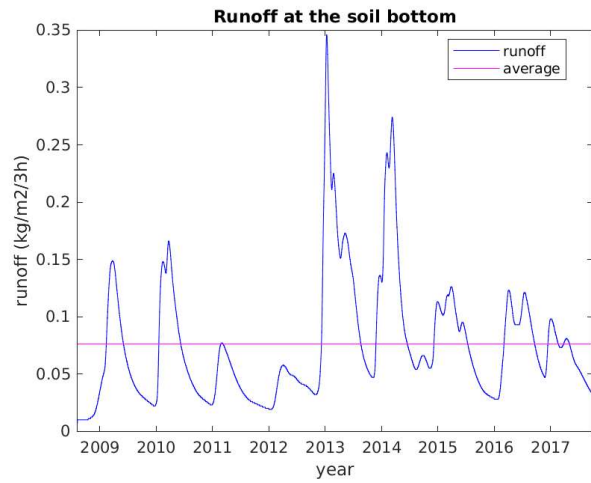
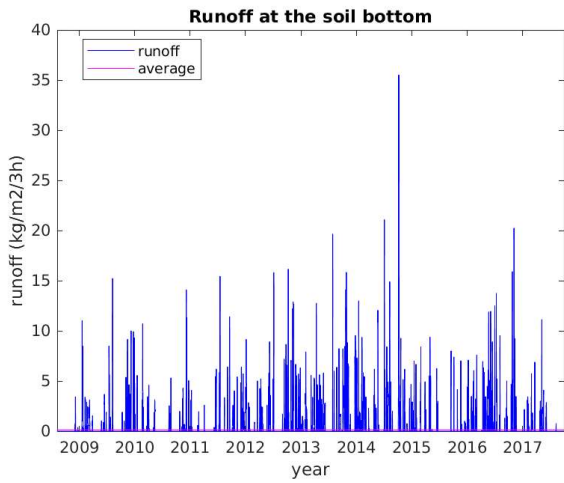
Figures 7-9: Alpine3D results: cumulative runoff vs cumulative discharge. Bucket,  $ER, rg = 1.8$  (left panel), Richards,  $ER, soil\ type = loam$  (right panel)



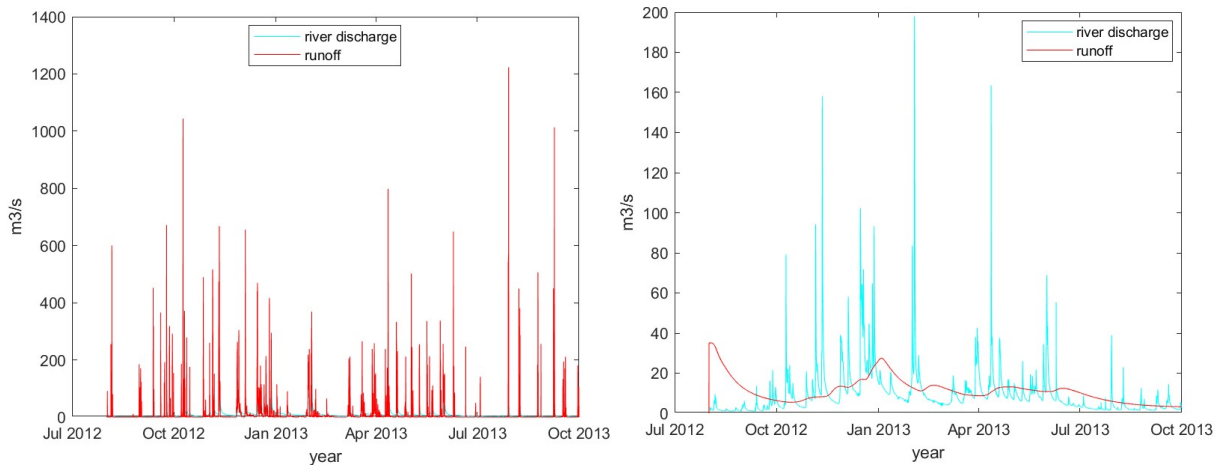
Figures 7-10: SNOWPACK results: cumulative runoff vs cumulative ET, measured and modelled. Extract relative to Alpine3D simulations' time window. Bucket,  $ER, rg = 1.8$  (left panel), Richards,  $ER, soil\ type = loam$  (right panel)



Figures 7-11: SNOWPACK results: cumulative runoff vs cumulative ET, measured and modelled. Full temporal window, as in other SNOWPACK plots. Bucket, ER, rg = 1.8 (left panel), Richards, ER, soil type = loam (right panel)



Figures 7-12: SNOWPACK produced runoff. Bucket, ER, rg = 1.8 (left panel), Richards, ER, soil type = loam (right panel)



*Figures 7-13: Alpine3D results: runoff vs discharge. Bucket, ER,  $rg = 1.8$  (left panel), Richards, ER, soil type = loam (right panel)*

## 8 CONCLUSIONS

The study of ground temperature and soil water dynamics is a matter of great interest in hydrology, agriculture, but also chemistry and geotechnical engineering. In this work, the model SNOWPACK is tested in fine-grained soils from eleven Swiss sites, nine of which belong to the low-altitude region of the Swiss Plateau. The focus lies upon the reproduction of four main quantities by the model: ground temperature (GT), liquid water content (LWC) or soil moisture, evapotranspiration (ET) and runoff.

Sensitivity analysis results in chapter 6 are divided by water infiltration model, whose choice is found to greatly impact SNOWPACK's output for all the four studied quantities. GT, for instance, is simulated remarkably better with the use of the Bucket model, contrary to the findings of Wever et al. (2015), who had achieved in a gravel alpine soil a better GT prediction with the Richards model, even if a big bias had remained with respect to the measurements. In Payerne, simulating GT with Bucket reduces the difference between observed and modelled data. This is particularly true in the warmer months (summer in primis, spring and partially autumn) and to a less extent in winter and autumn. On the other hand, Richards tends to underestimate GT by no less than 1-2 °C in all seasons.

ET and runoff modelling also depend largely on the infiltration model. Having to respect the soil water mass balance, these two quantities are mathematically complementary and their evaluation can be done at two levels. The first is by looking at ET field data, the second is by running Alpine3D over a whole catchment and comparing the produced runoff to river discharge data. Regarding the first method, the following can be said: being Richards equation the most physically based tool to describe soil water dynamics, it is with it that a more accurate ET is simulated. The simple Bucket model highly underestimates the real ET, reaching on average only 68% of it.

Passing to the second of the two exposed methods, a different point of view must be adopted. The three-dimensional hydrological model Alpine3D is run in the Broye catchment and the cumulative runoff, integrated over the whole area, is compared to the cumulative discharge. The results are congruent with the ET findings, as the soil runoff is found to overestimate discharge more with Bucket ( $rg = 1.8$  mm) than with Richards (by 43% and 21% respectively), all other things being equal. Looking at the temporal trend of the model produced runoff, the Bucket model leads to far too high discrete values: A better shape is obtained with Richards, which however generates a runoff that is much smoother than the river discharge temporal evolution.

A meteorological setting of great importance is the soil evaporation method, which has a bigger influence on the Bucket model. The results presented so far were achieved using the Evaporation Resistance (ER) method, which models the soil such that the first layer is always saturated. This fixing is particularly useful when a mechanistic model like Bucket is implemented. In fact, setting the Relative Humidity (RH) method leads to an almost null predicted ET and to higher GT by 1-2 °C than with ER. This makes the GT-ET interaction very clear: a higher amount of water evaporating from the soil, thus a greater latent heat flux  $q_l$  directed upwards, involves a heat loss for the soil in all seasons where ET is not negligible. Summarizing, the imposition of the RH method is only meaningful with Richards, where the uppermost layers hardly dry out entirely.

Soil parametrization can affect significantly the thermal and hydrological regimes. The variable  $rg$ , set to indicate the typical grain size in Bucket, together with the soil type definition in Richards, influence all quantities. GT gradients are increased with smaller soil particle size, due to the higher thermal resistance which they can oppose. The effect on ET is rather big because field capacity changes according to the chosen  $rg$  or soil type. This is more marked with Richards: increasing the field capacity from 0.13 to 0.26 (values relative to sand and loam respectively) induces an increase in modelled ET of more than 0.8 kg/m<sup>2</sup>-d with Richards and of 0.3 kg/m<sup>2</sup>-d with Bucket. Besides,  $rg$  and soil type are the only factors capable of influencing significantly the LWC: this grows where the simulated soil is a fine-grained one, whereas it diminishes evidently when the soil is more coarse-grained.

As far as GT goes, the thermal parameters specific heat capacity ( $c_m$ ) and thermal conductivity ( $\lambda_m$ ) bring the biggest influence on the GT-depth curve gradient and partially on the surface GT as well. Gradients prove higher when  $c_m$  is increased and when  $\lambda_m$  is decreased. GT is also found to be very sensitive to roughness length changes, with increasing values causing a drastic reduction in summer, then spring and autumn, temperatures. Furthermore, higher soil roughness length values can mimic the extra ET obtainable through the implementation of canopy in the model.

The modelling of vegetation covering the soil surface also plays a critical role. It is noted that the introduction of canopy, together with every parameter variation which contributes to its increased effect, causes a ground temperature reduction. Shelia et al. (2018) make the same observation with respect to the consideration of vegetation in the models HYDRUS-1D and CERES. Lowering Direct Throughfall (DT) is what causes the highest decrease in GT. ET, instead, responds with a general increase, especially to rises in Leaf Area Index (LAI), although smaller than what expected.

In chapter 7, the soil values obtained in Payerne are applied to ten sites bearing similar or equal soil characteristics and comparable meteorological context. A satisfying representation of ET is observed, while variable (positive and negative) bias are seen for GT and LWC.

The reproduced GT in the majority of the sites appear to be less negatively biased than in Payerne in winter and autumn, while the bias is often positive in summer and spring. A general GT overestimation is observed in the two sandy loam soils. The biggest issue is represented by the erroneous modelling of the GT-depth curve gradient in autumn (all the sites share this) and in some cases in winter (Reckenholz and Rietholzbach are the most evident). Higher thermal conductivities and/or lower specific heat capacities would be needed to represent the real thermal behavior, with the problem being that other seasons would then be simulated wrongly. On the bright side, most important GT variations at an annual and monthly scale are well captured. Summarizing, it can be stated that two soils which are theoretically equal may not be so in reality. To contribute to tackle this issue, a more complete vertical characterization of the soil would be needed, so to be sure that the modelled soil profile respects the actual one. As a matter of fact, soil can present great variability

The ET results from Bern and Rietholzbach are quite consistent with what has been found in Payerne. All three stations share an underestimated ET with the Bucket model, confirming its failure in such task. As for Richards, the fitting in Bern is almost identical to the one in Payerne, while it is generally better in Rietholzbach, where ET appears slightly underestimated in all seasons and the RMSE values are lower, thanks to better accuracy and better reproduction of the ET temporal variations.

When assessing soil moisture reproduction coming from Richards simulations, the results appear in some way contradictory with each other, as some reproductions are positively biased and others negatively. As already remarked by Wever et al. (2017), significant shifts between measured and modelled data can exist, as well as between different datasets for the same location. The same authors point out an excess soil freezing computed by SNOWPACK, which is here confirmed. Variations at the annual and monthly scale are well captured in most cases, except for periods depicted by a constant LWC not adequately reproduced by the model. Despite the mentioned issues, the simulations are overall satisfactory, with seven of the eleven sites reporting RMSE values below 0.05.

As already mentioned, a source of uncertainty on the results comes from the gaps existing between multiple datasets for GT and LWC. While for the first quantity it is possible to identify which dataset

holds erroneous measures, for the second one this task gets harder due to the rather similar measured values. The uncertainty in the Alpine3D simulations is also rather high because of the assumption of the same soil type over the whole hydrographic catchment. Soil not only is usually highly variable with depth, but it can change greatly just a few meters apart. Nonetheless, having tested several *rg* values ranging from silty clay to sand, and having obtained in all cases a neat overestimation of runoff compared to the river discharge, the drawn conclusions still hold valid.

Amongst the identified model limitations, there is surely the impossibility of reproducing satisfactorily ground temperature, soil moisture, evapotranspiration and runoff with a unique configuration. The infiltration model which proves most promising is the Richards equation model, which is also much more realistic. Although this is found to better simulate snowpack temperatures (Wever et al., 2015), it requires improvements in the simulation of ground temperatures, in order to avoid the underestimation that is often observed.

Further issues lie in the difficulties encountered to reproduce vegetation characterized by low heights and high Direct Throughfall values, which ought to be investigated in detail if SNOWPACK will continue to be implemented in medium-low altitude sites with open fields. Furthermore, the formulation to compute the soil bulk thermal conductivity must be revisited, referring to the existing models in literature and possibly differing depending on the soil type and on the water content. The new formula should assign more importance to the water thermal conductivity and the heat solver in the model should be modified in order to produce a realistic GT regime when lower conductivity values, comparable to the ones proposed in literature, are used as input.

Future studies should assess SNOWPACK's ability to simulate soil physical phenomena at lower time resolution, from the hourly to the weekly time scale. The model, if perfected in the simulation of ground temperatures, could become a precious tool to evaluate the entity and the temperature of subsurface flow. This, in turn, would allow to estimate with accuracy stream temperature and discharge using models such as Alpine3D and StreamFlow 1.0. The capability to make good previsions on soil and stream temperature, as well as on stream discharge, will be very useful when predicting climate change effect on geochemical, biologic and hydrologic cycles, along with flood risk management.

## BIBLIOGRAPHY

- Abu-Hamdeh, N. H., et Reeder, N. C. (2000). Soil Thermal Conductivity Effects of Density, Moisture, Salt Concentration, and Organic Matter. *Soil Science Society of America Journal*, 1285-1290.
- Andujar Marquez, J. M., et al. (2016). Ground Thermal Diffusivity Calculation by Direct Soil Temperature Measurement. Application to very Low Enthalpy Geothermal Energy Systems. *Sensors*.
- Bartelt, P., et Lehning, M. (2002). A physical SNOWPACK model for the Swiss avalanche warning: Part I: numerical model. *Cold Regions Science and Technology*, 123-145.
- Bavay, M., et Egger, T. (2014). MeteoIO 2.4.2: a preprocessing library for meteorological data.
- Brauchli, T., et al. (2017). Influence of slope-scale snowmelt on catchment response simulated with the Alpine3D model. *Water Resources Research*, 10723-10739.
- Briggs, L. J., et Shantz, H. L. (1912). The Wilting Coefficient and Its Indirect Determination. *Botanical Gazette*, 20-37.
- Byrne, K. A., et al. (2007). Carbon sequestration determined using farm scale carbon balance and eddy covariance. *Agriculture, Ecosystems et Environment*, 357-364.
- Campbell, G. S. (1974). A simple method for determining unsaturated hydraulic conductivity from moisture retention data. *Soil Science*, 311-315.
- Celia, M. A., et al. (1990). A general mass-conservative numerical solution for the unsaturated flow equation. *Water Resources Research*, 1483-1496.
- Comola, F., et al. (2015a). Scale-dependent effects of solar radiation patterns on the snow-dominated hydrologic response: Hydrologic signature of solar radiation. *Geophysical Research Letters*.
- Corbett, E. S., et Crouse, R. P. (1968). Rainfall interception by annual grass and chaparral losses compared. *Berkeley, Calif., Pacific SW. Forest et Range Exp. Sta.*
- Darcy, H. (1856). *Les fontaines publiques de la ville de Dijon*. Paris: Dalmont.
- De Marsily, G. (1986). *Quantitative Hydrogeology: Groundwater Hydrology for Engineers*. Academic Press.
- Duarte, A., et al. (2006). Thermal Properties of unsaturated soils. *Unsaturated Soils, Global Soil Partnership*, 1707-1718.
- Farouki, O. (1982). *Evaluation of Methods for Calculating Soil Thermal Conductivity*. Report 82-8, US Army.
- Fierz, C., et al. (2009). The International Classification for Seasonal Snow on the Ground. *Technical Documents in Hydrology*.
- Fourier, J. (1822). *Théorie analytique de la chaleur*. Paris: Firmin Didot Père et Fils.
- Freeze, R. A., et Cherry, J. A. (1979). *Groundwater*. Prentice-Hall. Inc.: Englewood Cliffs, N.J.
- Gallice, A., et al. (2016). Streamflow 1.0: an extension to the spatially distributed snow model Alpine3D for hydrological modelling and deterministic stream temperature prediction. *Geoscientific Model Development*, 4491-4519.
- Ghauman, B. S., et Lal, R. (1985). Thermal conductivity, thermal diffusivity, and thermal capacity of some Nigerian soils. *Soil Sciences*, 74-80.
- Gouttevin, I., et al. (2015). A two-layer canopy model with thermal inertia for an improved snowpack energy balance below needleleaf forest (model SNOWPACK, version 3.2.1, revision 741). *Geoscientific Model Development*, 2379-2398.
- Hipp, T. (n.d.). Master Thesis.
- Hollesen, J., et al. (2011). Future active layer dynamics and carbon dioxide production from thawing permafrost layers in Northeast Greenland. *Global Change Biology*, 911-926.
- Holtlag, A., et H., D. B. (1988). Applied modeling of the nighttime surface energy balance over land. *Journal of Applied Meteorology*, 689-704.

- Hurk, V. D., et al. (2000). Offline validation of the ERA40 surface scheme. *ECMWF Tech. Memo*, 295.
- Ippish, O., et al. (2006). Validity limits for the van Genuchten–Mualem model and implications for parameter estimation and numerical simulation. *Advances in Water Resources*, 1780-1789.
- Jansson, P. E., et al. (1999). Simulated evapotranspiration from the Norunda forest stand during the growing season of a dry year. *Agricultural and Forest Meteorology*, 621-628.
- Jansson, P. E., et Halldin, S. (1979). Model for the annual water and energy flow in a layered soil. Comparison of Forest and Energy Exchange Models. *Society for Ecological Modelling*, 145-163.
- Johansen, O. (1975). Thermal Conductivity of Soils and Rocks. *Proceedings of the Sixth International Congress of the Foundation Francaise d'Etudes Nordiques*, 407-420.
- Joint Technical Committee, E.-0. (2016). <https://structx.com/home.html>. Retrieved from STRUCTX: [https://structx.com/Soil\\_Properties\\_002.html](https://structx.com/Soil_Properties_002.html)
- Jones, J. W., et al. (2003). The DSSAT cropping system model. *European Journal of Agronomy*, 235-265.
- Kersten, M. S. (1949). Thermal Properties of Soils. *Engineering Experiment Station*.
- Kirchhoff, G. (1860). On the relation between the radiating and absorbing powers of different bodies for light and heat. *Annalen der Physik und Chemie*, 275-301.
- Kool, J. B., et van Genuchten, M. T. (1989). *HYDRUS, One-dimensional variably saturated flow and transport model, including hysteresis and root water uptake*. Herndon, VA: Hydrogeologic Inc.
- Koorevaar, P., et al. (1983). *Elements of Soil Physics*. Development in Soil Science 13.
- Kustas, W. P., et al. (1994). Local energy flux estimates for unstable conditions using variance data in semiarid rangelands. *Water Resources Research*, 1351-1361.
- Lehning, M., et al. (2002). A physical SNOWPACK model for the Swiss avalanche warning: Part II: Snow microstructure. *Cold Regions Science and Technology*, 147-167.
- Lehning, M., et al. (2002). A physical SNOWPACK model for the Swiss avalanche warning: Part III: meteorological forcing, thin layer formation and evaluation. *Cold Regions Science and Technology*, 169-184.
- Lehning, M., et al. (2006). Alpine3D: a detailed model of mountain surface processes and its application to snow hydrology. *Hydrological Processes*, 2111-2128.
- Lehning, M., et Bartelt, P. (2002). A physical SNOWPACK model for the Swiss avalanche warning: Part I: numerical model. *Cold Regions Science and Technology*, 123-145.
- Luetsch, M. (2005). A model and field analysis of the interaction between snow cover and alpine permafrost. *PhD thesis, University of Zurich*.
- Luetsch, M., et al. (2003). Numerical simulation of the interaction processes between snow cover and alpine permafrost. *In Proceedings of the Eighth International Conference on Permafrost*, 697-702.
- Luetsch, M., et al. (2008). A sensitivity study of factors influencing warm/thin permafrost in the Swiss Alps. *Journal of Glaciology*.
- Martynov, G. A. (1959). Principles of Geocryology, Part I. *Academy of Sciences*.
- Michlmayr, G., et al. (2008). Application of the Alpine3D model for glacier mass balance and glacier runoff studies at Goldbergkees, Austria. *Hydrological Processes*, 3941-3949.
- Philip, J. R., et de Vries, D. A. (1957). Moisture movement in porous materials under temperature gradients. *American Geophysical Union*, 222-232.
- Richards, L. A. (1931). Capillary conduction of liquids through porous mediums. *Physics* 1:5, 318-333.
- Riha, S. J., et al. (1980). A Finite Element Calculation for Determining Thermal Conductivity. *Soil Science Society of America Journal*, 1323-1325.

- Rockström, J., et al. (1998). Seasonal rainfall partitioning under runoff and runoff conditions on sandy soil in Niger. On-farm measurements and water balance modelling. *Journal of Hydrology*, 68-92.
- Romano, M., et al. (2011). Parameterization of a bucket model for soil-vegetation-atmosphere modeling under seasonal climatic regimes. *Hydrology and Earth System Sciences*, 3877-3893.
- Russo, D. (1988). Determining soil hydraulic properties by parameter estimation: On the selection of a model for the hydraulic properties. *Water Resources Research*, 453-459.
- Rutter, N., et al. (2009). Evaluation of forest snow processes models (SnowMIP2). *Journal of geophysical research*.
- Saito, H., et al. (2006). Numerical analysis of coupled water vapor and heat transport in the vadose zone. *Vadose Zone Journal*, 784-800.
- Sándor, R., et Fodor, N. (2012). Simulation of Soil Temperature Dynamics with Models Using Different Concepts. *The Scientific World Journal*, Article ID 590287, <http://dx.doi.org/10.1100/2012/590287>.
- Saxton, K. E., et al. (1986). Estimating generalized soil-water characteristics from texture. *Soil Science Society of America Journal*, 1031-1036.
- Schaap, M. G., et al. (2001). Rosetta: a computer program for estimating soil hydraulic parameters with hierarchical pedotransfer functions. *Journal of Hydrology*, 163-176.
- Schlogl, S., et al. (2016). Sensitivity of Alpine3D modeled snow cover to modifications in dem resolution, station coverage and meteorological input quantities. *Environmental Modelling and Software*, 387-396.
- Schlögl, S., et al. (2017). How do Stability Corrections Perform in the Stable Boundary Layer Over Snow? *Boundary-Layer Meteorology*, 161-180.
- Shelia, V., et al. (2018). Coupling DSSAT and HYDRUS-1D for simulations of soil water dynamics in the soil-plant-atmosphere system. *Journal of Hydrology and Hydromechanics*, 232-245.
- Stearns, C. R., et Weidner, G. A. (1993). Sensible and latent heat flux estimates in Antarctica. *Antarctic Research Series*, 109-138.
- St-Hilaire, A., et al. (2000). Water temperature modelling in a small forested stream: implication of forest canopy and soil temperature. *Canadian Journal of Civil Engineering*, 1095-1108.
- Tavman, L. H. (1996). Effective thermal conductivity of granular porous materials. *International Communications in Heat and Mass Transfer*, 169-176.
- Taylor, S. A., et Jackson, R. D. (1965). Heat capacity and specific heat. *American Society of Agronomy*, 345-348.
- Thimo, P. (2013). Recent heat flow in the Alps – Geothermal energy. *MSc. Angewandte Geowissenschaften*.
- van Genuchten, M. T. (1978). *Mass transport in saturated-unsaturated media: one-dimensional solutions*. Princeton University, NJ: Water Resources Program.
- Van Genuchten, M. T. (1980). A Closed-form Equation for Predicting the Hydraulic Conductivity of Unsaturated Soils. *Soil Science Society of America Journal*.
- van Genuchten, M. T. (1987). *A numerical model for water and solute movement in and below the root zone*. Riverside, California: U.S. Salinity laboratory, USDA, ARS.
- Van Wijk, W. R. (1963). *Physics of plant environment*.
- Vedova, B. D., et al. (1991). Heat flow in the tectonic provinces of the European Geotraverse. *Tectonophysics*, 57-74.
- Vogel, T. (1987). *Numerical model of two-dimensional flow in a variably saturated porous medium*. Wageningen, The Netherlands: Dept. of Hydraulics and Catchment Hydrology, Agricultural University.

- Watson, D. J. (1947). Comparative physiological studies on the growth of field crops: I. Variation in net assimilation rate and leaf area between species and varieties and within and between years. *Annals of Botany*, 41-76.
- Wever, N., et al. (2014). Solving Richards Equation for snow improves snowpack meltwater. *The Cryosphere*, 257-274.
- Wever, N., et al. (2015). Verification of the multi-layer SNOWPACK model with different water transport schemes. *The Cryosphere*, 2271-2293.
- Wever, N., et al. (2017). Simulating the influence of snow surface processes on soil moisture dynamics and streamflow generation in an alpine catchment. *Hydrology and Earth System Sciences*, 4053-4071.
- Yadav, M. R., et Saxena, G. S. (1973). Effect of Compaction and Moisture Content on Specific Heat and Thermal Capacity of Soils. *Journal of the Indian Society of Soil Science*, 129-132.

## APPENDICES

### A. Rosetta soil classification and class mean hydraulic parameters

Table 0-1 below provides class-average values of the seven hydraulic parameters for the twelve USDA textural classes. This table represents the first model of the hierarchical sequence. For the  $\theta_r$ ,  $\theta_s$ ,  $\alpha$ ,  $n$  and  $K_s$  parameters, the values are the result of averaging multiple values for each textural class.  $K_s$  and  $L$  were generated by entering the class average values of  $\theta_r$ ,  $\theta_s$ ,  $\alpha$  and  $n$  into Model C2 (see Rosetta's help file). This implies that  $K_o$  and  $L$  may not be very reliable, as they are computed based on predicted parameters. The values in parenthesis show the standard deviation uncertainty of the class average values.

Table 0-1: Rosetta class average values of hydraulic parameters

Texture Class	N	$\theta_r$		$\theta_s$		$\log(\alpha)$		$\log(n)$		$K_s$		$K_o$		$L$	
		cm <sup>3</sup> /cm <sup>3</sup>	( )	cm <sup>3</sup> /cm <sup>3</sup>	( )	log(1/cm)	( )	log10	( )	log(cm/day)	( )	log(cm/day)	( )	( )	
Clay	84	0.098	(0.107)	0.459	(0.079)	-1.825	(0.68)	0.098	(0.07)	1.169	(0.92)	0.472	(0.26)	-1.561	(1.39)
C loam	140	0.079	(0.076)	0.442	(0.079)	-1.801	(0.69)	0.151	(0.12)	0.913	(1.09)	0.699	(0.23)	-0.763	(0.90)
Loam	242	0.061	(0.073)	0.399	(0.098)	-1.954	(0.73)	0.168	(0.13)	1.081	(0.92)	0.568	(0.21)	-0.371	(0.84)
L Sand	201	0.049	(0.042)	0.390	(0.070)	-1.459	(0.47)	0.242	(0.16)	2.022	(0.64)	1.386	(0.24)	-0.874	(0.59)
Sand	308	0.053	(0.029)	0.375	(0.055)	-1.453	(0.25)	0.502	(0.18)	2.808	(0.59)	1.389	(0.24)	-0.930	(0.49)
S Clay	11	0.117	(0.114)	0.385	(0.046)	-1.476	(0.57)	0.082	(0.06)	1.055	(0.89)	0.637	(0.34)	-3.665	(1.80)
S C L	87	0.063	(0.078)	0.384	(0.061)	-1.676	(0.71)	0.124	(0.12)	1.120	(0.85)	0.841	(0.24)	-1.280	(0.99)
S loam	476	0.039	(0.054)	0.387	(0.085)	-1.574	(0.56)	0.161	(0.11)	1.583	(0.66)	1.190	(0.21)	-0.861	(0.73)
Silt	6	0.050	(0.041)	0.489	(0.078)	-2.182	(0.30)	0.225	(0.13)	1.641	(0.27)	0.524	(0.32)	0.624	(1.57)
Si Clay	28	0.111	(0.119)	0.481	(0.080)	-1.790	(0.64)	0.121	(0.10)	0.983	(0.57)	0.501	(0.27)	-1.287	(1.23)
Si C L	172	0.090	(0.082)	0.482	(0.086)	-2.076	(0.59)	0.182	(0.13)	1.046	(0.76)	0.349	(0.26)	-0.156	(1.23)
Si Loam	330	0.065	(0.073)	0.439	(0.093)	-2.296	(0.57)	0.221	(0.14)	1.261	(0.74)	0.243	(0.26)	0.365	(1.42)

## B. A complete scheme of the formulas behind the methods Evaporation Resistance (ER) and Relative Humidity (RH)

The bulk aerodynamic equation for computing latent heat exchange  $q_l$  ( $W/m^2$ ) can be written in the form:

$$q_l = \beta \cdot (e_a - e_s) \quad (31)$$

where:

$\beta$  = aerodynamic resistance (m/s)

$e_a$  = air vapor pressure (Pa)

$$e_a = \varphi \cdot \text{vaporSaturationPressure}(T_a) \quad (32)$$

where:

$\varphi$  = relative humidity of air (/)

*vaporSaturationPressure* is the function describing the equilibrium vapor pressure according to the temperature, based on Antoine's equation.

$e_s$  is the vapor pressure in the uppermost layer, which can be either snow or soil. Its computation can differ and requires the following variables to be presented:

$T_{ss}$  = surface temperature (K)

$T_{se}$  = temperature of uppermost layer, at 1 cm in this case (K)

$P_{vap,1} = \text{vaporSaturationPressure}(T_{ss})$

$P_{vap,2} = \text{vaporSaturationPressure}(T_{se})$

With snow, saturation is assumed.

If  $T_{ss} < 0$  °C

$$e_s = P_{vap,1}$$

If  $T_{ss} > 0$  °C

$$e_s = P_{vap,2}$$

Without snow:

If  $T_{ss} < 0$  °C

$$e_s = P_{vap,1}$$

If  $T_{ss} > 0$  °C

If evaporation method = ER

$$e_s = P_{vap,2}$$

If evaporation method = RH

$$e_s = P_{vap,2} \cdot RelativeHumidity(\text{topsoil layer})$$

*RelativeHumidity*: The formulation is based on Saito et al. (2006). *RelativeHumidity* is calculated from the pressure head using a thermodynamic relationship between liquid water and water vapor in soil pores (Philip et de Vries, 1957).

If infiltration method = Richards

$$\text{Return } \max \left( 0; \min \left( 1; e^{\frac{h \cdot g}{gas\_constant \cdot T_e}} \right) \right) \quad (33)$$

Else

If  $\theta_w < \theta_{fc}$

$$\text{Return } 0.5 \cdot \left( 1 - \cos \left( \min \left( \pi; \frac{\theta_w \cdot \pi}{\theta_{fc} \cdot 1.6} \right) \right) \right) \quad (34)$$

else

return 1

where:

$h$  = capillary pressure head (m)

$g$  = gravitational acceleration constant (m/s<sup>2</sup>)

$gas\_constant$  = 461.9 (J/kg·K)

$T_e$  = temperature of uppermost element (K)

$\beta$  is computed according to this formula, originated from Kustas et al. (1994):

$$\beta = \frac{c \cdot 0.622 \cdot lh\_sublimation}{gas\_const\_air \cdot T_{air}} \quad (35)$$

$lh\_sublimation$  = latent heat of vaporization or sublimation =  $2.838 \cdot 10^6$  J/kg

$gas\_const\_air$  = 287 J/kg·K

$c$  is the heat exchange coefficient due to vapor exchange (m/s) and it is computed differently whether the evaporation method is ER or RH.

If the evaporation method is RH,  $c$  will be based on the height  $z_0$  and on  $psi\_m$ , a variable that takes care of the stability correction for atmospheric turbulence. This formulation is described in the function *compSensibleHeatCoefficient* of the SNOWPACK code.

When the evaporation method is ER, an additional resistance  $R_{soil}$ , dependent on the relative saturation of the topsoil layer, is used to reduce the heat exchange coefficient  $c$  in the case of evaporation.

The modification of  $c$  is only applied when  $e_s \geq e_a$  et  $T(\text{topsoil element}) \geq 0$  °C .

$$R_a = \frac{1}{c} \quad (36)$$

$$c_2 = \frac{1}{R_a + \frac{R_{soil,min}}{\max(relsatmin, \min\left(1, \frac{\theta_w}{\theta_{fc}}\right))}} \quad (37)$$

where:

$R_a$  is the atmospheric resistance (s/m)

$R_{soil,min}$  = 50 s/m is the minimum soil resistance in the top layer (Hurk et al., 2000)

$relsatmin$  = 0.05 is the minimum relative humidity in the top layer

$c_2$  is the corrected heat exchange coefficient, to be introduced in equation (35) instead of  $c$ .

All the quantities refer to the uppermost layer.

### C. Simulations' temporal length and availability of data

The second column indicates the period for which both meteorological data and soil information are available; the third column specifies the lowest and highest depth for which soil information is provided; columns from 4 to 6 declare the availability of the written meteorological quantities; the final column expresses the possibility of running Alpine3D in the relative hydrographic catchment.

*Table 0-2: Duration of the simulations and available information for each site*

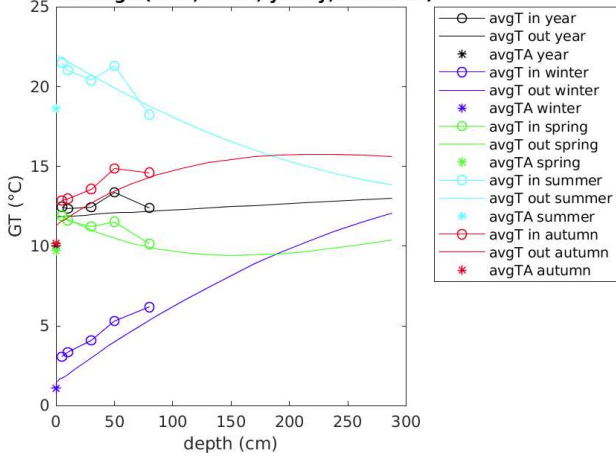
ID	Dataset period	Depths (cm)	ET	OLWR	OSWR	Alpine3D
BAS	08-2009 : 10-2017	5 to 120				
BER	08-2009 : 10-2017	5 to 120	YES			
CHN/CGI	01-2008 : 11-2017	5 to 80			YES	
LAG/NABLAE	08-2009 : 11-2017	5 to 45				
MAG/CAD	08-2009 : 10-2017	5 to 80		YES	YES	
PAY	08-2008 : 10-2017	5 to 80	YES	YES	YES	YES
PLA/PLF	01-2008 : 11-2017	5 to 120			YES	
REC	08-2009 : 11-2017	5 to 150				
RIE/RHB	05-2009 : 01-2017	5 to 110	YES	YES	YES	YES
SIO	08-2009 : 11-2017	5 to 120				
TAE	05-2010 : 10-2017	5 to 50		YES	YES	
WYN	05-2010 : 11-2017	5 to 50				

## D. Ground temperature plots

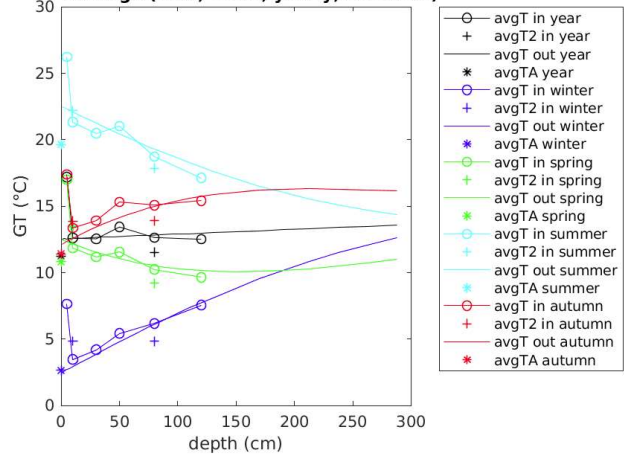
The full set of plots described in section 7.1 is here reported. Both measured and modelled ground temperatures are divided by season, averaged throughout the whole time series and displayed against soil depth. Figures found in Part I were obtained with the Bucket infiltration model and the Evaporation Resistance method, whereas those found in Part II come from the application of the Richards equation model and the same evaporation method.

### I. Bucket, ER

GT average (mod, meas; yearly, seasonal)



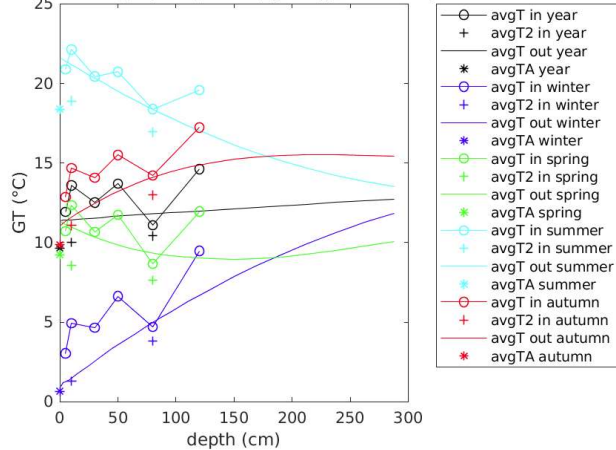
GT average (mod, meas; yearly, seasonal)



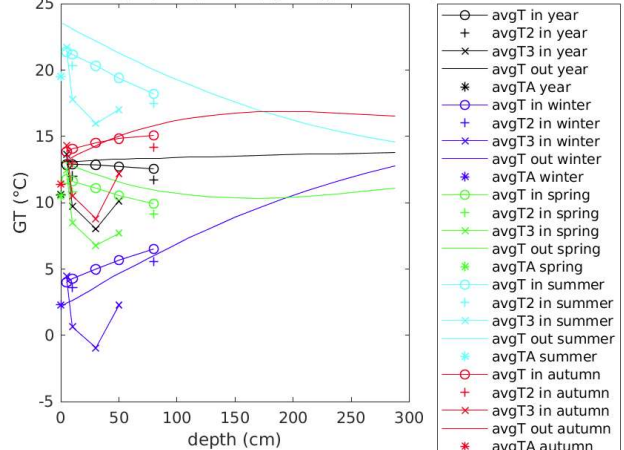
Figures 0-1: Seasonal and yearly average GT vs depth, modelled and measured.

Payerne (left panel), Basel (right panel)

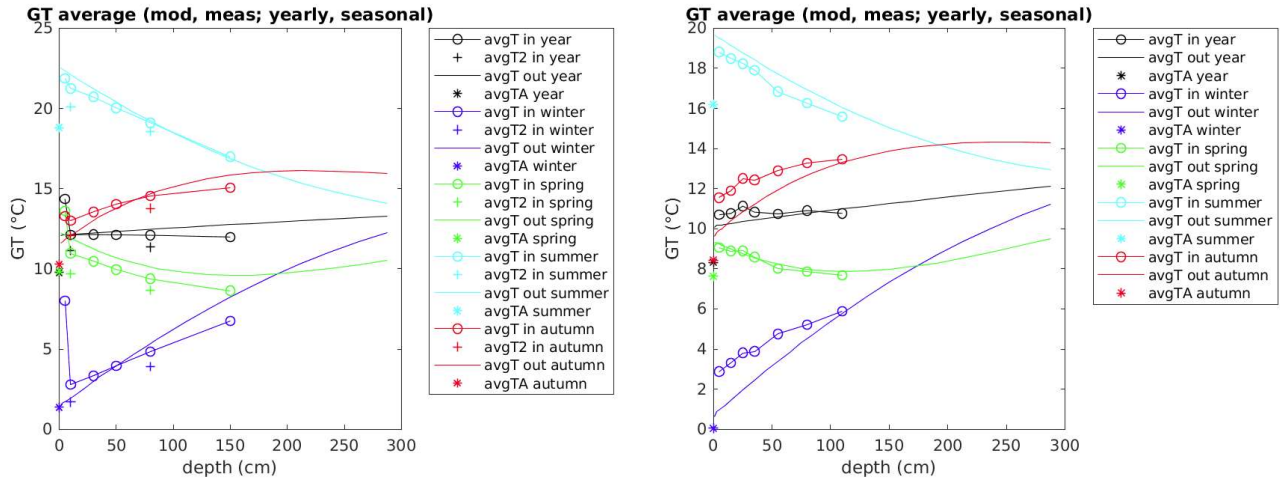
GT average (mod, meas; yearly, seasonal)



GT average (mod, meas; yearly, seasonal)



Figures 0-2: Seasonal and yearly average GT vs depth, modelled and measured. Bern  
(left panel), Nyon Changins (right panel)



Figures 0-3: Seasonal and yearly average GT vs depth, modelled and measured. Reckenholz (left panel), Rietholzbach (right panel)

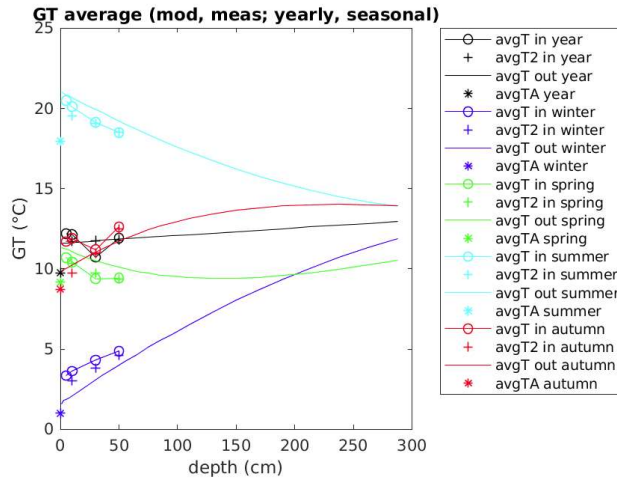
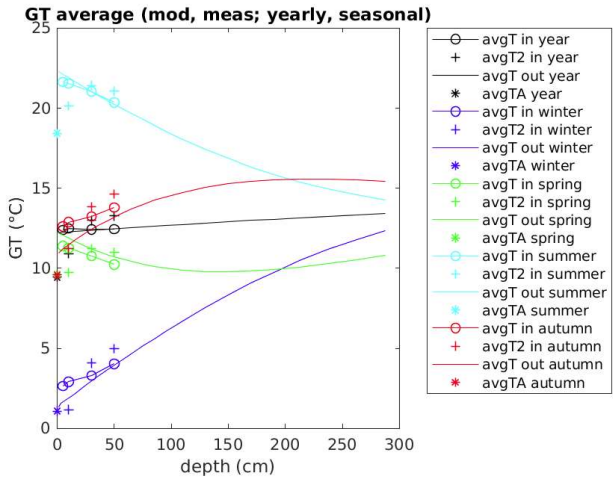
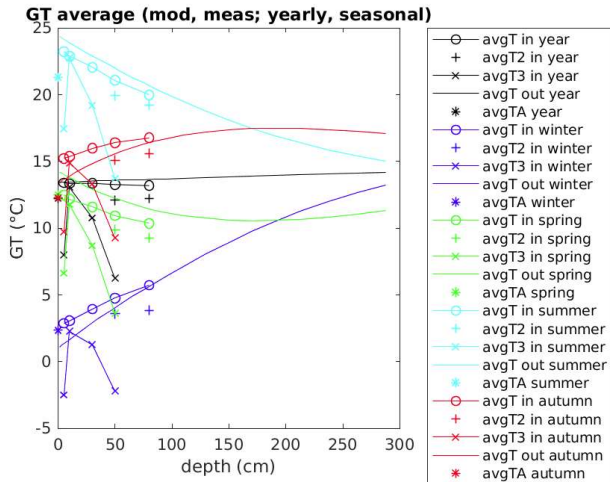
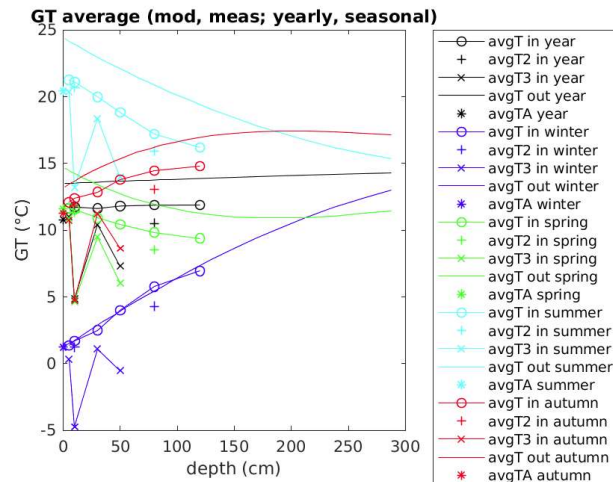
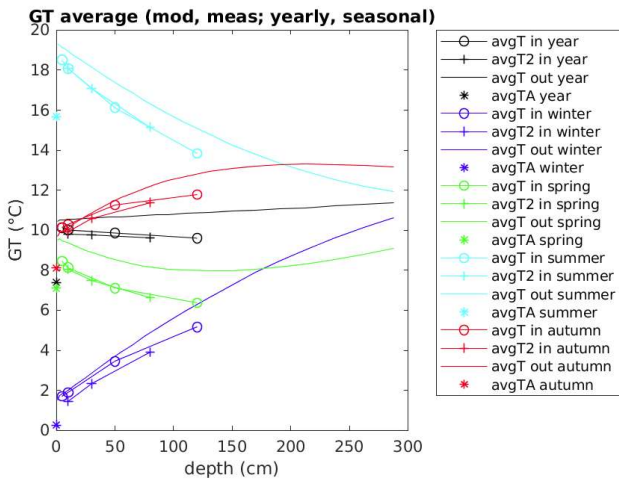


Figure 0-4: Seasonal and yearly average GT vs depth, modelled and measured.

Taenikon



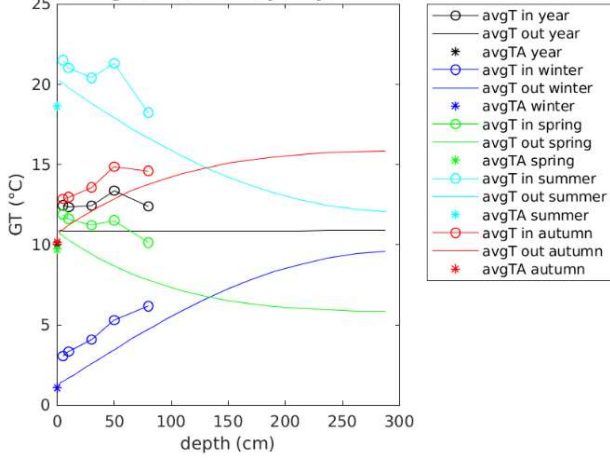
Figures 0-5: Seasonal and yearly average GT vs depth, modelled and measured.  
Magadino Cadenazzo (left panel), Wynau (right panel)



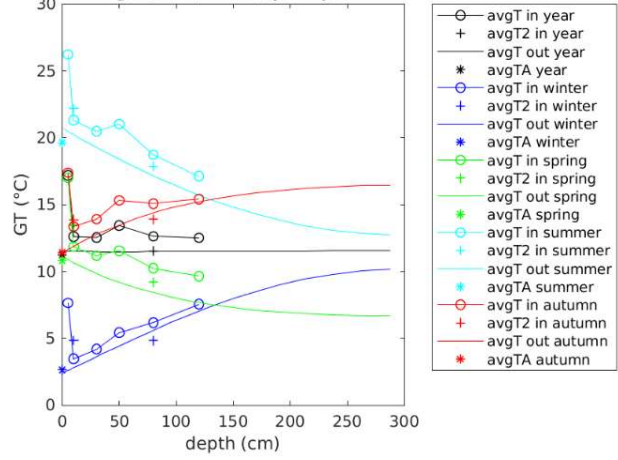
Figures 0-6: Seasonal and yearly average GT vs depth, modelled and measured.  
Plaffeien (left panel), Sion (right panel)

## II. Richards, ER

GT average (mod, meas; yearly, seasonal)



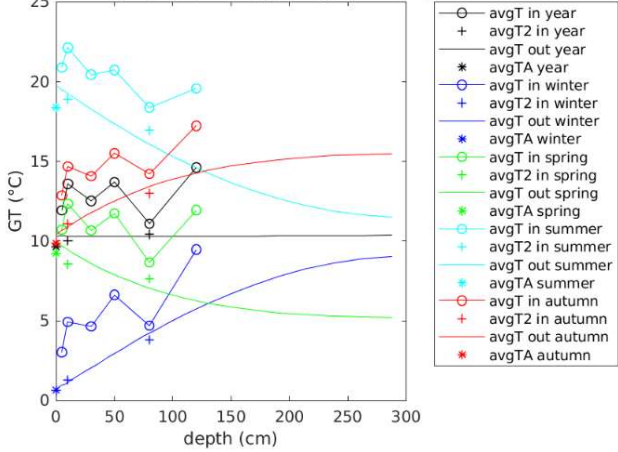
GT average (mod, meas; yearly, seasonal)



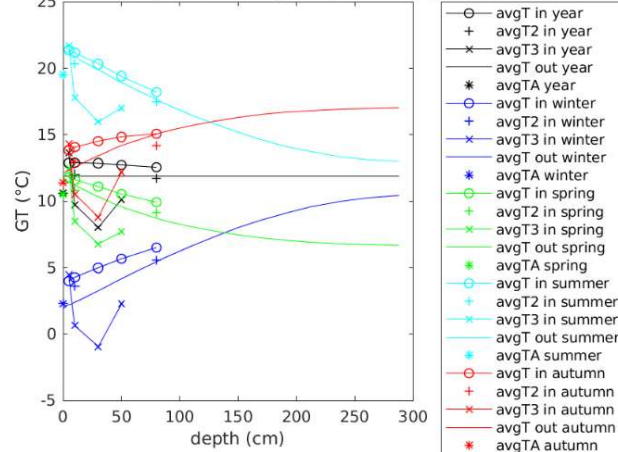
Figures 0-7: Seasonal and yearly average GT vs depth, modelled and measured.

Payerne (left panel), Basel (right panel)

GT average (mod, meas; yearly, seasonal)

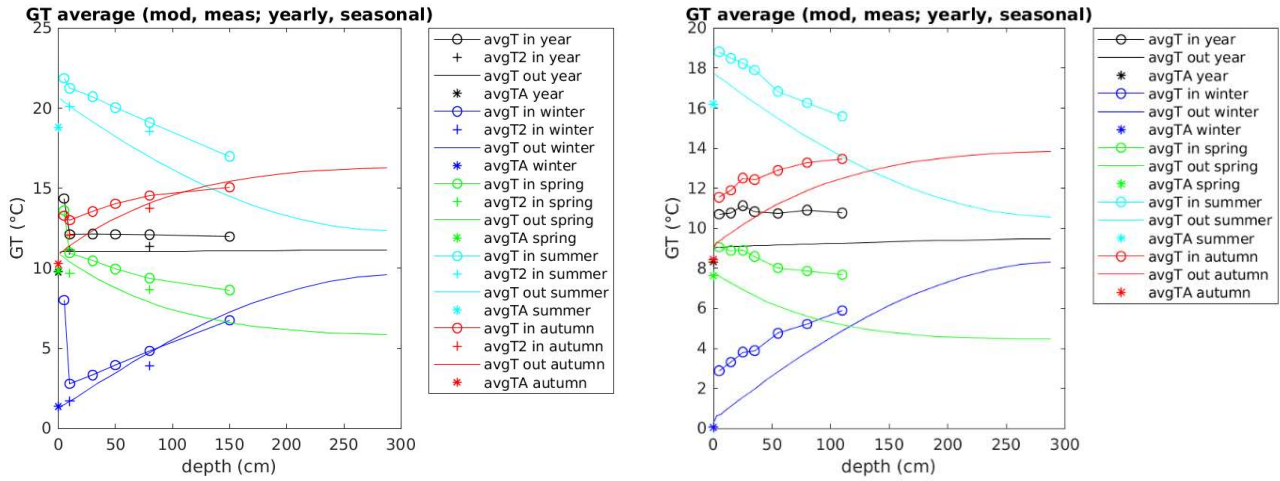


GT average (mod, meas; yearly, seasonal)



Figures 0-8: Seasonal and yearly average GT vs depth, modelled and measured. Bern

(left panel), Nyon Changins (right panel)



Figures 0-9: Seasonal and yearly average GT vs depth, modelled and measured.  
 Reckenholz (left panel), Rietholzbach (right panel)

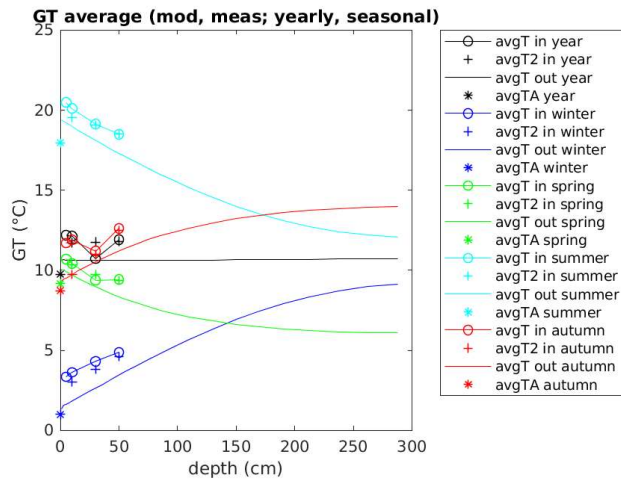
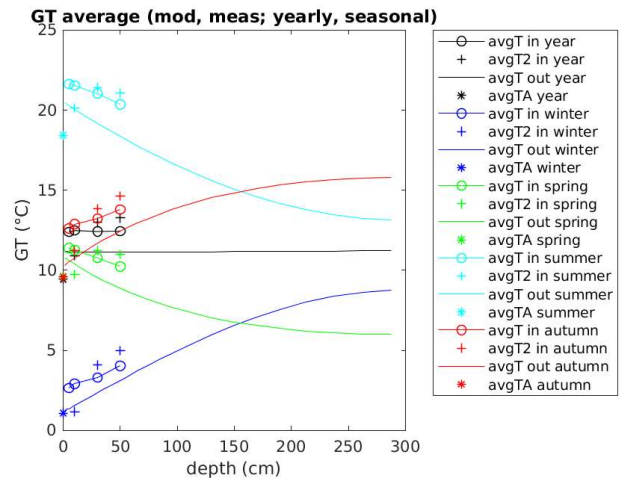
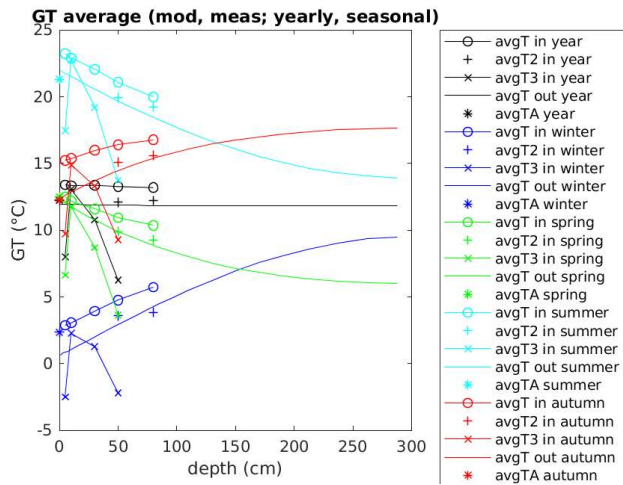
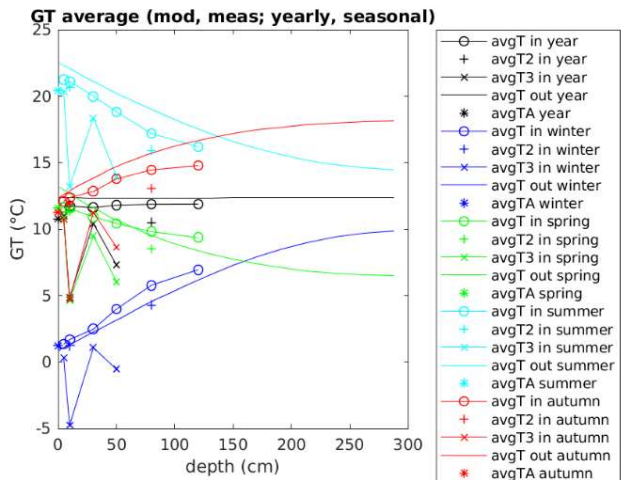
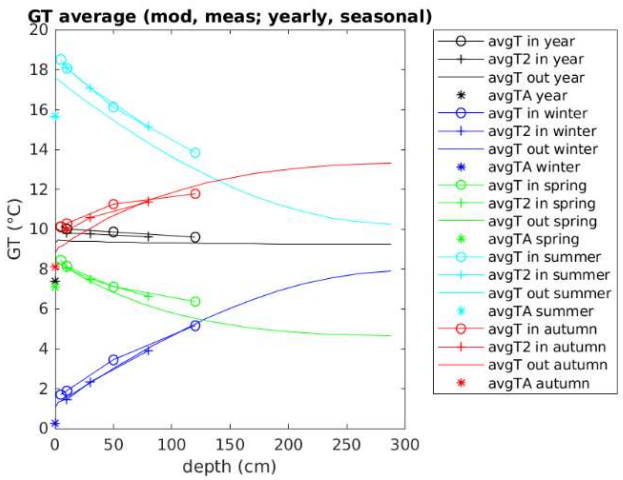


Figure 0-10: Seasonal and yearly average GT vs depth, modelled and measured.  
 Taenikon



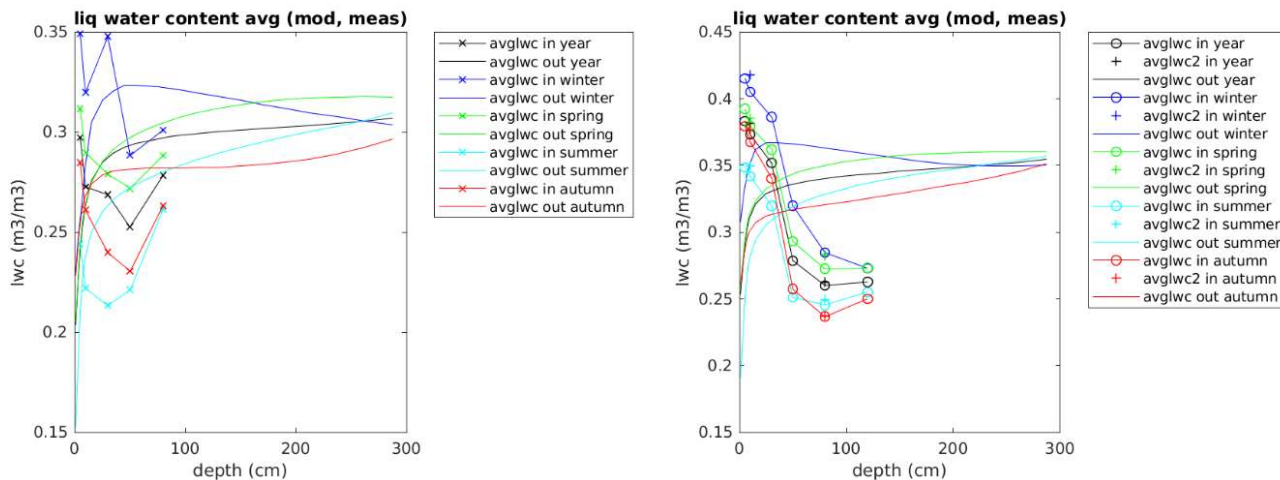
Figures 0-11: Seasonal and yearly average GT vs depth, modelled and measured.  
Magadino Cadenazzo (left panel), Wynau (right panel)



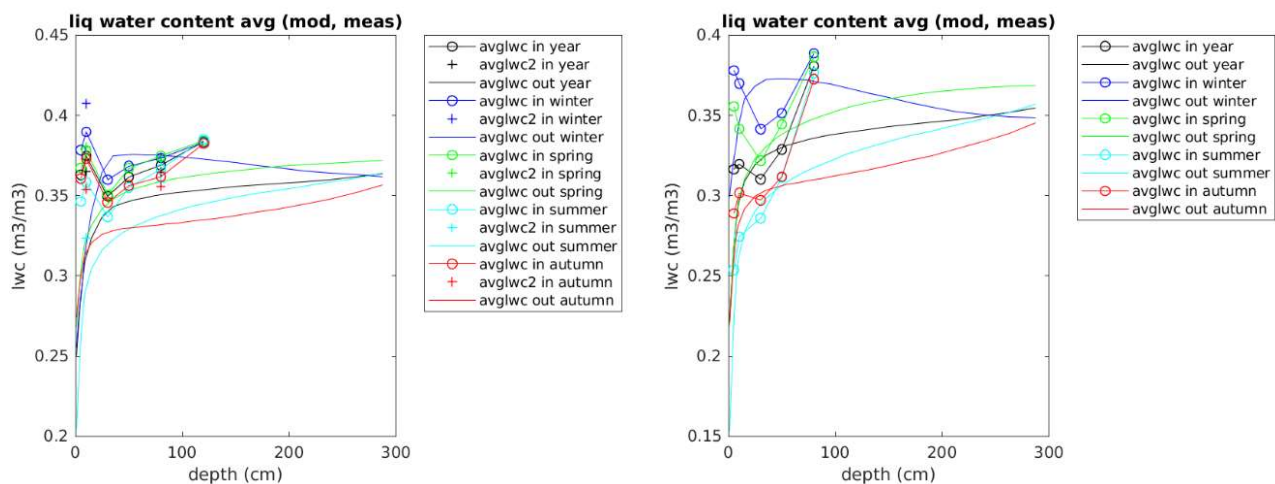
Figures 0-12: Seasonal and yearly average GT vs depth, modelled and measured.  
Plaffeien (left panel), Sion (right panel)

## E. Soil moisture plots

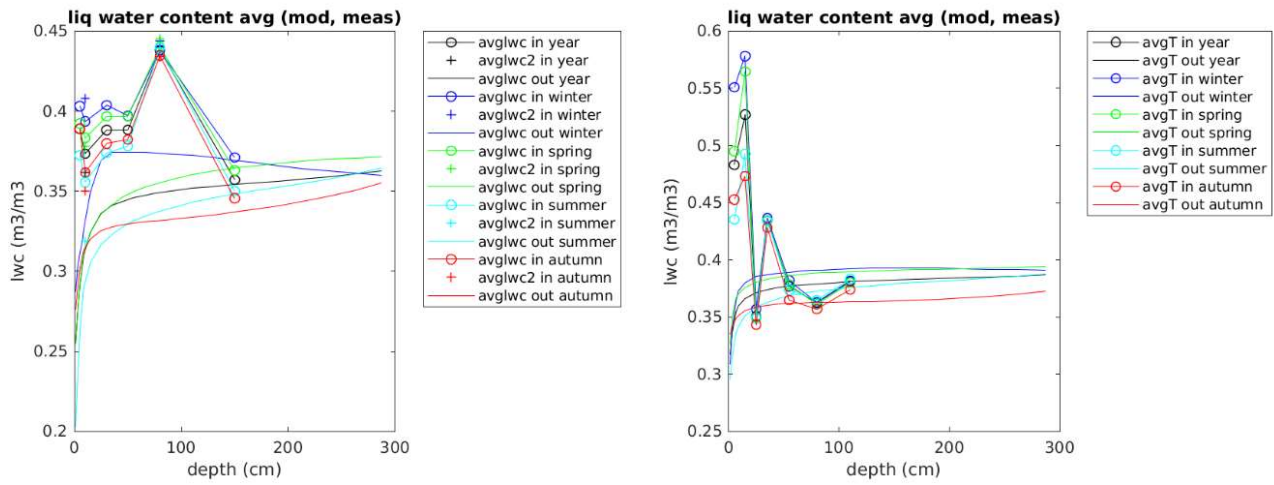
The full set of plots described in section 7.3 is here reported. Both measured and modelled soil moisture data are divided by season, averaged throughout the whole time series and displayed against soil depth. All the figures were obtained with the Richards equation infiltration model and the Evaporation Resistance method.



Figures 0-13: Seasonal and yearly average soil moisture vs depth, modelled and measured. Payerne (left panel), Basel (right panel)



Figures 0-14: Seasonal and yearly average soil moisture vs depth, modelled and measured. Bern (left panel), Nyon Changins (right panel)



Figures 0-15: Seasonal and yearly average soil moisture vs depth, modelled and measured. Reckenholz (left panel), Rietholzbach (right panel)

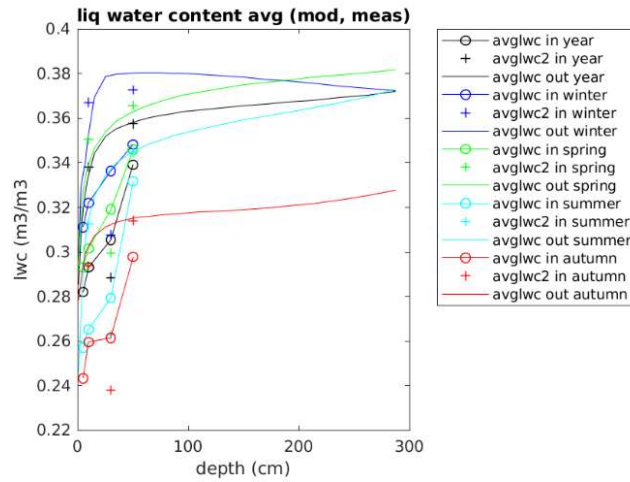
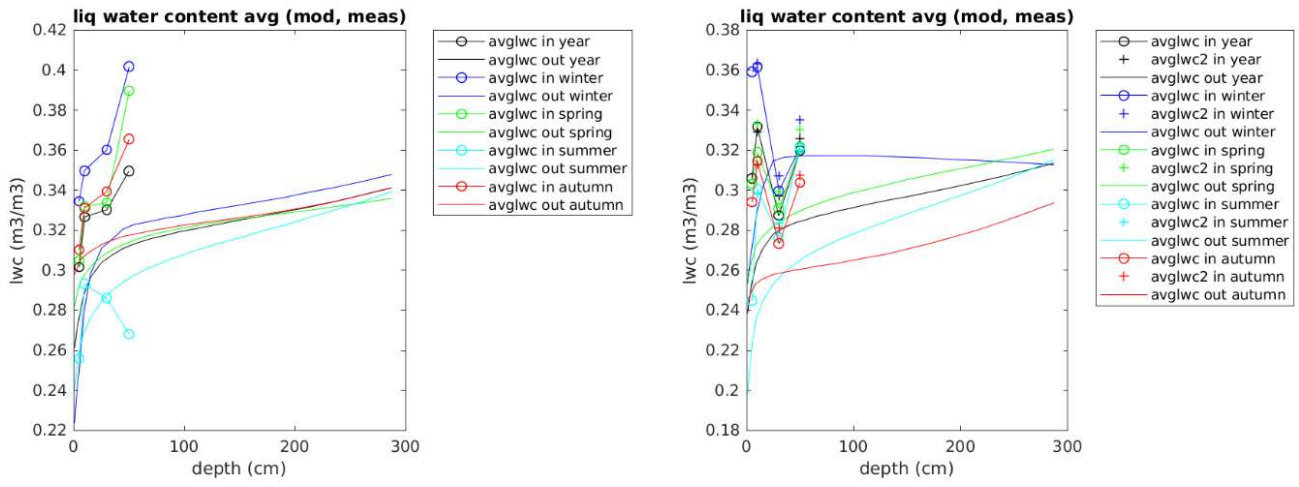
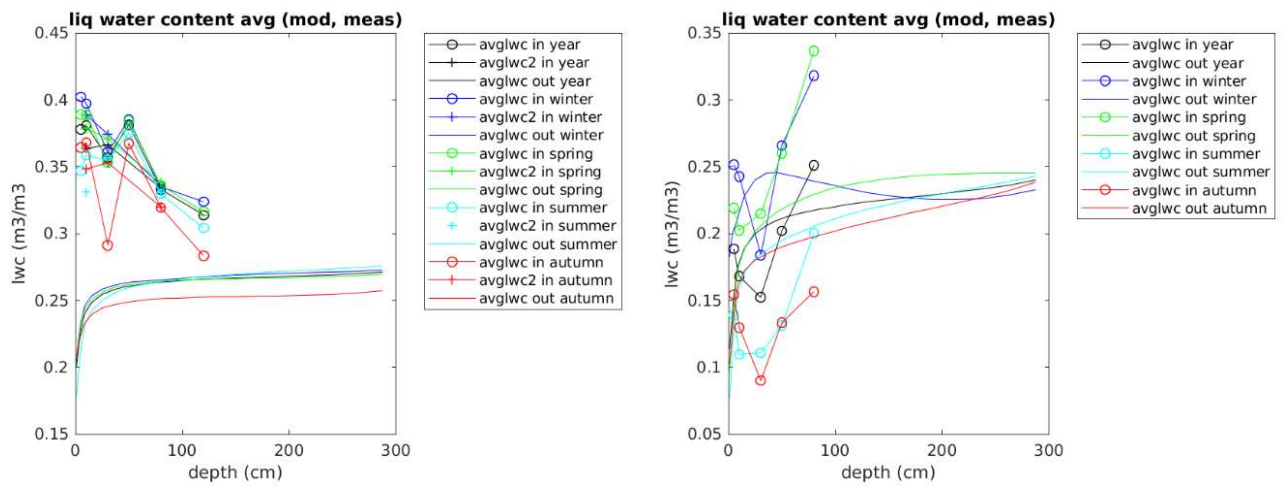


Figure 0-16: Seasonal and yearly average soil moisture vs depth, modelled and measured. Taenikon



Figures 0-17: Seasonal and yearly average soil moisture vs depth, modelled and measured. Magadino Cadenazzo (left panel), Wynau (right panel)



Figures 0-18: Seasonal and yearly average soil moisture vs depth, modelled and measured. Plaffeien (left panel), Sion (right panel)